NASA CR-54234

VON KARMAN CENTER

SNAP-8 DIVISION

SNAP-8 SEALS-TO-SPACE DEVELOPMENT TEST PROGRAM

VOL. III – DYNAMIC SLINGER

A REPORT TO

NATIONAL AERONAUTICS AND SPACE ADMINISTRATION

CONTRACT NO. NAS 5-417

REPORT NO. 2808 (TOPICAL) / MAY 1964 / COPY NO. 23

AEROJET GENERAL TIRE GENERAL

NASA CR-54234
N65 17272

SNAP-8 SEALS-TO-SPACE DEVELOPMENT TEST PROGRAM

VOLUME III - DYNAMIC SLINGER

By R. L. Lessley
I. L. Marburger

Contract No. NAS 5-417

a topical report to

NASA - LEWIS RESEARCH CENTER
SNAP-8 PROJECT OFFICE
H. O. SLONE, SNAP-8 PROJECT MANAGER

Report No. 2808 (Topical) May 1964

AEROJET-GENERAL CORPORATION
A SUBSIDIARY OF THE GENERAL TIRE & RUBBER COMPANY

CONTRACT FULFILLMENT STATEMENT

This is Volume III of a four-volume topical report covering the SNAP-8 Seals-to-Space Development Test Program, and is submitted in partial fulfillment of NASA Contract No. NAS 5-417.

FOREWORD

The SNAP-8 seals-to-space concept involves the use of visco pump, molecular pump, and dynamic slinger elements. The seals-to-space program encompassed basic test work on each of these components for the purpose of demonstrating satisfactory performance for SNAP-8 operating conditions. In addition to the basic component tests, an overall integrated seal test rig was built and operated. This rig provided a nearly perfect simulation of the SNAP-8 turbine alternator assembly seal-to-space configuration and thermal environment, and demonstrated the satisfactory performance of the seal.

Volumes I through III of this report cover the work done on the visco pump, molecular pump, and dynamic slinger elements. Volume IV describes the design and operation of the integrated seal simulator.

The SNAP-8 Seals-to-Space Development Test Program was carried out under the auspices of the SNAP-8 Division, Von Karman Center, Aerojet-General Corporation, as part of the SNAP-8 Contract work.

Mr. C. G. Boone, Chief Engineer for the SNAP-8 Division, had overall responsibility for the SNAP-8 Seals-to-Space Development Test Program. Mr. R. L. Lessley, Engineering Department, SNAP-8 Division, had direct responsibility for the program. Assisting Mr. Lessley were E. A. Haglund, J. N. Hodgson, and I. L. Marburger, all of the Engineering Department, SNAP-8 Division.

CONTENTS

CONTENTS (cont.)

CONTENTS (cont.)

SUMMARY

17272

The seal-to-space concept advocated for use in the SNAP-8 power conversion system rotating assemblies utilizes two basic elements. The first element creates a liquid-vapor interface (i.e., a line of demarcation between liquid and vapor). The second element restricts leakage of the vapors which emanate from the liquid-vapor interface. A dynamic slinger has been selected as the liquid-vapor interface element for the current SNAP-8 seal-to-space configuration. In order for the slinger to fulfill its intended role, however, the liquid-vapor interface must be stable. Otherwise droplets may be generated by the interface which can possibly pass on through the seal.

A series of tests was conducted in which oil and mercury slingers were operated at the specific conditions encountered in the SNAP-8 rotating assemblies. The purpose of these tests was to demonstrate that the slinger interfaces actually do provide a positive demarcation between liquid and vapor and thus create a barrier to prevent leakage of raw liquid. The slinger housings contained transparent sections which permitted observation of the interface during operation. Pumping and drag data were also collected.

The oil slinger tests revealed the presence on the slinger static wall of a film that could serve as a vehicle for the transport of oil past the interface. It was found that this problem could be avoided by coating the slinger walls with a non-wettable material such as Teflon. Tests of mercury slingers revealed a small population of liquid droplets within the interface radius. A modification to the slinger configuration successfully eliminated this droplet formation. Thus, satisfactory slinger performance at SNAP-8 operating conditions is possible for both oil and for mercury.

Author

I. INTRODUCTION

The current SNAP-8 seal concept is illustrated in Figure 1. The purpose of the seal is to prevent mixing of the turbine mercury with the bearing oil. This is accomplished by venting a section of the shaft to space and permitting a small controlled leakage of each liquid to the space vent cavity. The magnitude of this leakage is controlled by mercury and oil seals-to-space. Each seal consists of (a) an element for creating a liquid-vapor interface to prevent passage of raw liquid, and (b) an element for restricting the leakage of vapors emanating from the liquid-vapor interface.

The main elements of mercury seal in Figure 1 are (a) a seal cooler, which causes the seal region next to the turbine to remain full of mercury condensate; (b) a herringbone visco pump, which prevents liquid mercury from centrifuging into the turbine wheel housing; (c) a vaneless slinger (consisting of a step in the shaft), which establishes a liquid-vapor interface; and (d) a molecular pump which restricts leakage of vapors from the slinger liquid-vapor interface. Leakage is further reduced by the tendency of the seal cooler to refrigerate the liquid-vapor interface, thereby reducing the density of the leakage vapors.

The oil seal is similar in construction. It consists of (a) a dynamic slinger, which establishes the liquid-vapor interface; and (b) a molecular pump for restriction of vapor leakage.

This report deals with the role of the dynamic slinger in this seal-to-space concept. Since its sole function is to prevent the loss of raw liquid, it is imperative that the slinger liquid-vapor interface provide a positive demarcation between liquid and vapor in the seal. This can be done only if the interface is stable. Under certain operating conditions, liquid-vapor interfaces obtained in dynamic slingers are unstable (Reference 1). In such cases the interface can actually generate droplets which are discharged in a radially inward direction. Since general laws governing stability of such an interface have not yet been formulated, tests were required to demonstrate the stability of the slinger interfaces at SNAP-8 operating conditions with ET-378 oil and mercury. The same test effort also permitted measurement of pumping and drag coefficients.

II. PROGRAM OBJECTIVES

Program objectives were as follows:

A. To determine adequacy of mercury slinger liquid-vapor interface for use in SNAP-8 seals-to-space

B. To determine adequacy of ET-378 oil slinger liquid-vapor interface for SNAP-8 seals-to-space

C. To determine influence of slinger axial clearance on interface stability for oil and mercury slingers

D. To measure slinger pumping and drag coefficients.

III. TEST APPARATUS AND METHODS

A. OIL SLINGER TESTS

1. Slinger Configurations

Both vaned and vaneless slingers were evaluated in the oil slinger tests. This was done because during the early part of the program, system considerations had required a lubricating oil return pressure of 15 psia at the periphery of the oil slinger. The bearing operation is based on the effective scavenging of the bearing cavity. In the arrangement of Figure 1, this means that the 15 psia return pressure must be generated in the pumping continuum contained between the slinger and the outer race of the bearing. In order to generate 15 psia with such a limited submergence of the slinger disk, it was necessary to select a vaned slinger configuration. Later when the slinger return pressure was reduced from 15 psia to 5 psia it was possible to abandon the vaned slingers in favor of vaneless slingers. Thus the oil slinger tests involved both vaned and vaneless slinger configurations, although only the vaneless slingers were used in the actual SNAP-8 rotating assemblies. Some of the configurations tested are shown in Figures 2 to 5.

2. Oil Test Rig

The first of two test rigs used for evaluation of oil slingers is shown in Figures 6 and 7. The test rig consisted of a 2.5-in.-dia slinger disk and drive spindle in a transparent lucite housing. The transparent housing permitted viewing of the slinger interface during 12,000-rpm operation. The test rig was driven by a 12,000-rpm, 400-cycle, 3-phase, forced-air-cooled induction motor. The rig had provisions for varying axial clearance of the slinger on successive buildups. During each run, radial engagement between the slinger disk and the liquid was varied by controlling liquid pressure applied at the slinger periphery. Provisions were made for applying a vacuum to the slinger interface in order to prevent any influence of atmospheric air on interface stability.

Loop schematics used for water and for oil tests are presented in Figures 8 and 9. This test rig was operated until elevated temperatures encountered during oil tests caused cracking and general deterioration of the lucite housing. It was then replaced by the rig pictured in Figures 10 and 11.

The new test rig incorporated metal housings and was designed for operation over a wider range of pressures and temperatures. A transparent face plate made of a clear polyester was located by the outboard face of the slinger. This permitted photographs of the slinger interface during testing. A cross section of the rig is shown in Figure 12.

Instrumentation penetration included slinger outlet pressure and temperature. Vacuum ports were provided to the interface cavities on each side of the slinger disk. A magnetic speed pickup was provided for shaft speed measurement. Pressures were measured with Heise gages having a maximum error of 0.25 to 0.5 psi. Temperature readings were obtained from iron-constantan thermocouples with a Symplytrol meter read-out (maximum error of 5°F).

3. Procedure for Oil Tests

Prior to the running of each test, the oil was heated to 200°F and allowed to de-gas under a vacuum for 2 to 4 hours. The test loop pump motor was started and the oil was allowed to circulate in a by-pass circuit. Pressurized buffer oil was valved into the region between the two shaft seals. A vacuum was then applied to the slinger cavity and the test rig motor was started. The slinger inlet and outlet valves were then manipulated to introduce the working fluid and to establish the desired interface location and outlet pressure level. Flow of water through housing cooling passages was modulated to attain the desired temperature of the slinger oil. When visual observation of the interface indicated steady-state operation had been achieved, a photograph was taken of the interface and recordings were taken of system pressures, temperatures, and shaft speed. The motor power was then interrupted and a deceleration trace was recorded on an oscillograph. This deceleration trace, together with another deceleration trace taken with no liquid in the slinger, provided information from which power loss of the partially submerged slinger was calculated (see Appendix A for a description of the method).

The data just described was recorded for several radial engagement values and several axial clearance values for both vaned and vaneless slingers. The entire set of tests was repeated over a range of oil temperatures to permit correlation of the pumping and drag coefficients with Reynolds Number.

B. MERCURY SLINGER TESTS

1. Mercury Test Rig

The Mercury Slinger Test Rig is shown in Figure 13 and Figure 14. A 2.0-in.-dia smooth slinger was mounted on a shaft supported by two grease-lubricated bearings. The bearing housing was constructed from 300 series stainless steel and contained a cooling annulus on the motor side. The stainless-steel test section housing also contained a cooling annulus and had provisions in the slinger face area to accept a transparent quartz insert. The insert permitted viewing of the slinger interface. The test section housing was attached to the bearing housing by a mating thread. With this arrangement, the test section housing could be rotated to change the slinger axial clearance without disassembling the machine. Flexible flow and instrument lines were to be provided on the test section to allow such adjustments.

The test cavity was isolated from the bearing cavity by three segmented carbon shaft seals. Liquid mercury was circulated between the two seals nearest the test cavity, and a vacuum was drawn in the cavity formed by the second

and third seals. Instrument penetrations included interface cavity vacuum, outlet temperature and pressure, and buffer seal outlet temperature. The test rig was driven by a 400-cycle, 3-phase, 20,000-rpm motor. The speed was reduced to 12,000 rpm by controlling the frequency of the power supply.

A schematic of the loop used for mercury slinger tests is shown in Figure 15. A photograph with the test rig in place is shown in Figure 16. This loop was designated as LMS-1. Instrumentation provided in the loop included seal rig inlet temperature and pressure, seal rig inlet flow orifice (Δp), mercury supply tank pressure, buffer seal inlet pressure, buffer seal inlet and outlet temperature, and shaft speed. Pressure transducers in conjunction with L&N Recorders were used for all pressure measurements. The accuracy of this combination was $\pm 2\%$ of the reading. All temperatures were obtained with the use of copper constantan thermocouples in conjunction with a Brown recorder. Temperature measurement accuracy was $\pm 2\%$ of the reading.

Shaft speed was obtained with the use of an induction speed pickup and a Hewlett-Packard counter. Speed is also monitored by a strobotac.

2. Procedure for Mercury Tests

The test procedures for a typical test are as follows: Cooling water was introduced to the test section cooling annulus and the motor side cooling annulus. One of the buffer seal tanks was pressurized with N_2 and flow was established from one buffer seal tank, through the test rig buffer seal area to the second buffer seal tank. Instruments were checked for zero readings and the vacuum pump was turned on. The power source was adjusted to provide the correct motor input corresponding to a desired speed. The drive motor was then turned on and the speed checked with the strobotac. The speed was adjusted where necessary. A "dry" deceleration was then taken for later use in determining the test rig friction hp loss. The "dry" deceleration procedure consists of switching the drive motor off and recording the resultant deceleration transient on an oscillograph. The signal to the oscillograph was generated by a magnetic speed pickup. The drive motor was then restarted. The slinger cavity and the aft seal cavity was evacuated to 1 mm or lower. Next the mercury supply tank was pressurized to roughly the desired slinger outlet pressure and the test rig charge valve was opened. This charged the slinger cavity with mercury. The resulting slinger discharge pressure was observed and the mercury supply tank pressure was adjusted as necessary to trim it to the desired level. Data for the static flow condition was then taken and a photograph of the liquid-vapor interface was obtained. A "wet" deceleration was then taken in the manner previously described. The interface region was studied in order to detect any leakage from the interface region.

IV. RESULTS

A. OIL SLINGER TESTS

1. Interface Stability

a. Vaneless Slinger

The interfaces obtained with vaneless slingers were found to be considerably smoother than those obtained with vaned slingers. It is

therefore quite fortunate that, during the course of the slinger program, SNAP-8 system considerations permitted reduction of the slinger discharge pressure from the original requirement of 15 psia to 5 psia. This reduction in pumping requirement allowed replacement of vaned slingers with vaneless slingers. As a result, the interface of the oil seal-to-space is relatively smooth and stable.

Figures 17, 18, and 19 show the interfaces obtained with a 2.5-in.-dia vaneless slinger turning at 12,000 rpm. The fluid is ET-378 oil and the axial clearance values range from 0.011 to 0.062 in. The pictures show considerable variation in interface smoothness with axial clearance. The interface obtained with an 0.011-in. axial clearance (Figure 17) is very smooth. The interfaces obtained with clearances of 0.031 in. (Figure 18) and 0.062 in. (Figure 19) are considerably more turbulent. Possibly the presence of an excessive amount of dissolved air in the ET-378 oil somewhat aggravated the liquid-vapor interfaces of Figures 18 and 19. Nevertheless, it is clear that an important change in the character of the interface occurs as axial clearance is increased from 0.011 to 0.031 in. Accordingly, the axial clearance of the seal-to-space slingers in the SNAP-8 rotating assemblies has been held to a minimum practical value (i.e., 0.010 to 0.020 in.).

The pictures reveal the presence of a liquid film on the static face within the interface radius. The thickness and mobility of this film appear to be proportionate to the axial clearance. During the operating condition shown in Figure 17, the film was hardly noticeable. It was quite evident at larger axial clearances, however. Since the slinger shaft was horizontally oriented, the force of gravity was sufficient to cause a noticeable movement of the film away from the interface (in the upper portion of the slinger) and into the interface (in the lower portion of the slinger). The nature of this movement is illustrated in Figure 20.

The presence of a liquid film within the slinger interface radius is extremely significant. The primary function of the slinger in the seal-to-space concept is to provide a positive demarcation between liquid and vapor (i.e., to provide a barrier past which liquid cannot flow). Possibly the film observed in the slinger tests would remain immobile in a zero-g environment. It also appears unlikely that even a mobile slinger film could penetrate the scavenging action of the adjacent close-clearance molecular pump (Figure 1). This later contention is born out by the low oil leakage rates measured in tests of the Model A Seal Simulator (see Volume IV of this report). Nevertheless, it is quite clear that this problem would not exist if the slinger had a non-wetting liquid-surface combination. No such film is observed in the mercury slinger tests reported in Section IV,B.

Figure 21 illustrates how a non-wetting liquid-surface combination prevents formation of a liquid film on the static wall. There it is seen that the surface tension force is the only force tending to prevent the momentum force from forming a liquid film on the static wall; the surface tension force acts in opposition to the momentum force only in the presence of a non-wetting liquid-surface combination. Thus, it appears that the liquid film could be eliminated or diminished by coating the slinger walls with a non-wetting

material such as Teflon. Additional slinger tests, with a coating of Dow Corning Silicon Vacuum Grease on the transparent static wall, revealed the effectiveness of a non-wetting surface. Subsequently, such a film of Teflon was specified for oil slinger walls of the space seals in the SNAP-8 power conversion system rotating assemblies.

b. Vaned Slingers

Since the system requirements of the SNAP-8 rotating assemblies permitted use of vaneless slingers, the data obtained for vaned slingers was ultimately found to have no direct application to SNAP-8. Nevertheless, a brief discussion of the interfaces observed for vaned slingers is presented below.

Figure 22 shows a 2.5-in.-dia shrouded 12-vane slinger operating at 12,000 rpm. The axial clearance is 0.011 in. The interface is seen to be very turbulent, although its appearance is somewhat aggravated by the fact that the oil was not well degassed and the interface vacuum caused formation of a bubble-like froth in the vicinity of the interface. Adequate de-gassing procedures had not been developed at the time of this test. Nevertheless, it is evident that the interface is considerably more turbulent than is desired for use as a seal-to-space.

The oil film within the central unvaned section was relatively immobile and essentially trapped since the action of the vanes tended to prevent it from joining the fluid at the slinger periphery. No tests were conducted with a non-wetting coating on the static wall. It is not known just what improvement might be obtained by such means.

The reasons for covering the vane tips with a shroud are illustrated in Figure 23. There the interface resulting from a test of an unshrouded vaned slinger is shown. In such tests, severe vibration and increased drag were observed when the radial engagement between the vanes and the liquid was small. Pictures such as the one shown in Figure 23 revealed a pronounced interaction between the vane tips and the liquid, which caused a wedge-shaped wake behind each slinger tip. Since the vibration and energy loss appeared to be caused by flow across the tips of the vanes, it was reasoned that addition of a rim at the outer diameter of the slinger would significantly alter the flow pattern. This proved indeed to be the case. The vibration disappeared and the power loss was reduced to two-thirds of its previous value. The shroud was adopted for all subsequent vaned slinger tests.

2. Pumping Coefficients

Figures 24 through 29 show the pumping coefficients obtained for vaneless and for vaned slingers. Each curve sheet shows the influence of engagement ratio and Reynolds Number. Separate curve sheets are presented for each of three axial clearances. The results show the pumping coefficients to be essentially unaffected by Reynolds Number. The influence of engagement ratio on pumping coefficient is small. A small decrease in pumping coefficient at high engagement ratio is observed for vaneless slingers. The exact opposite trend

seems to hold true for vaned slingers, but again the effect is small. Increased axial clearance causes a decrease in pumping coefficient for vaneless slingers whereas, for the range of clearances tested, increased clearance improves the pumping coefficient for the vaned slinger. All of these effects are small, however. In general, it is clear that pumping coefficients are 0.4 to 0.5 for vaneless slingers and 0.9 to 1.0 for vaned slingers.

3. Drag Coefficients

Figures 30 through 35 show the drag coefficients obtained for vaneless and vaned slingers. The curves for both vaneless and vaned slingers show a small increase in drag as axial clearance increases from 0.011 to 0.062 in. The small negative slope of the curves is in general agreement with the data reported for completely submerged disks by Daily and Nece (References 2, 3, and 4).

The data from the pumping and drag curves were used to calculate power loss of the oil slingers for the SNAP-8 Turbine-Alternator Assembly and Mercury Pump Motor Assembly. The TAA uses Size 208 anti-friction bearings and rotates at 12,000 rpm while the Hg PMA uses Size 207 bearings and rotates at 7800 rpm. The resulting power loss values are presented in Figures 36 and 37. For an average oil temperature of 250°F, the power loss per slinger for the TAA and Hg PMA is 0.67 hp and 0.15 hp, respectively (for 5 psia return pressure). It is interesting to note what the power requirement would have been had vaned slingers been required. The power loss data of Figures 38 and 39 show a power requirement of 1.30 hp for each TAA slinger and 0.375 hp for each Hg PMA slinger (for 15 psia return pressure). Thus the vaneless slinger offers a considerable power saving in addition to the superior liquid-vapor interface characteristic discussed earlier.

B. MERCURY SLINGER TESTS

1. Interface Stability

The mercury slinger tests were not nearly as broad in scope as the oil slinger tests. No generalized plots of pumping and drag coefficients were obtained. Instead, all attention was directed at interface behavior and pumping performance at specific SNAP-8 operating conditions. The greatest attention was given to the question of interface stability.

Figures 40, 41, and 42 show mercury slinger liquid-vapor interfaces at running conditions duplicating those of the turbine seal-to-space (i.e., 2-in. OD disk, 12,000 rpm, with an applied pressure of 20 psia). A vacuum was applied to the interface cavity. Three axial clearance values were investigated: 0.010, 0.018, and 0.025 in. The 20-psi applied pressure causes an engagement of only 0.080 in. with the slinger, so the liquid-vapor interface is located very near the OD of the slinger. A slot in the transparent end plate located just below the interface tends to obscure the view of the interface. The nature of this slot, included for the purpose of introducing a cold mercury through flow, is illustrated by Figure 43. Figures 40, 41, and 42 represent conditions with no through flow, however.

The interface is distinguished best in Figures 41 and 42. It is seen to be generally smooth and stable in nature. In each case, however, a small population of liquid droplets is observed within the interface radius. The diameter of these droplets appears to be proportional to the axial clearance of the slinger. The droplets were relatively immobile (they tended to wander about the interface cavity slowly and in a random manner). It is possible that these droplets were caused by an interaction between the liquid-vapor interface and the annular-slot in the transparent face plate.

The presence of these droplets raises a significant question: namely, can these liquid droplets pass through the molecular pump flow restrictor and escape through the seal as raw liquid leakage? It is quite probable that such leakage cannot occur. The liquid droplets are larger than the radial clearance within the molecular pump. Also, the molecular pump configuration should provide an effective scavenging action. Nevertheless, it was decided that modified slinger configurations should be tested in an effort to eliminate the generation of liquid droplets.

The configuration illustrated in Figure 44 provided a stable interface which also generated no liquid droplets. This configuration was tested with a transparent face plate and demonstrated that the droplets were eliminated. A microflash photograph taken during this demonstration is shown in Figure 45. There it is seen that the interface cavity is clear of droplets. The droplets visible in the center were trapped in the shaft hub cavity during startup of the test. Mercury visible at a larger radius is liquid which seeped in behind a plastic ring which was pressed into the transparent face plate. The clear region between the plastic ring and the hub cavity is the significant part of the picture, since it reveals a complete absence of droplets. As a result of these tests, the slinger configuration shown in Figure 44 was incorporated into the SNAP-8 turbine seal-to-space and the Model A and Model B Seal Simulators. Successful tests of the seal simulators have confirmed the effectiveness of this mercury slinger configuration.

2. Interface Stability with Through Flow

The seal-to-space design adopted for use in the SNAP-8 turbine is the one illustrated in Figure 1 and discussed earlier in this report. The illustration is accurate in most details although it does not illustrate the modified slinger configuration discussed above. This seal configuration is the same configuration that was tested successfully in the Model B Seal Simulator. A somewhat different configuration was tested in the Model A Seal Simulator. The major difference between the two configurations is that the Model B (Figure 1) configuration uses an oil heat exchanger to cool the mercury slinger interface whereas the Model A configuration cools the interface by introducing a flow of cold (210°F) mercury at the interface. This is done in a manner similar to that illustrated in Figure 46. The purpose of the annular slot in the transparent face plate of Figure 43 was to demonstrate whether or not this method of introducing flow at the interface causes undue disturbance of the interface. The results, shown in Figure 47, revealed an instable interaction between the through flow and the interface. A smooth flow of mercury into the slinger interface was obtained only

when the flow was introduced in a radially outward direction. The configuration which permitted this is shown in Figure 48. This configuration was incorporated into the Model A Seal Simulator. Subsequent tests of the Model A Seal Simulator further demonstrated the adequacy of the method of introducing interface coolant to the slinger interface.

V. CONCLUSIONS

A. OIL SLINGERS

1. Axial clearance of the vaneless slinger in the oil seal-to-space should be small. An axial clearance no larger than 0.010 to 0.20 in. is recommended.

2. Static and dynamic surfaces adjacent to the liquid-vapor interface of the oil slinger in the seals-to-space should be coated with a 0.001 to 0.003 in. thickness of Teflon or an alternate material not wetted by ET-378 oil.

3. Slingers having a small engagement with the liquid have pumping coefficients essentially the same as those for fully submerged slingers. Pumping coefficients are sufficient to permit generation of 5 psia return pressure with fully scavenged bearing operation for SNAP-8 TAA and Hg PMA. Liquid-vapor interface will ride on outer race of adjacent bearings.

4. Slinger power consumption for SNAP-8 rotating assemblies is 0.67 hp for each TAA slinger and 0.15 hp for each Hg PMA slinger.

B. MERCURY SLINGER

1. The vaneless slinger configuration illustrated in Figure 44 gives a stable interface that provides a positive demarcation between liquid and vapor. This slinger configuration is recommended for use in the TAA seal-to-space.

2. The vaneless slinger provides pumping such that a 2-in. slinger turning at 12,000 rpm can generate 20 psi with a radial engagement of 0.080 to 0.100 in.

3. Influence of axial clearance on the slinger interface is not critical. However, it should be kept less than 0.025 in. since this was the largest value tested.

REFERENCES

1. Dynamic Shaft Seals in Space, Quarterly Report No. 5, Contract AF 33(657)-8469, General Electric, Missile and Space Division, Cincinnati, Ohio.

2. Roughness and Chamber Dimension Effects on Induced Flow and Frictional Resistance of Enclosed Rotating Disks, MIT Hydrodynamics Laboratory Technical Report 27, May 1958.

3. J. W. Daily and R. E. Nece, "Chamber Dimension Effects on Induced Flow and Frictional Resistance of Enclosed Rotating Disks," ASME Journal of Basic Engineering, March 1960, p. 217.

4. R. E. Nece and J. W. Daily, "Roughness Effects on Frictional Resistance of Enclosed Rotating Disks," ASME Journal of Basic Engineering, Sept. 1960, p. 553.

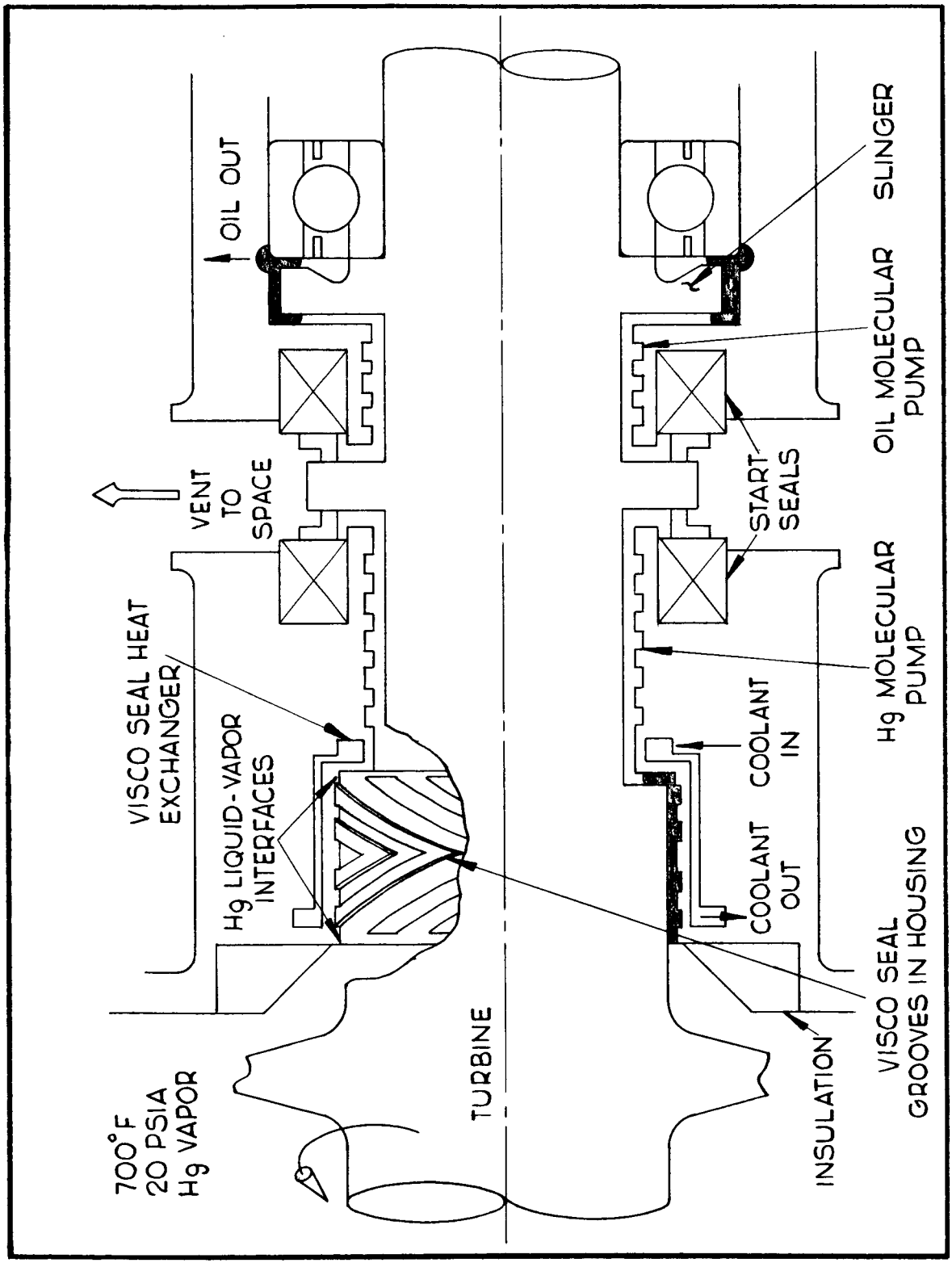

Seal Configuration for Model B Seal Simulator

Figure 1

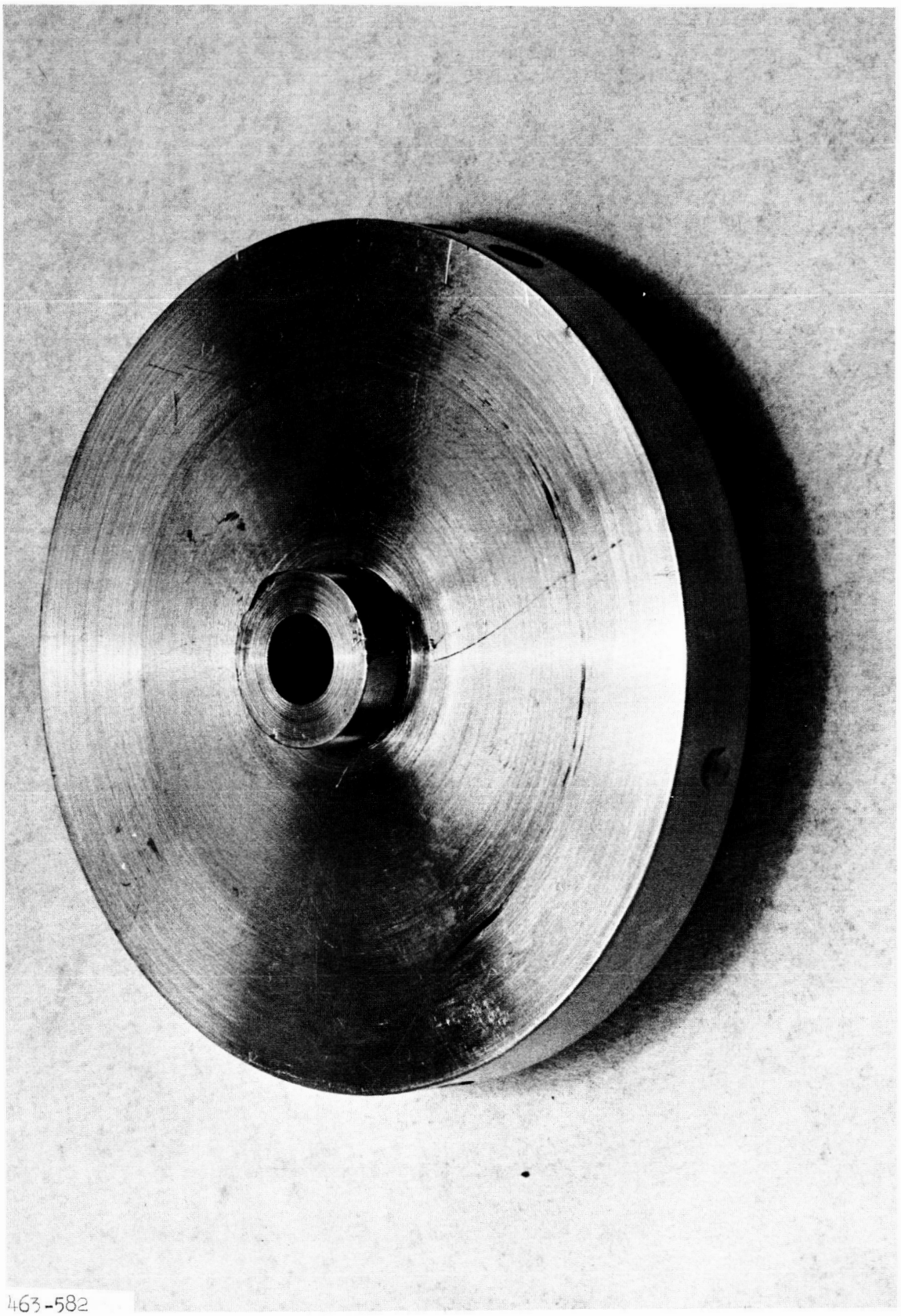

Vaneless Dynamic Seal - Slinger Seal Test

Figure 2

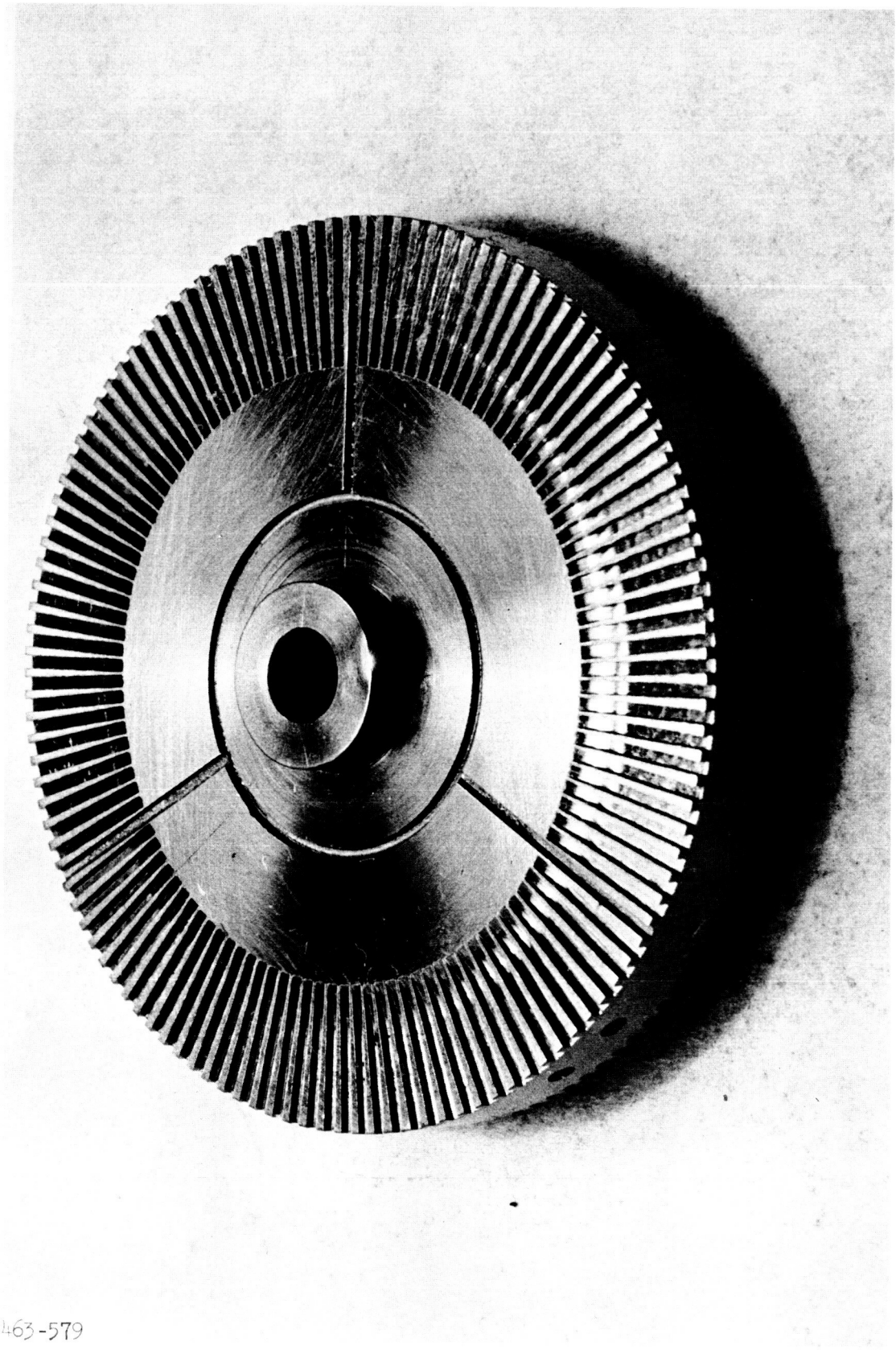

463-579

120-Vane Dynamic Seal - Slinger Seal Test

Figure 3

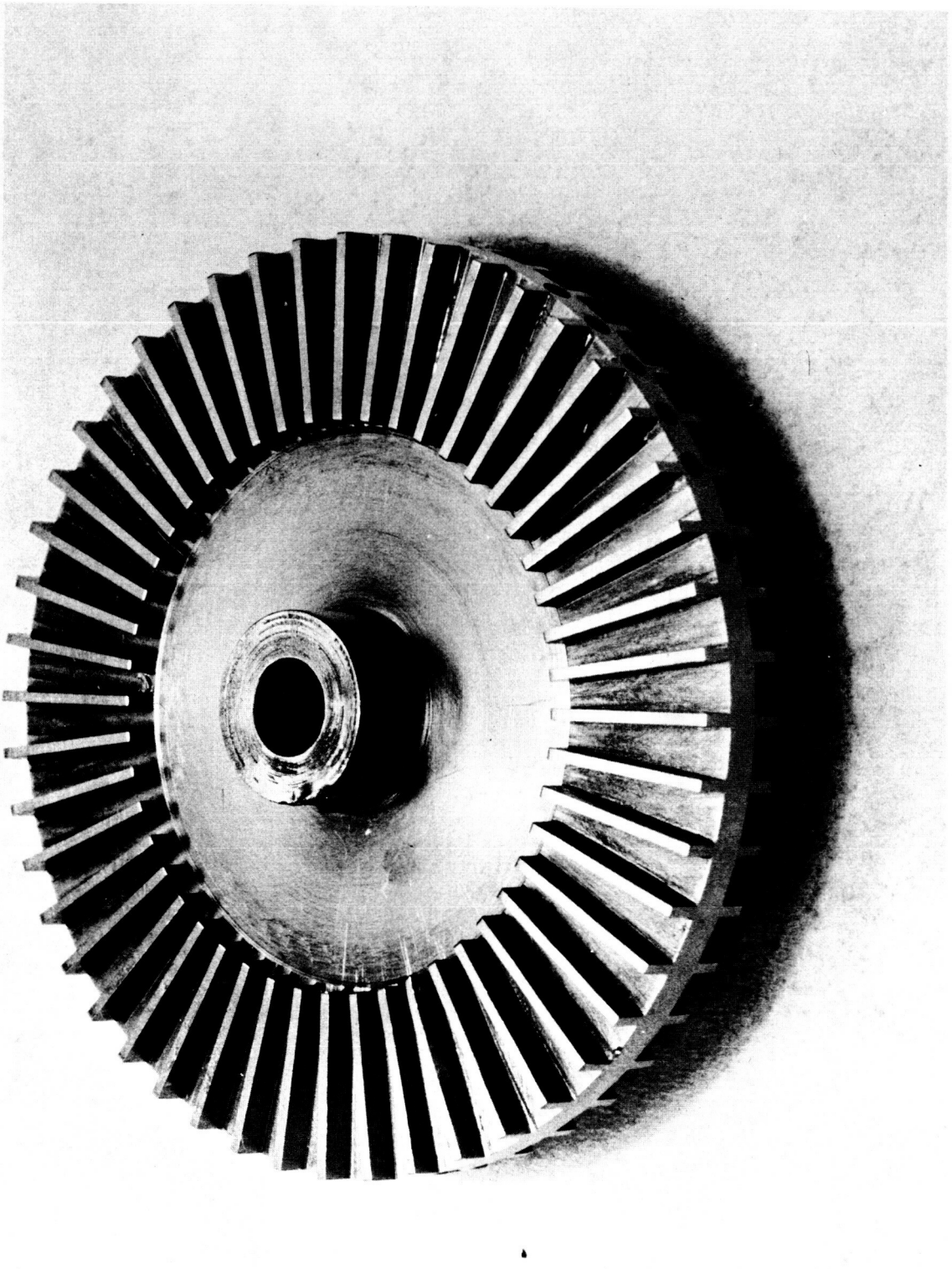

48-Vane Dynamic Seal - Slinger Seal Test

463-580

Figure 4

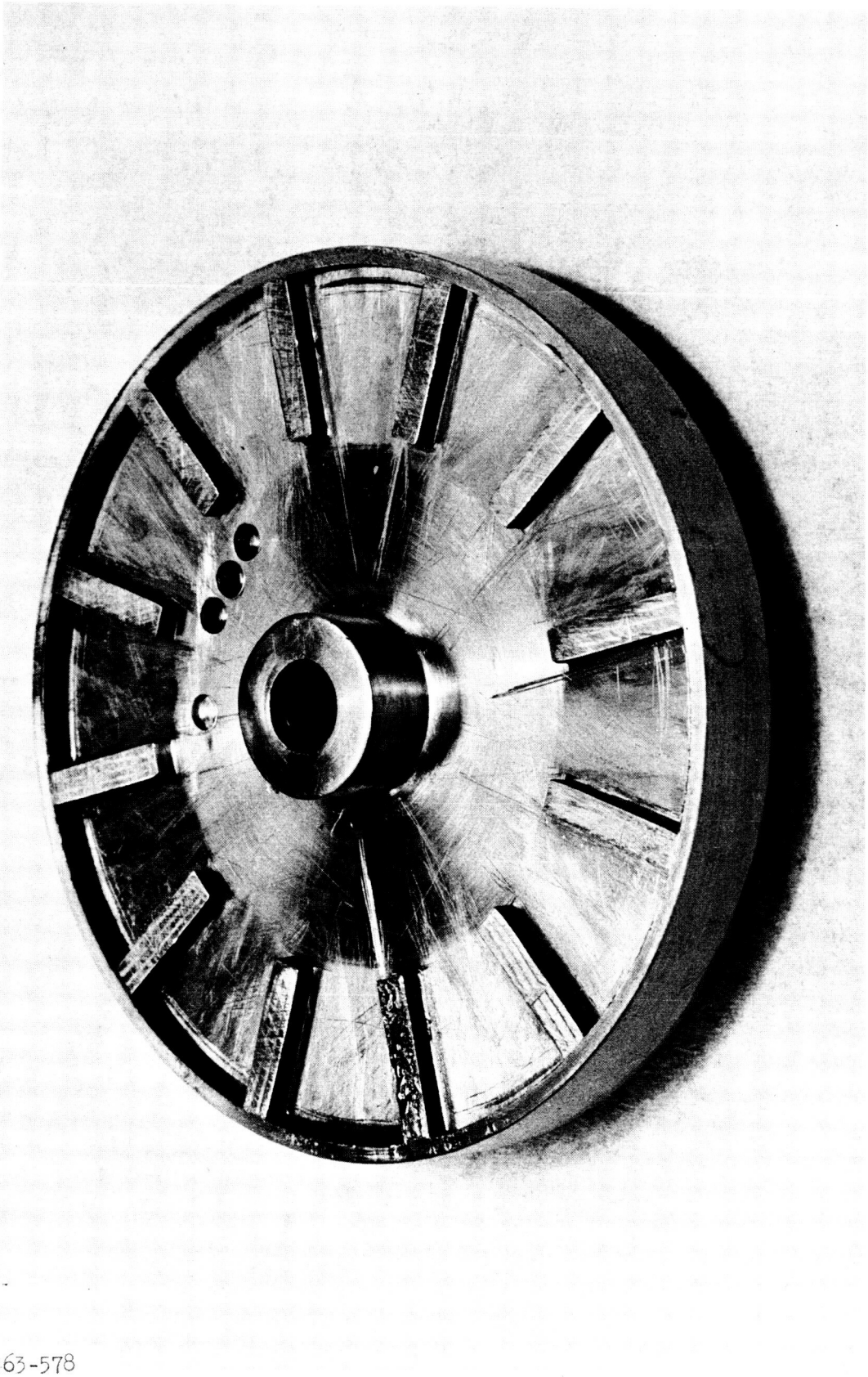

12-Vane, Shrouded Dynamic Seal - Slinger Seal Test

463-578

Figure 5

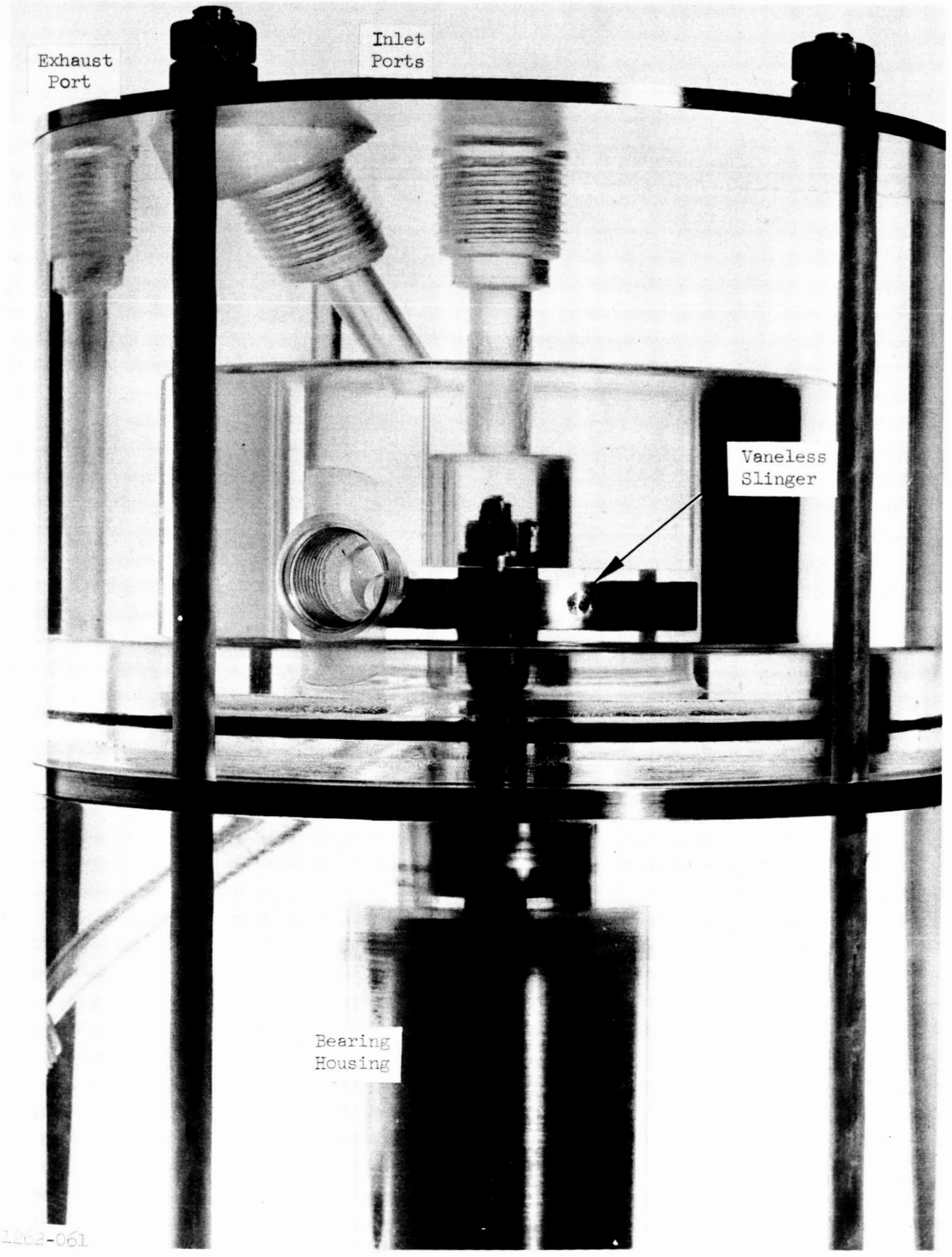

Slinger Seal Test Model

Figure 6

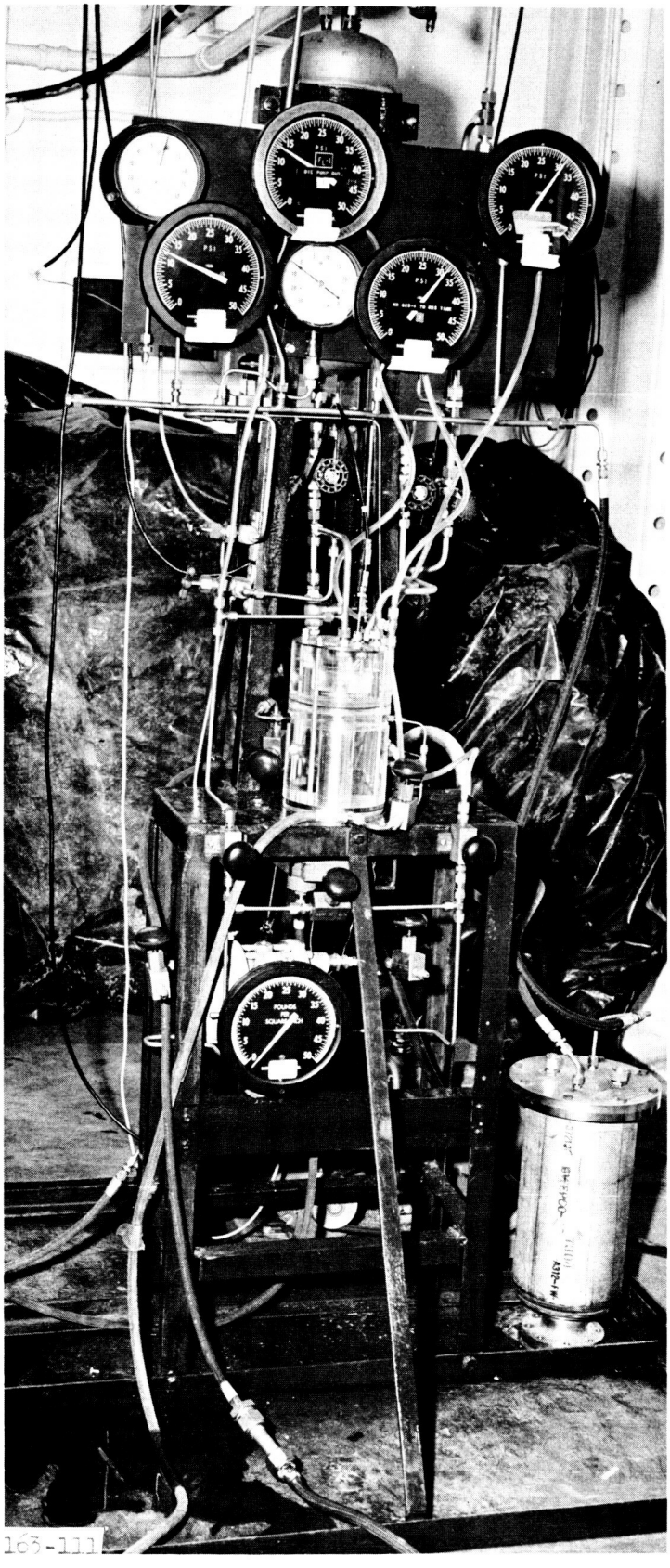

LWL-3 Slinger Seal Test Loop

Figure 7

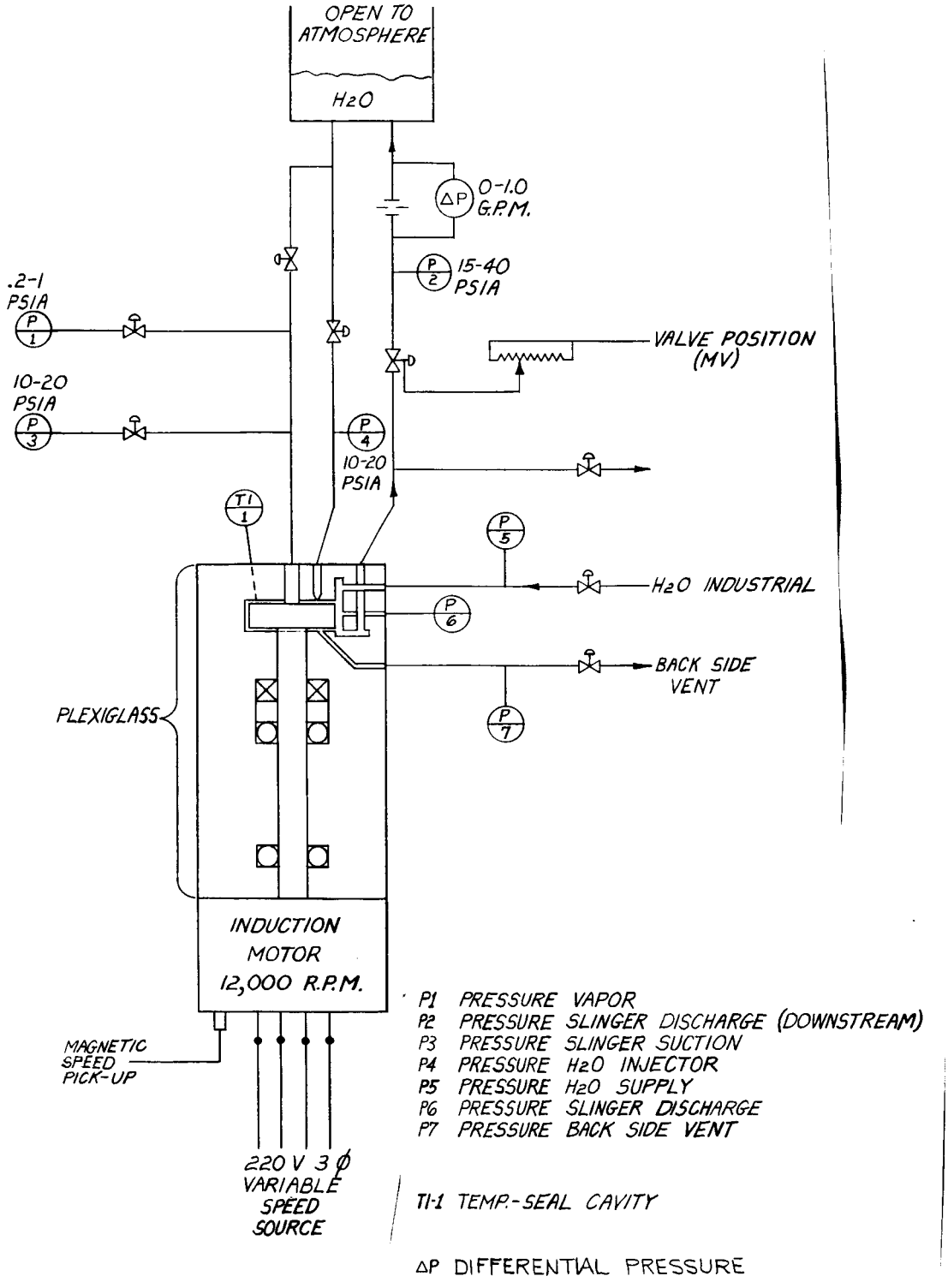

Dynamic Seal, LWL-3 P and I Diagram, Water

Figure 8

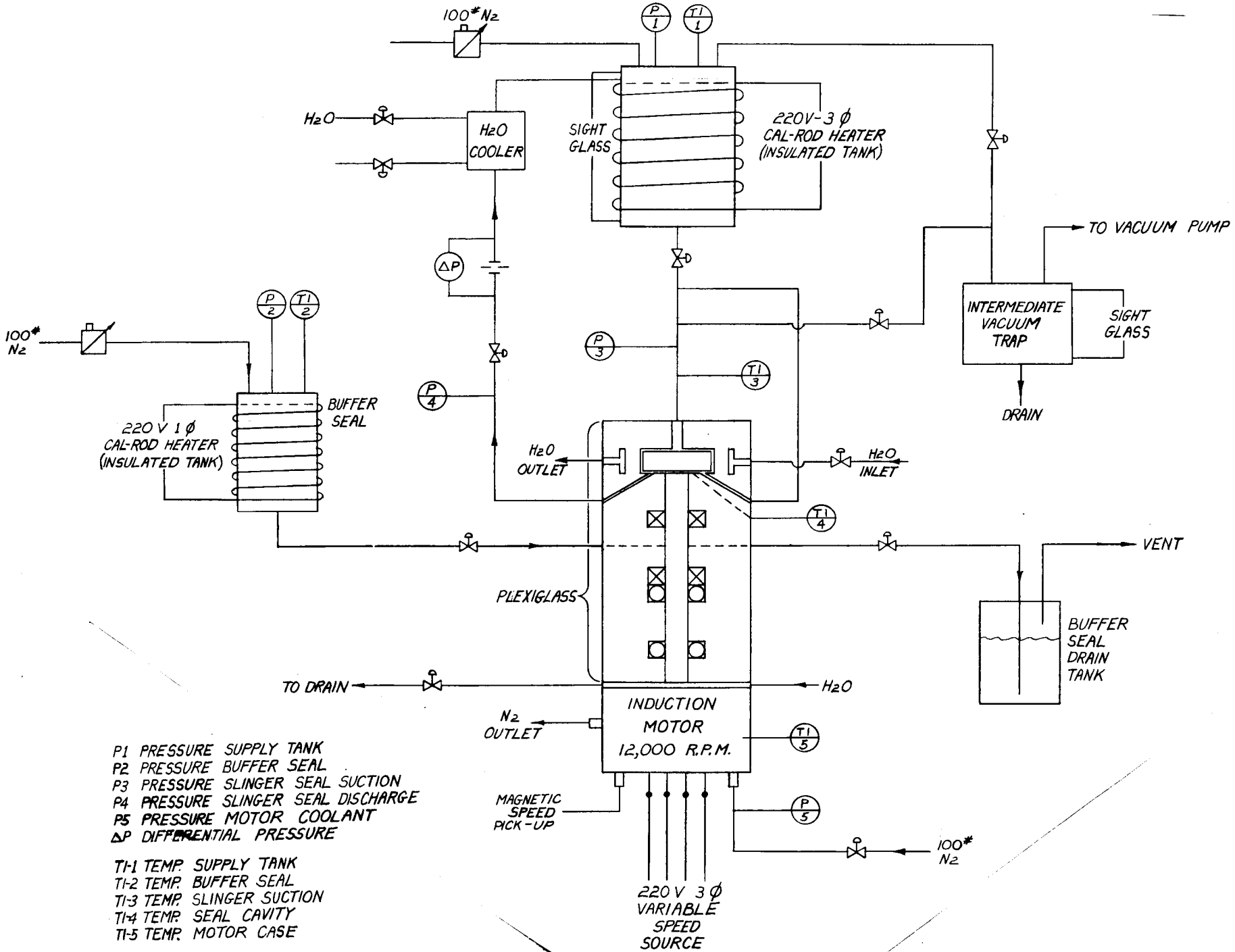

Dynamic Seal, LOS-1 P and I Diagram, OS-124 Oil

Figure 9

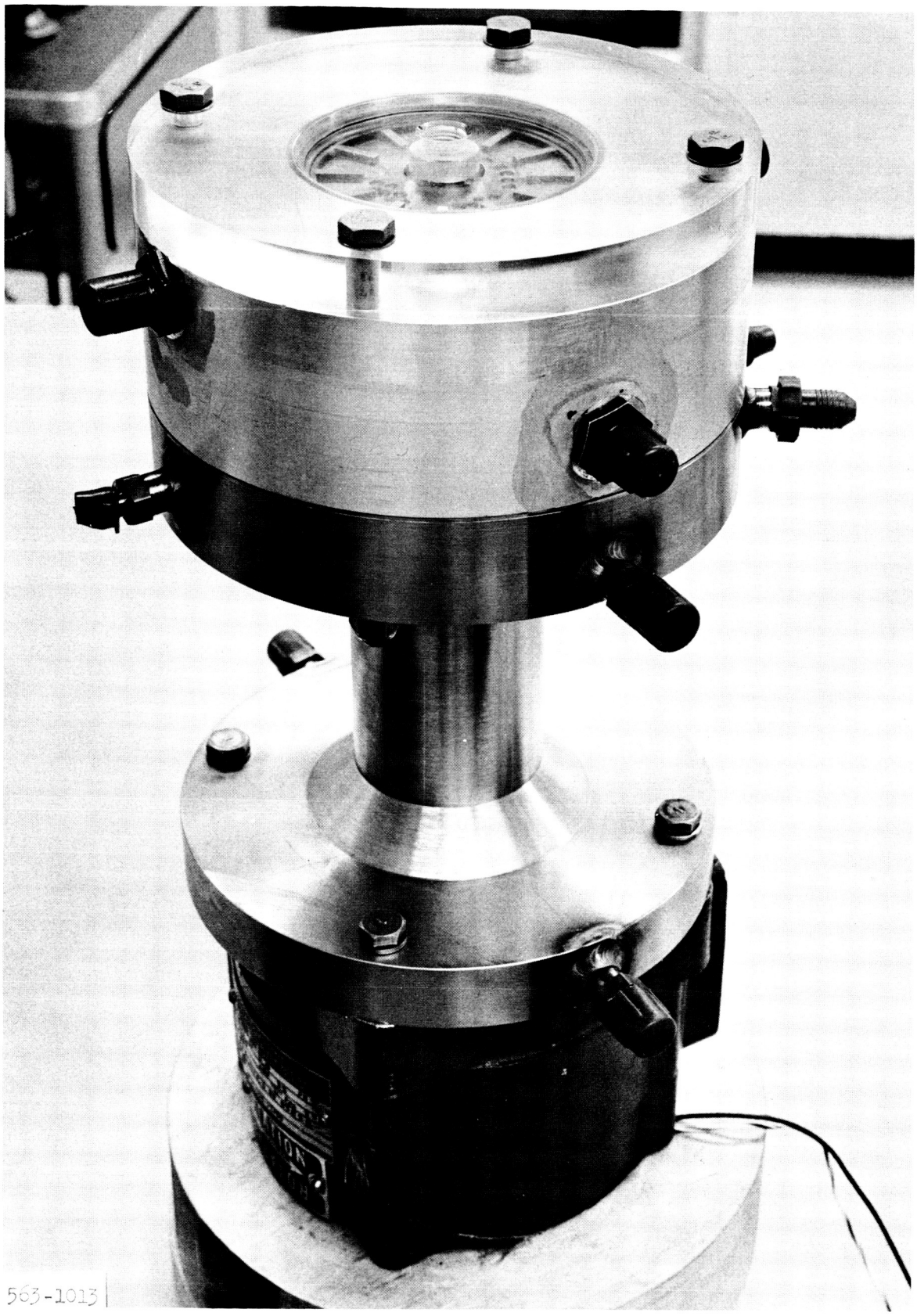

Oil Slinger Test Rig

Figure 10

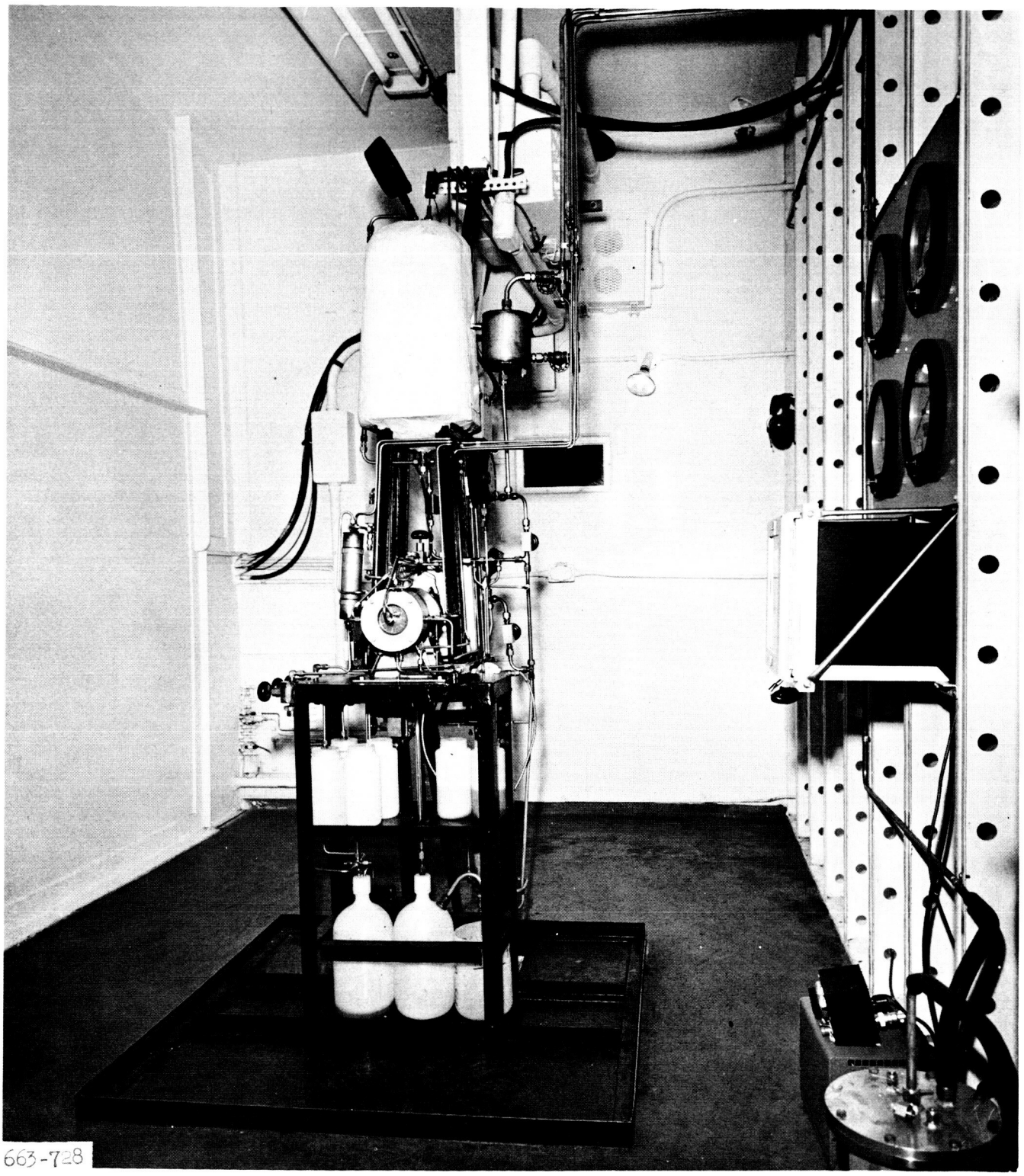

LOS-1 Test Loop

Figure 11

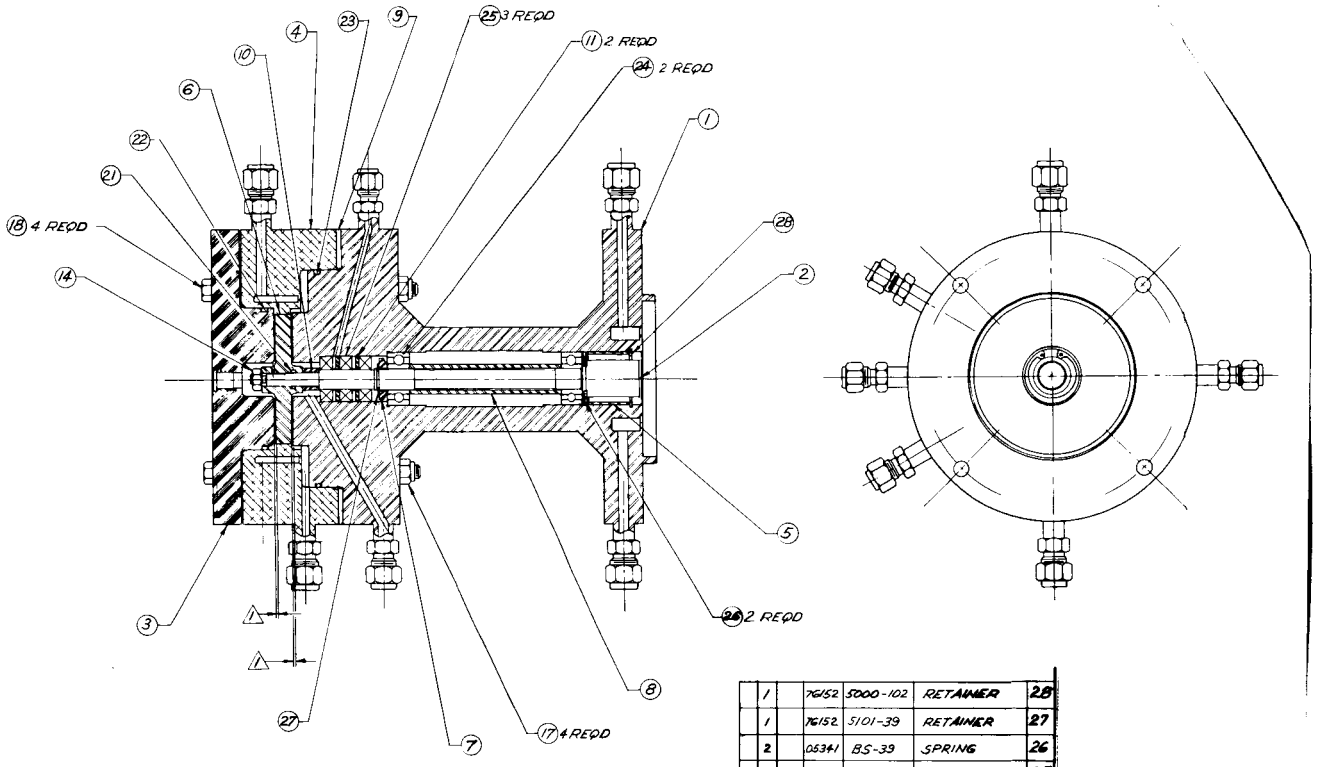

	1		76152	5000-102	RETAINER	28
	1		76152	5101-39	RETAINER	27
	2		05341	BS-39	SPRING	26
	3		71890	B103006	SEAL	25
	2		70854	100SS7X1K5	BEARING	24
	1		83259	2-155-77-545	O-RING	23
	1		83259	2-145-77-545	O-RING	22
	1		83259	2-10-77-545	O-RING	21
						20
						19
	4			MS35308-22	SCREW	18
	4			MS21044-C4	NUT	17
						16
						15
	1			AN320C3	NUT	14
						13
						12
	2			090376-1	SPACER	11
	1			090375-1	SPACER	10
	1			090374-1	SHIM	9
	1			090373-1	SPACER	8
	1			090372-1	RETAINER	7
	1			090371-1	SLINGER ASSY	6
	1			090370-1	SPACER	5
	1			090369-1	HOUSING ASSY	4
	1			090368-1	END CAP	3
	1			090367-1	SHAFT	2
	1			090366-1	HOUSING ASSY	1
QTY. REQD	✓	SYM	CODE IDENT NO.	PART OR IDENTIFYING NO.	NOMENCLATURE OR DESCRIPTION	ITEM NO.

Oil Slinger Test Rig Assembly

Figure 12

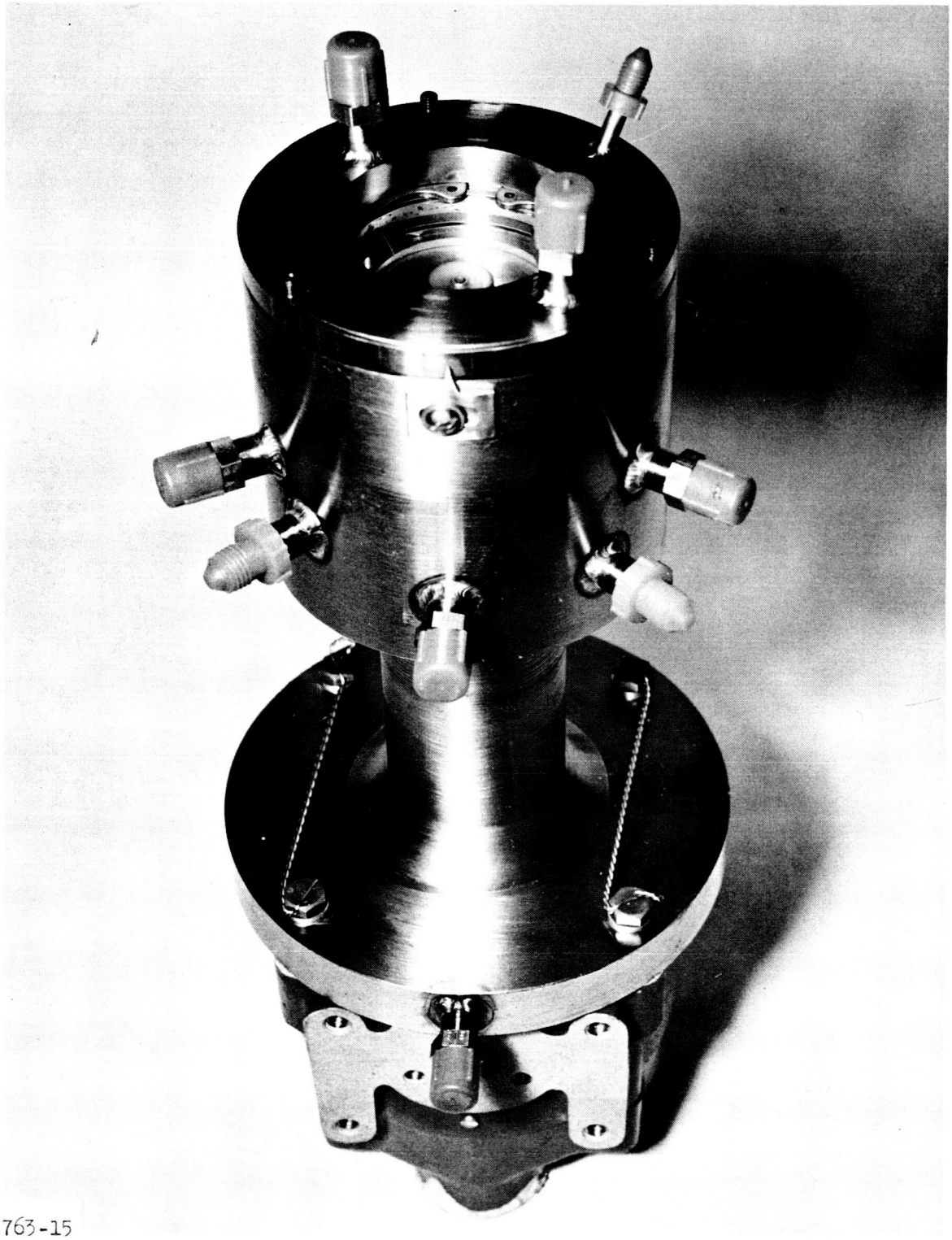

763-15

Mercury Slinger Test Rig

Figure 13

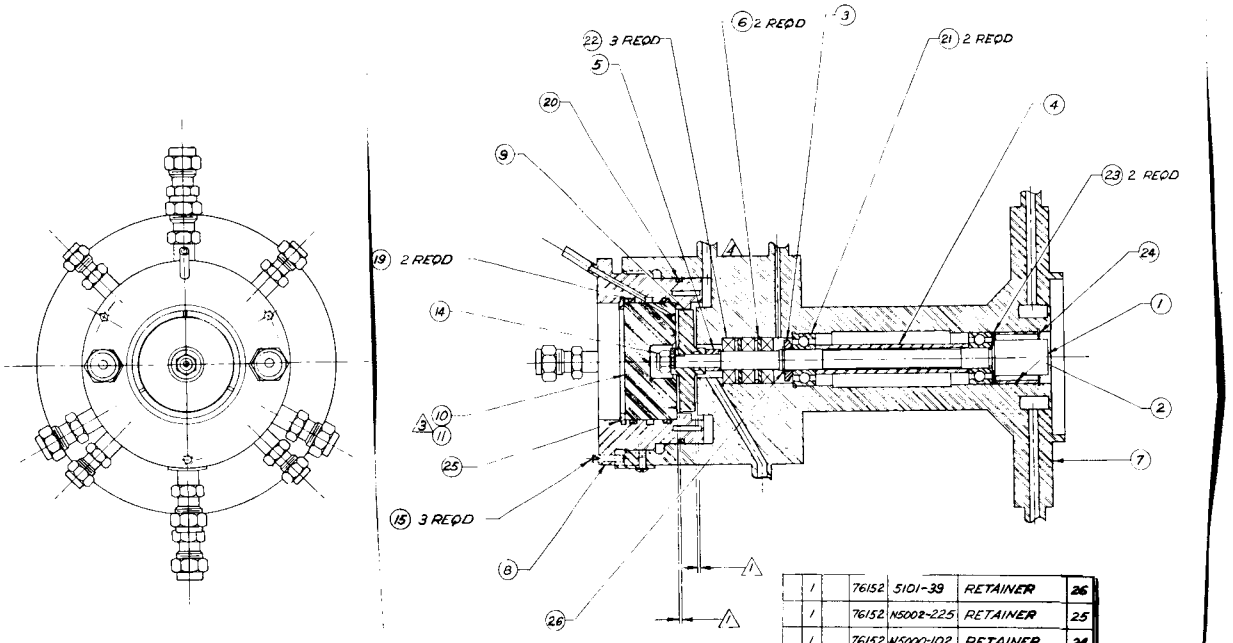

QTY REQD	SYM	CODE IDENT NO.	PART OR IDENTIFYING NO.	NOMENCLATURE OR DESCRIPTION	ITEM NO.
1		76152	5101-39	RETAINER	26
1		76152	N5002-225	RETAINER	25
1		76152	N5000-102	RETAINER	24
2		05341	BS-39	SPRING	23
3		71840	B10900G	SEAL	22
2		70854	100SSTX1K5	BEARING	21
1		83259	2-151-77-545	O-RING	20
2		83259	2-140-77-545	O-RING	19
					18
					17
					16
3			AN565 AC8H10	SET SCREW	15
1			AN363C1032	NUT	14
					13
					12
1			090787-1	END CAP	11
1			090786-1	END CAP	10
1			090785-1	SLINGER	9
1			090784-1	HOUSING ASSY	8
1			090783-1	HOUSING ASSY	7
2			090376-1	SPACER	6
1			090375-1	SPACER	5
1			090373-1	SPACER	4
1			090372-1	RETAINER	3
1			090370-1	SPACER	2
1			090367-1	SHAFT	1

Mercury Slinger Test Rig Assembly

Figure 14

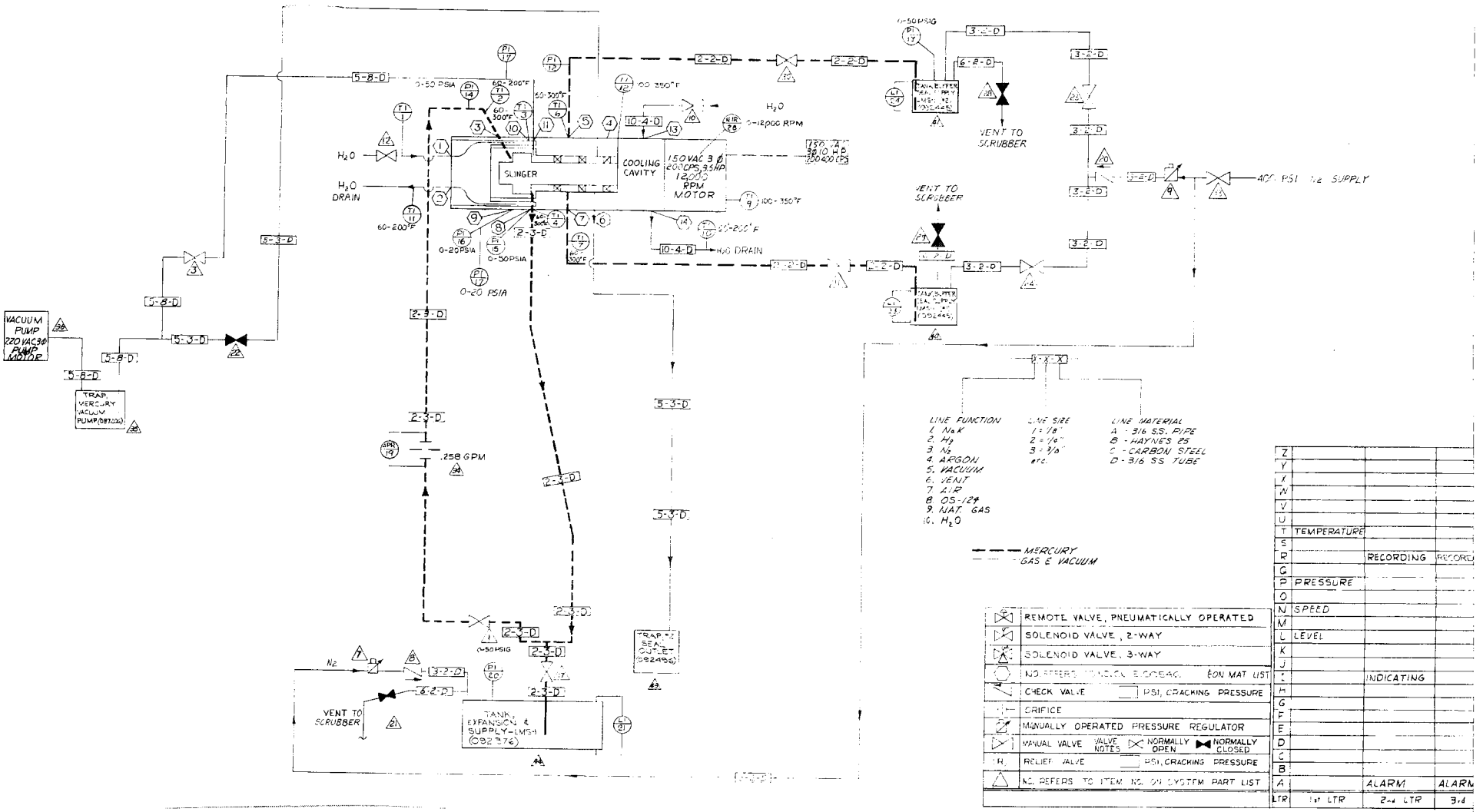

IMS-1 Instrumentation Diagram

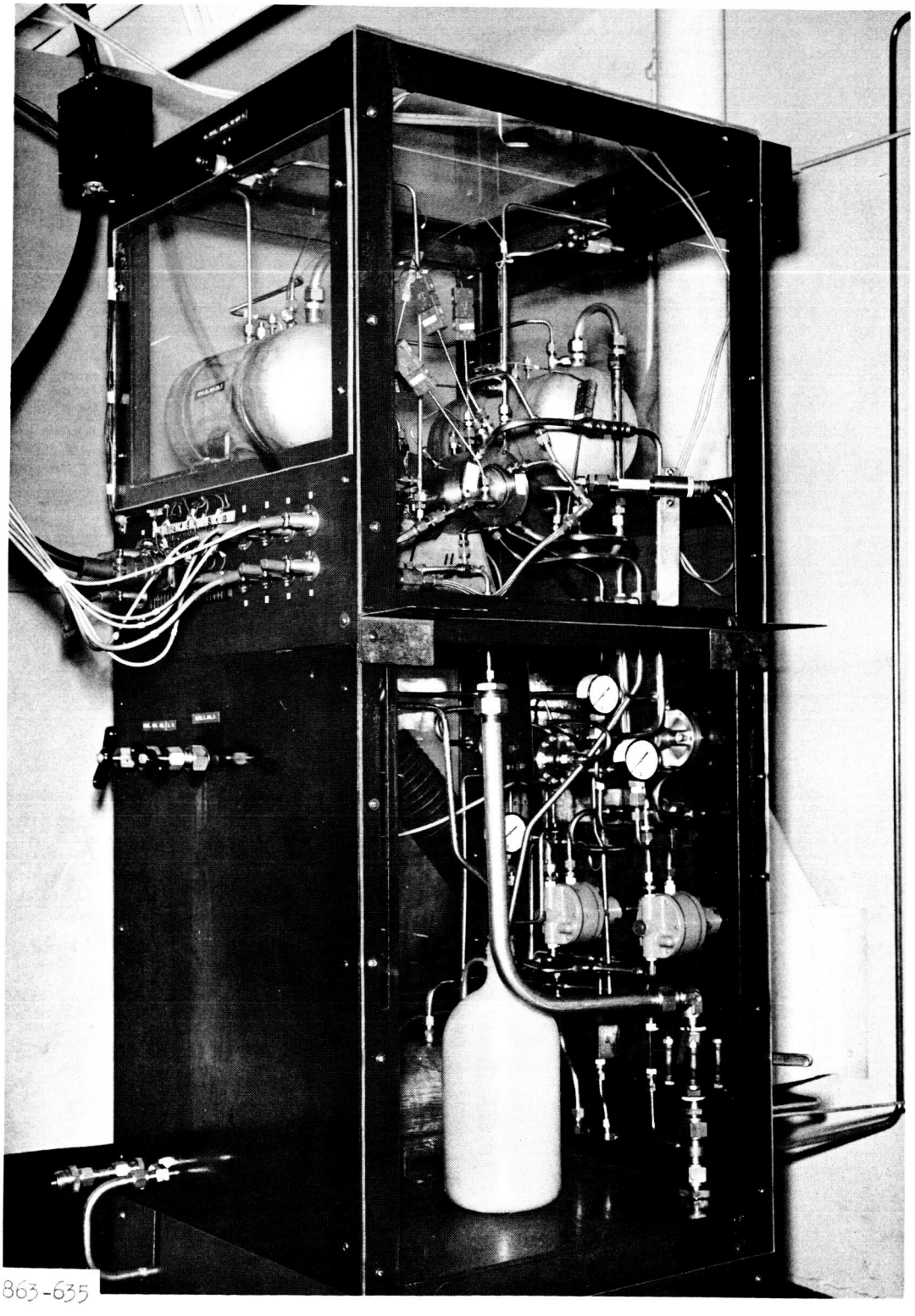

LMS-1 Test Loop

Figure 16

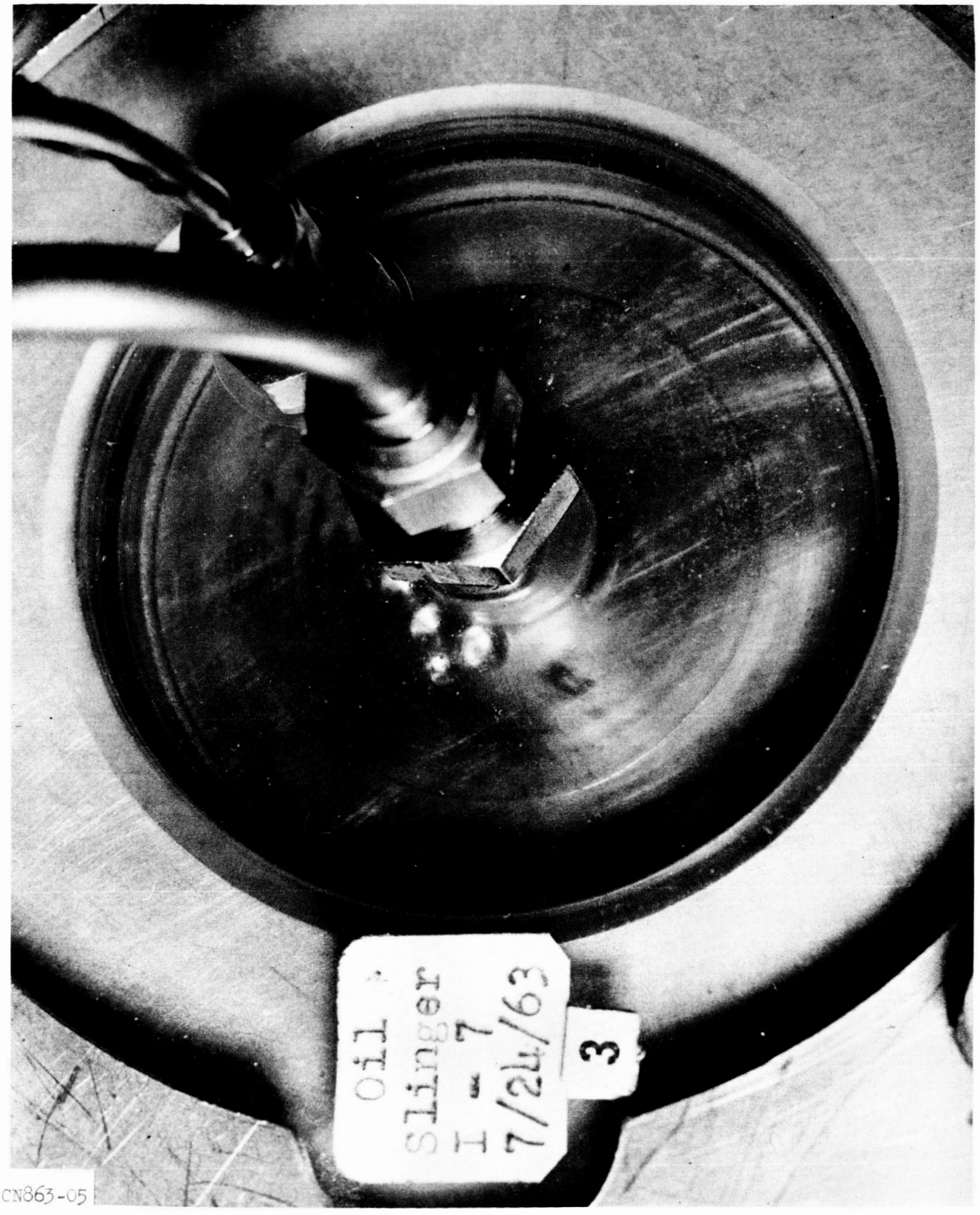

Vaneless Slinger Interface, ET-378
(12,000 rpm; 0.011 in. Axial Clearance)

Figure 17

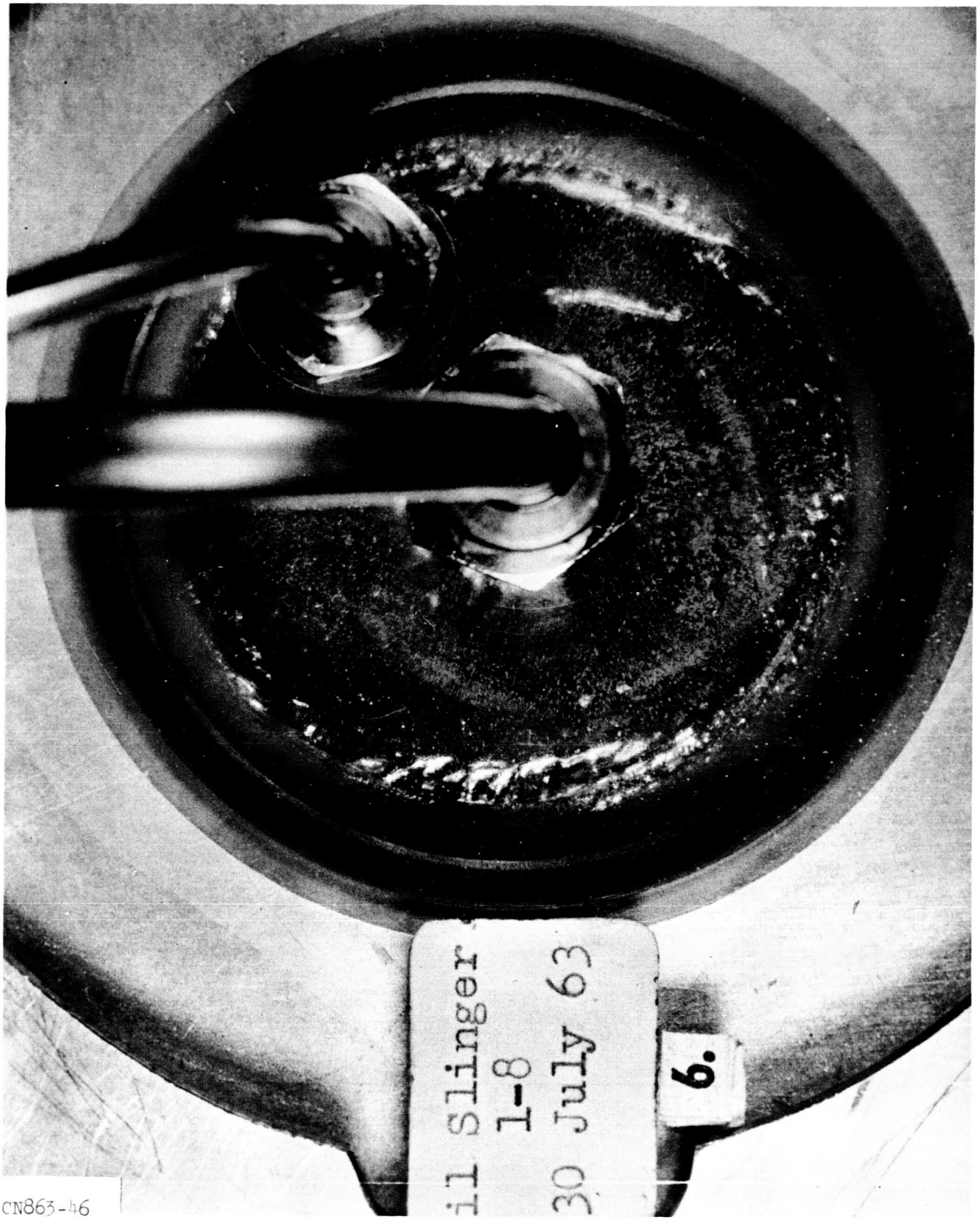

Vaneless Slinger Interface, ET-378
(12,000 rpm; 0.031 in. Axial Clearance)

Figure 18

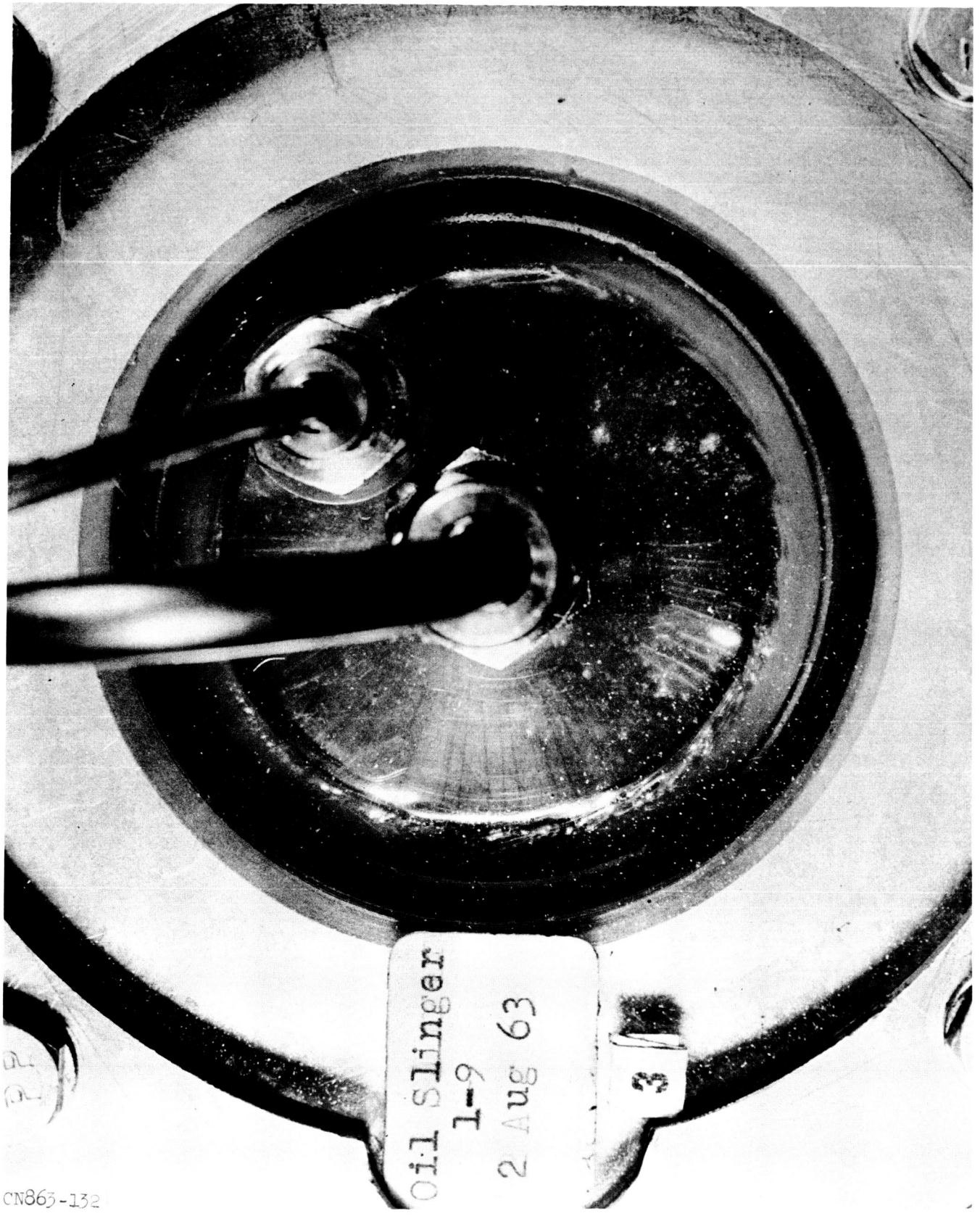

Vaneless Slinger Interface, ET-378
(12,000 rpm; 0.062 in. Axial Clearance)

Figure 19

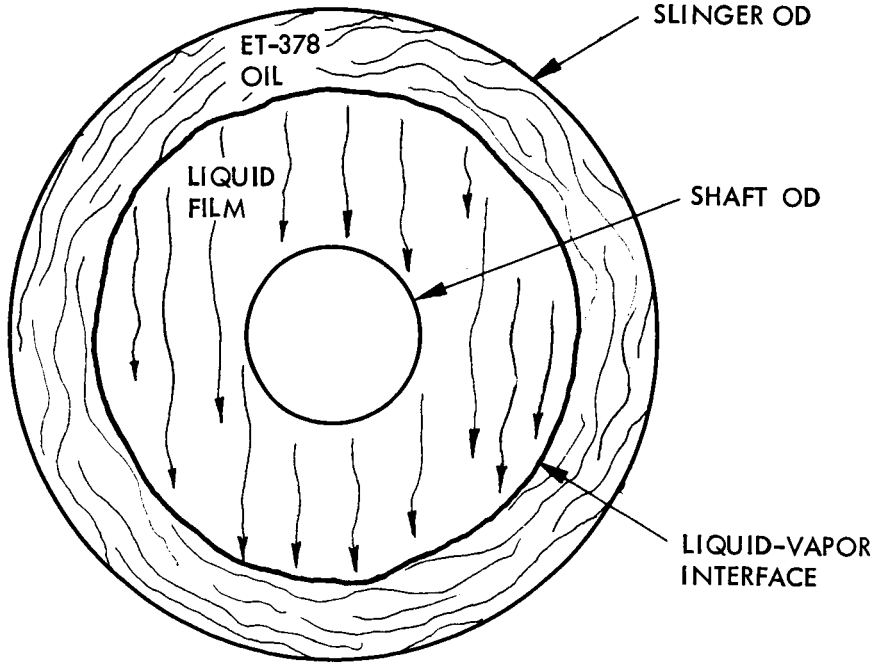

MOVEMENT OF FILM ON STATIC WALL
WITHIN SLINGER INTERFACE RADIUS
(HORIZONTALLY ORIENTED SHAFT)

10-067-115

Figure 20

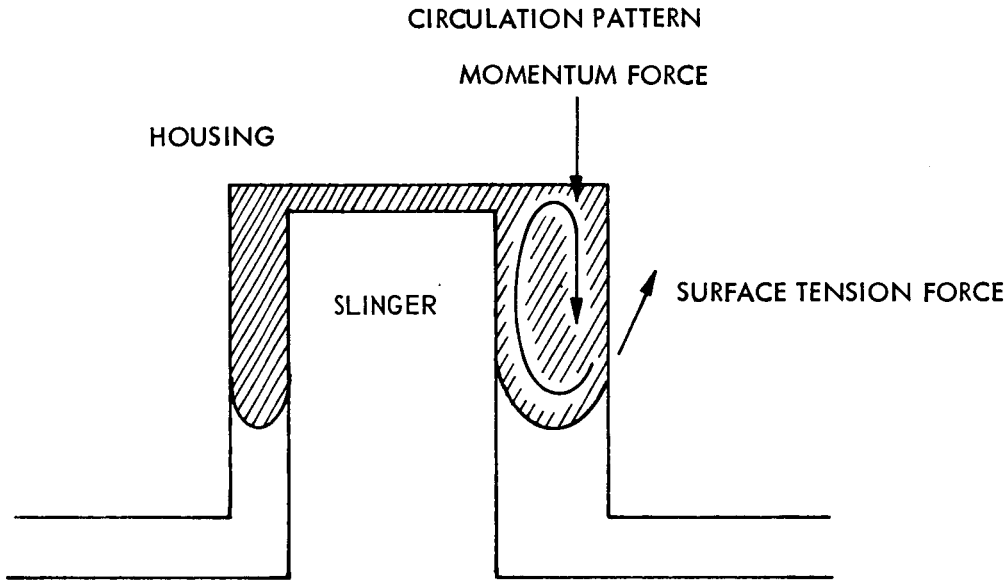

EFFECT OF NON-WETTING LIQUID-SURFACE COMBINATION ON SLINGER INTERFACE

10-067-118

Figure 21

Vaned Slinger Interface, ET-378
(12,100 rpm; 0.013 in. Axial Clearance, 12-Vane Shrouded Configuration)

Figure 22

12 Vane Slinger
½ in. long vanes
x.075 x.075
Clockwise Rotation
12,300 rpm
OS-124
.012 in. axial
clearance
P_d = 22.0 psia

P_s = 1.0 psia

T_c = 160°F

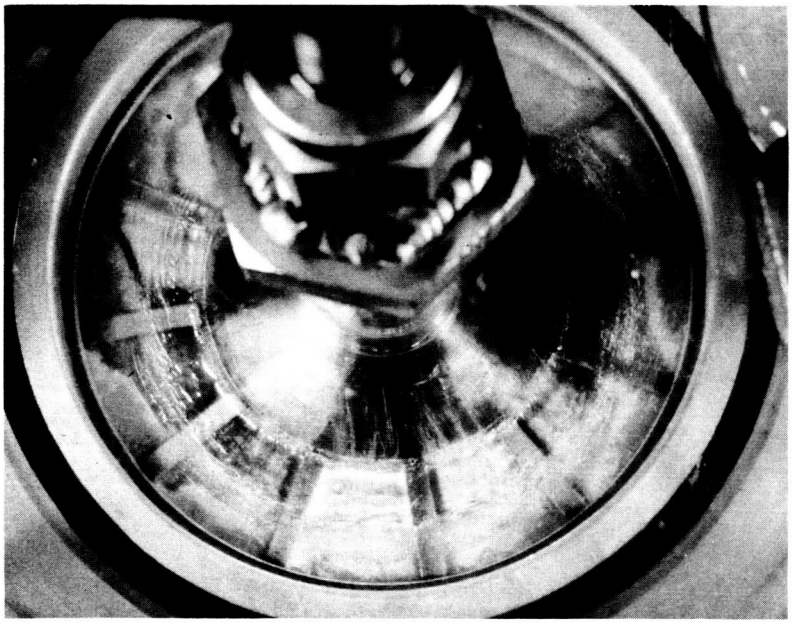

Vaned Slinger Interface, OS-124
(12,300 rpm; 0.012 in. Axial Clearance, 12-Vane Configuration Without Shroud)

Figure 23

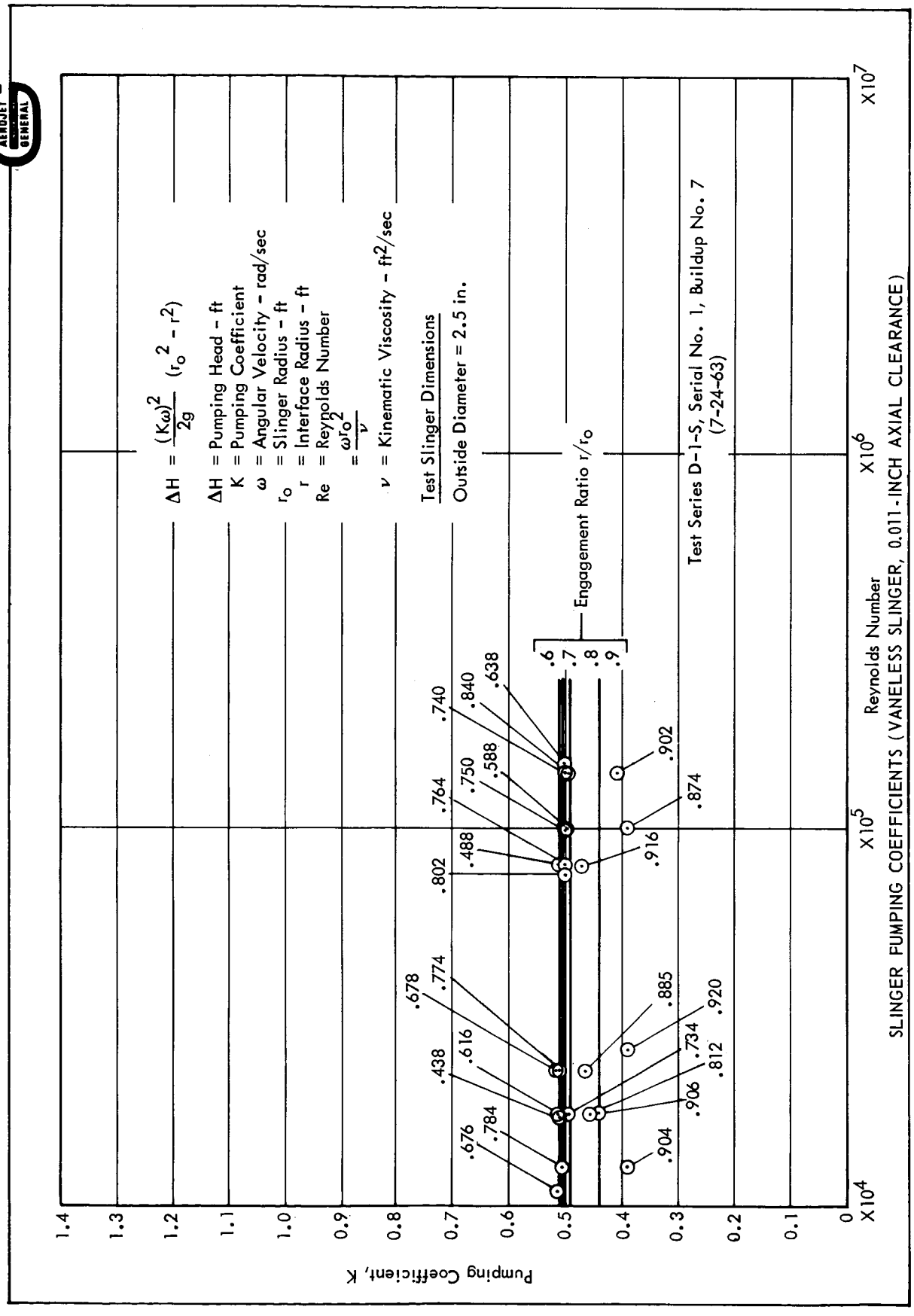
AEROJET GENERAL
SLINGER PUMPING COEFFICIENTS (VANELESS SLINGER, 0.011-INCH AXIAL CLEARANCE)
Test Series D-1-S, Serial No. 1, Buildup No. 7
(7-24-63)
Test Slinger Dimensions
Outside Diameter = 2.5 in.
ΔH = (Kω)²/2g (r_o² - r²)
ΔH = Pumping Head - ft
K = Pumping Coefficient
ω = Angular Velocity - rad/sec
r_o = Slinger Radius - ft
r = Interface Radius - ft
Re = Reynolds Number = ωr_o²/ν
ν = Kinematic Viscosity - ft²/sec
Engagement Ratio r/r_o
.6
.7
.8
.9
Pumping Coefficient, K
Reynolds Number
X10⁴
X10⁵
X10⁶
X10⁷
0
0.1
0.2
0.3
0.4
0.5
0.6
0.7
0.8
0.9
1.0
1.1
1.2
1.3
1.4
.438
.616
.676
.678
.774
.784
.802
.488
.764
.750
.588
.740
.840
.638
.902
.874
.916
.885
.920
.734
.812
.906
.904

Figure 24

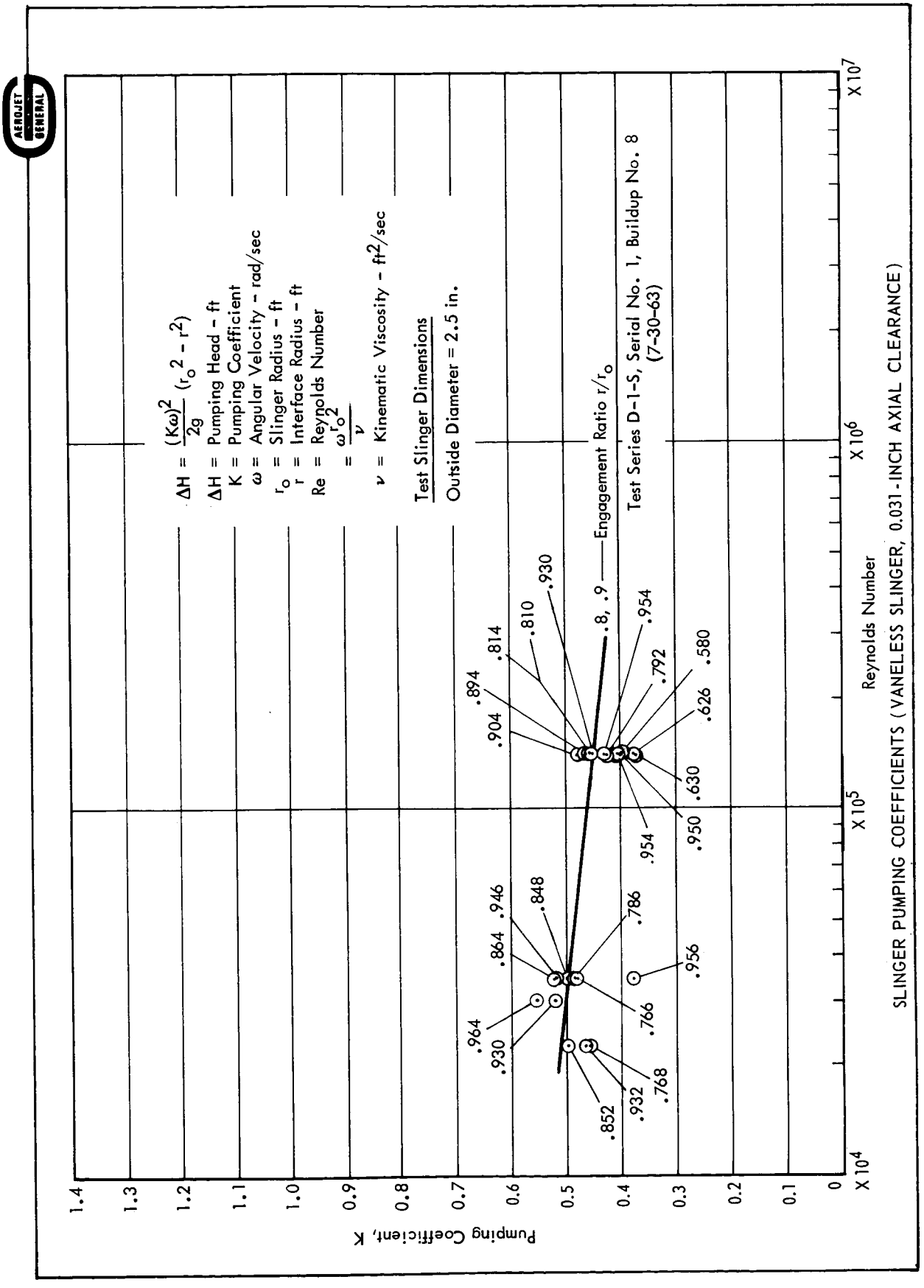
AEROJET GENERAL
$\Delta H = \frac{(K\omega)^2}{2g}(r_o^2 - r^2)$
ΔH = Pumping Head - ft
K = Pumping Coefficient
ω = Angular Velocity - rad/sec
r_o = Slinger Radius - ft
r = Interface Radius - ft
Re = Reynolds Number
$= \frac{\omega r_o^2}{\nu}$
ν = Kinematic Viscosity - ft²/sec
Test Slinger Dimensions
Outside Diameter = 2.5 in.
Test Series D-1-S, Serial No. 1, Buildup No. 8
(7-30-63)
.8, .9 — Engagement Ratio r/r_o
Pumping Coefficient, K
Reynolds Number
SLINGER PUMPING COEFFICIENTS (VANELESS SLINGER, 0.031-INCH AXIAL CLEARANCE)
1.4
1.3
1.2
1.1
1.0
0.9
0.8
0.7
0.6
0.5
0.4
0.3
0.2
0.1
0
X 10⁴
X 10⁵
X 10⁶
X 10⁷
.964
.930
.852
.932
.768
.766
.956
.786
.848
.946
.864
.954
.950
.630
.626
.580
.792
.954
.904
.894
.814
.810
.930

Figure 25

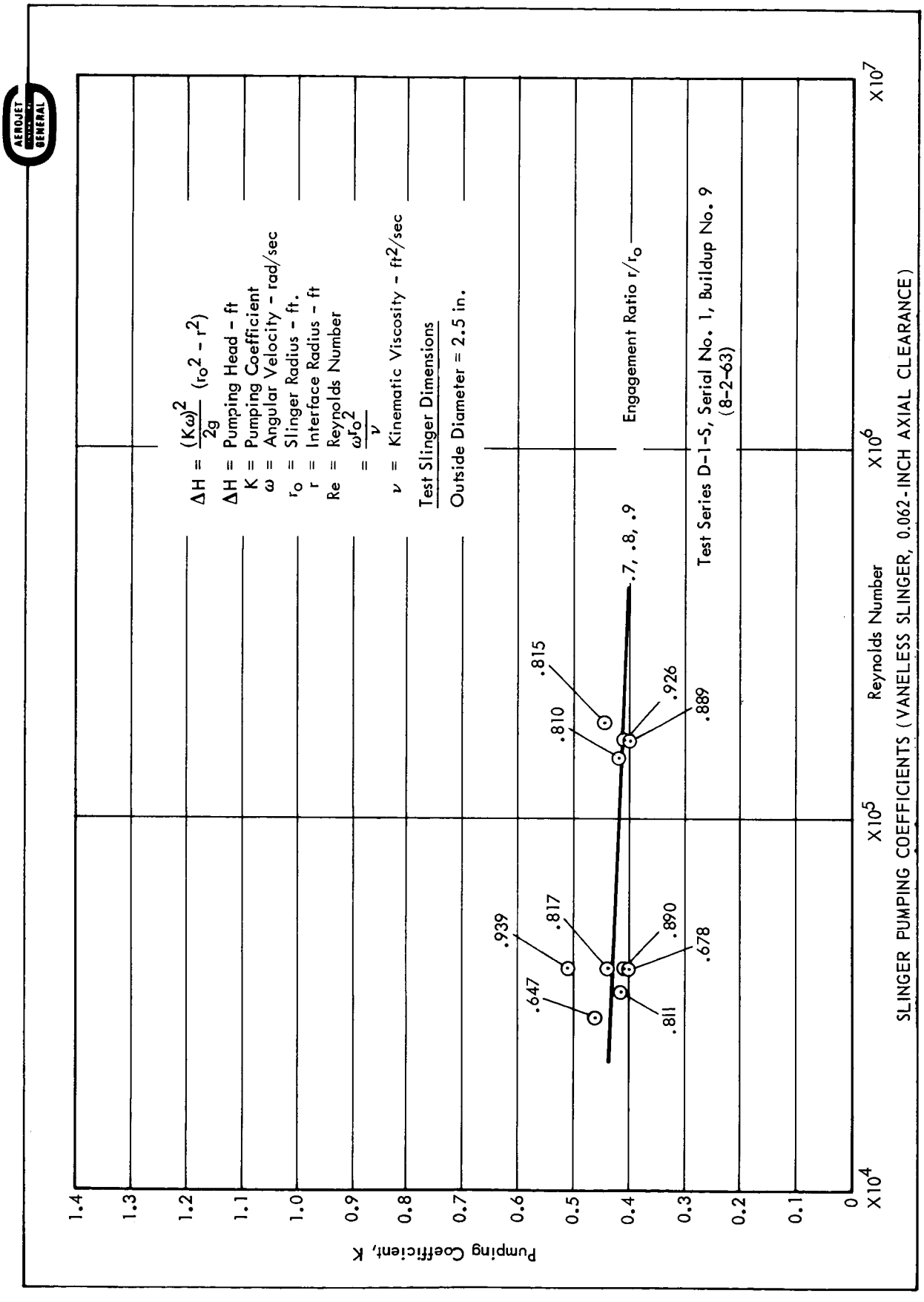
AEROJET GENERAL
SLINGER PUMPING COEFFICIENTS (VANELESS SLINGER, 0.062-INCH AXIAL CLEARANCE)
Test Series D-1-S, Serial No. 1, Buildup No. 9
(8-2-63)
Pumping Coefficient, K
Reynolds Number
Engagement Ratio r/ro
.7, .8, .9
.939
.647
.817
.815
.810
.811
.678
.890
.889
.926
ΔH = (Kω)²/2g (ro² - r²)
ΔH = Pumping Head - ft
K = Pumping Coefficient
ω = Angular Velocity - rad/sec
ro = Slinger Radius - ft.
r = Interface Radius - ft
Re = Reynolds Number
= ωro²/ν
ν = Kinematic Viscosity - ft²/sec
Test Slinger Dimensions
Outside Diameter = 2.5 in.

Figure 26

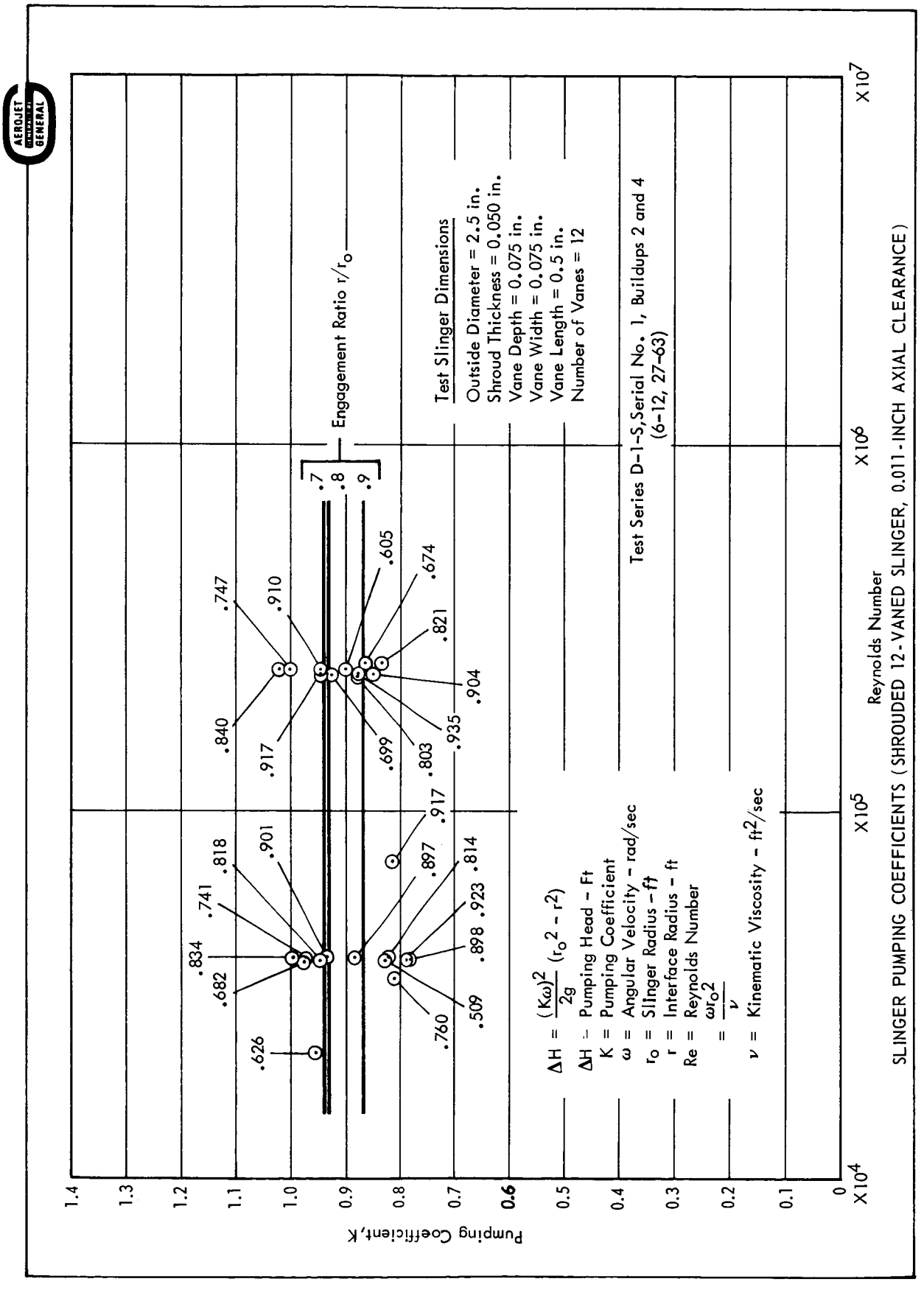
AEROJET GENERAL
SLINGER PUMPING COEFFICIENTS (SHROUDED 12-VANED SLINGER, 0.011-INCH AXIAL CLEARANCE)
Test Series D-1-S, Serial No. 1, Buildups 2 and 4 (6-12, 27-63)
Test Slinger Dimensions
Outside Diameter = 2.5 in.
Shroud Thickness = 0.050 in.
Vane Depth = 0.075 in.
Vane Width = 0.075 in.
Vane Length = 0.5 in.
Number of Vanes = 12
Engagement Ratio r/ro
.7
.8
.9
Pumping Coefficient, k
Reynolds Number
X10^4
X10^5
X10^6
X10^7
ΔH = (Kω)^2/2g (ro^2 - r^2)
ΔH = Pumping Head - Ft
K = Pumping Coefficient
ω = Angular Velocity - rad/sec
ro = Slinger Radius - ft
r = Interface Radius - ft
Re = Reynolds Number = ωro^2/ν
ν = Kinematic Viscosity - ft^2/sec

Figure 27

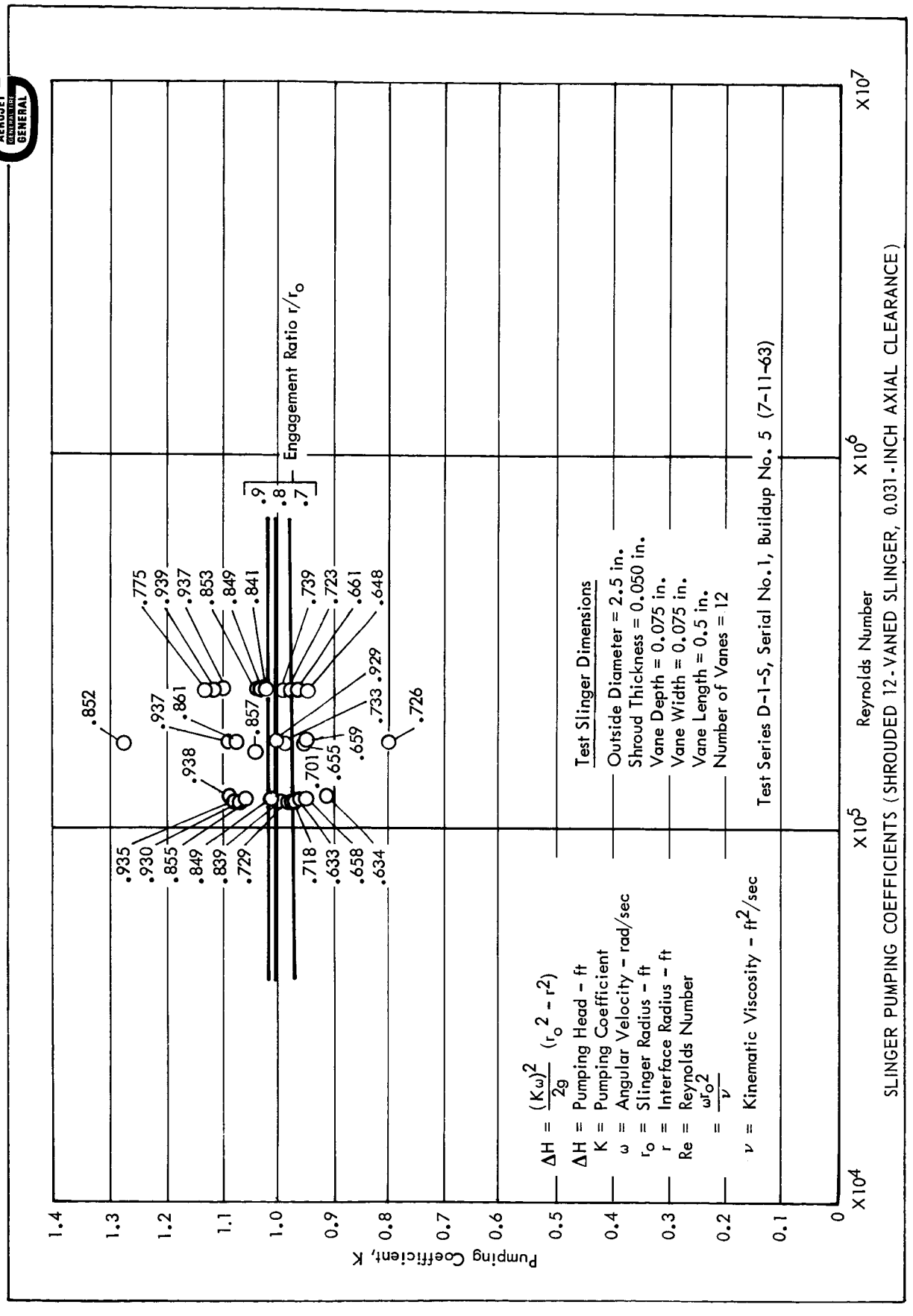
AEROJET GENERAL
Pumping Coefficient, K
Engagement Ratio r/r_o
.9
.8
.7
.852
.775
.939
.937
.853
.849
.841
.739
.723
.661
.648
.937
.861
.857
.938
.701
.655
.659
.733
.929
.726
.935
.930
.855
.849
.839
.729
.718
.633
.658
.634
ΔH = (Kω)²/2g (r_o² - r²)
ΔH = Pumping Head - ft
K = Pumping Coefficient
ω = Angular Velocity - rad/sec
r_o = Slinger Radius - ft
r = Interface Radius - ft
Re = Reynolds Number = ωr_o²/ν
ν = Kinematic Viscosity - ft²/sec
Test Slinger Dimensions
Outside Diameter = 2.5 in.
Shroud Thickness = 0.050 in.
Vane Depth = 0.075 in.
Vane Width = 0.075 in.
Vane Length = 0.5 in.
Number of Vanes = 12
Test Series D-1-S, Serial No. 1, Buildup No. 5 (7-11-63)
Reynolds Number
X10⁴
X10⁵
X10⁶
X10⁷
SLINGER PUMPING COEFFICIENTS (SHROUDED 12-VANED SLINGER, 0.031-INCH AXIAL CLEARANCE)

Figure 28

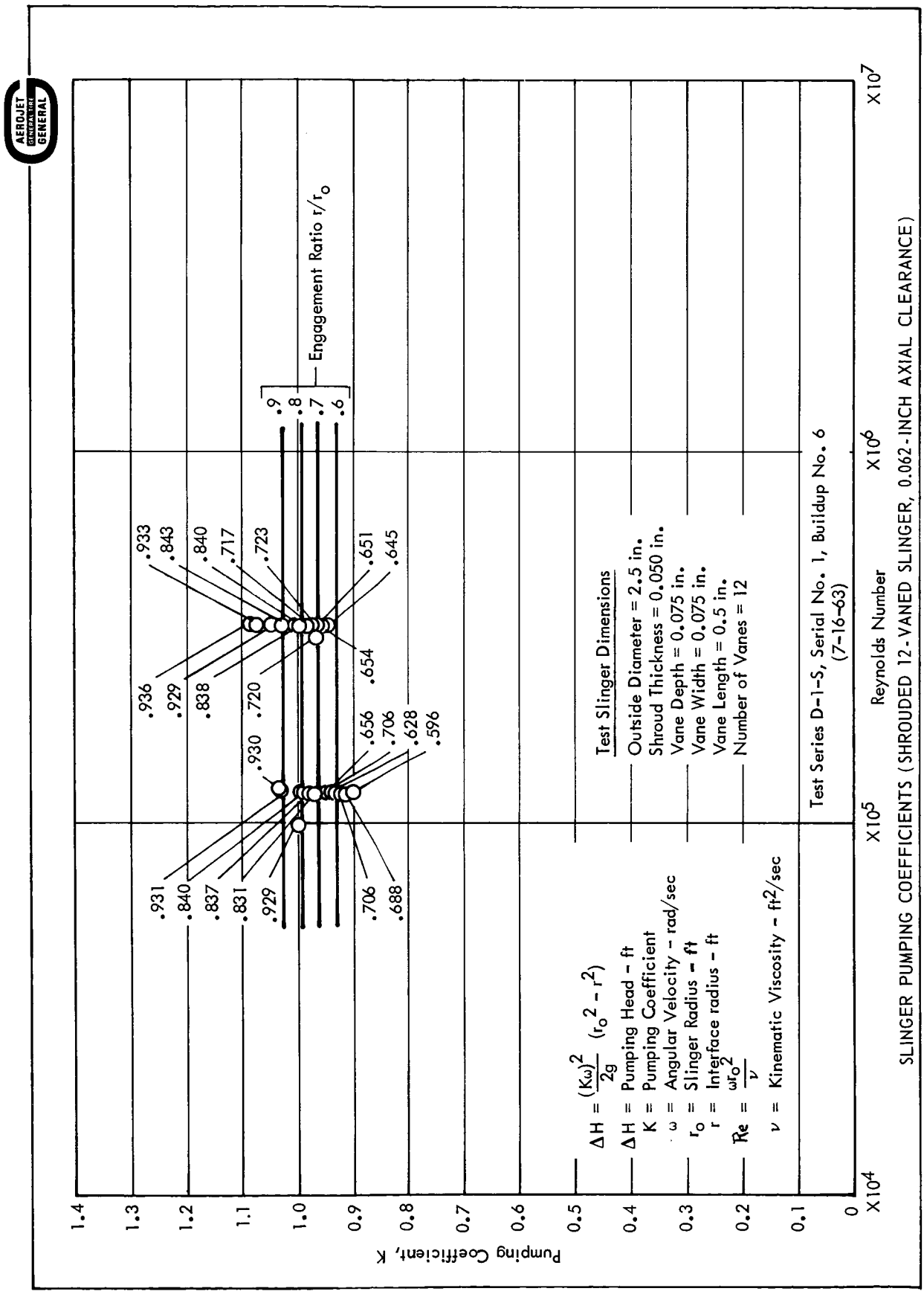
AEROJET GENERAL
SLINGER PUMPING COEFFICIENTS (SHROUDED 12-VANED SLINGER, 0.062-INCH AXIAL CLEARANCE)
Test Series D-1-S, Serial No. 1, Buildup No. 6 (7-16-63)
Pumping Coefficient, K
Reynolds Number
Engagement Ratio r/r_o
.9
.8
.7
.6
.933
.843
.840
.717
.723
.936
.929
.838
.720
.930
.651
.645
.654
.656
.706
.628
.596
.931
.840
.837
.831
.929
.706
.688
Test Slinger Dimensions
Outside Diameter = 2.5 in.
Shroud Thickness = 0.050 in.
Vane Depth = 0.075 in.
Vane Width = 0.075 in.
Vane Length = 0.5 in.
Number of Vanes = 12
ΔH = (Kω)²/2g (r_o² - r²)
ΔH = Pumping Head - ft
K = Pumping Coefficient
ω = Angular Velocity - rad/sec
r_o = Slinger Radius - ft
r = Interface radius - ft
Re = ωr_o²/ν
ν = Kinematic Viscosity - ft²/sec
1.4
1.3
1.2
1.1
1.0
0.9
0.8
0.7
0.6
0.5
0.4
0.3
0.2
0.1
0
X10⁴
X10⁵
X10⁶
X10⁷

Figure 29

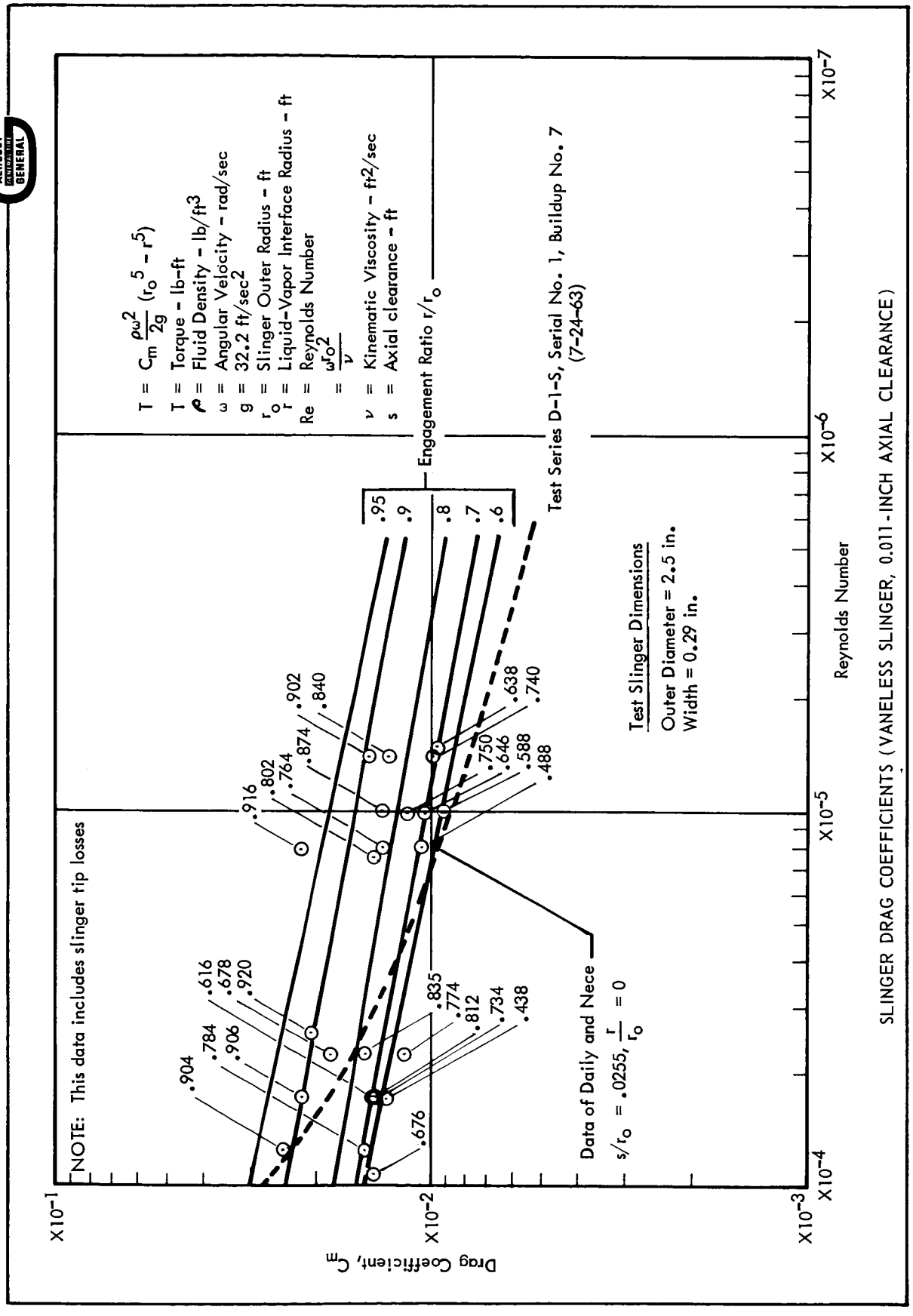
AEROJET GENERAL
SLINGER DRAG COEFFICIENTS (VANELESS SLINGER, 0.011-INCH AXIAL CLEARANCE)
Test Series D-1-S, Serial No. 1, Buildup No. 7 (7-24-63)
$T = C_m \frac{\rho\omega^2}{2g} (r_o^5 - r^5)$
T = Torque - lb-ft
ρ = Fluid Density - lb/ft³
ω = Angular Velocity - rad/sec
g = 32.2 ft/sec²
r_o = Slinger Outer Radius - ft
r = Liquid-Vapor Interface Radius - ft
Re = Reynolds Number $= \frac{\omega r_o^2}{\nu}$
ν = Kinematic Viscosity - ft²/sec
s = Axial clearance - ft
Engagement Ratio r/r_o
.95
.9
.8
.7
.6
Test Slinger Dimensions
Outer Diameter = 2.5 in.
Width = 0.29 in.
Data of Daily and Nece
s/r_o = .0255, $\frac{r}{r_o}$ = 0
NOTE: This data includes slinger tip losses
Drag Coefficient, C_m
Reynolds Number
X10⁻¹
X10⁻²
X10⁻³
X10⁻⁴
X10⁻⁵
X10⁻⁶
X10⁻⁷
.904
.784
.906
.616
.678
.920
.676
.835
.774
.812
.734
.438
.916
.802
.764
.874
.902
.840
.638
.740
.750
.646
.588
.488

Figure 30

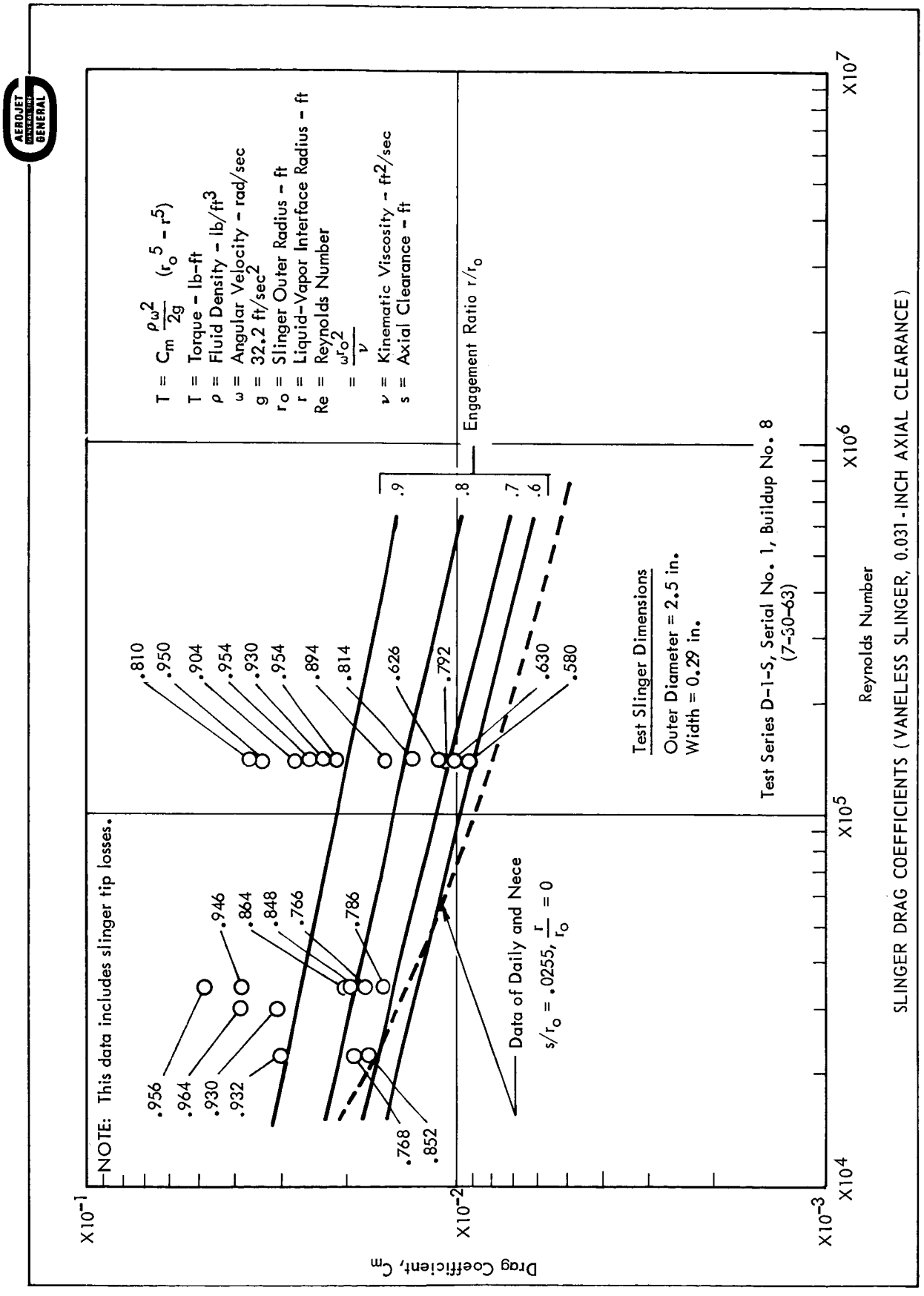
AEROJET GENERAL TIRE GENERAL
SLINGER DRAG COEFFICIENTS (VANELESS SLINGER, 0.031-INCH AXIAL CLEARANCE)
Drag Coefficient, C_m
Reynolds Number
Engagement Ratio r/r_o
$T = C_m \frac{\rho\omega^2}{2g} (r_o^5 - r^5)$
T = Torque - lb-ft
ρ = Fluid Density - lb/ft³
ω = Angular Velocity - rad/sec
g = 32.2 ft/sec²
r_o = Slinger Outer Radius - ft
r = Liquid-Vapor Interface Radius - ft
Re = Reynolds Number $= \frac{\omega r_o^2}{\nu}$
ν = Kinematic Viscosity - ft²/sec
s = Axial Clearance - ft
Test Slinger Dimensions
Outer Diameter = 2.5 in.
Width = 0.29 in.
Test Series D-1-S, Serial No. 1, Buildup No. 8 (7-30-63)
Data of Daily and Nece
$s/r_o = .0255, \frac{r}{r_o} = 0$
NOTE: This data includes slinger tip losses.
.9
.8
.7
.6
.810
.950
.904
.954
.930
.954
.894
.814
.626
.792
.630
.580
.946
.864
.848
.766
.786
.956
.964
.930
.932
.768
.852
X10⁻¹
X10⁻²
X10⁻³
X10⁴
X10⁵
X10⁶
X10⁷

Figure 31

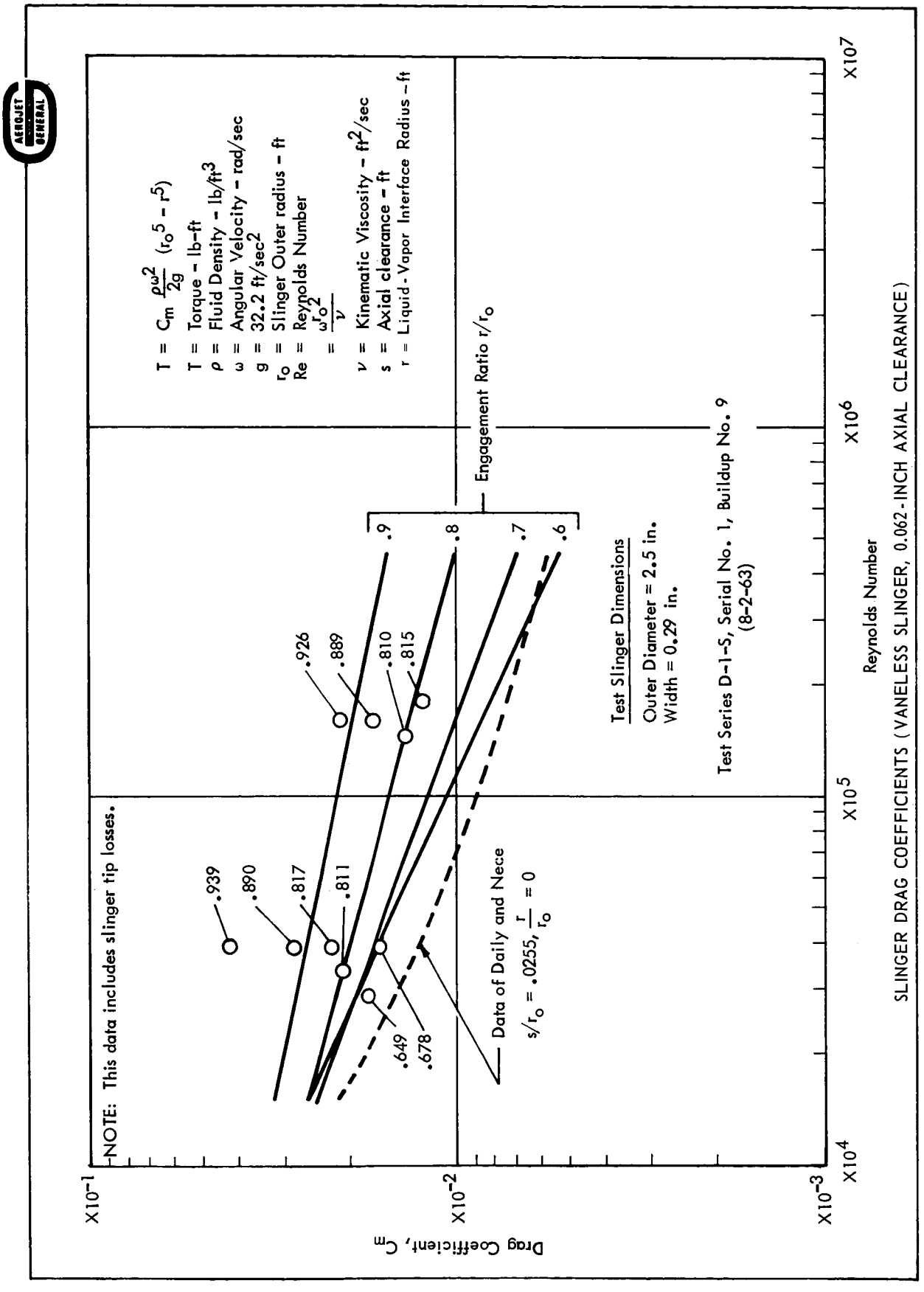
SLINGER DRAG COEFFICIENTS (VANELESS SLINGER, 0.062-INCH AXIAL CLEARANCE)
AEROJET GENERAL
T = $C_m \frac{\rho\omega^2}{2g} (r_o^5 - r^5)$
T = Torque - lb-ft
ρ = Fluid Density - lb/ft³
ω = Angular Velocity - rad/sec
g = 32.2 ft/sec²
r_o = Slinger Outer radius - ft
Re = Reynolds Number = $\frac{\omega r_o^2}{\nu}$
ν = Kinematic Viscosity - ft²/sec
s = Axial clearance - ft
r = Liquid - Vapor Interface Radius - ft
Engagement Ratio r/r_o
.9
.8
.7
.6
Test Slinger Dimensions
Outer Diameter = 2.5 in.
Width = 0.29 in.
Test Series D-1-S, Serial No. 1, Buildup No. 9
(8-2-63)
.926
.889
.810
.815
.939
.890
.817
.811
.649
.678
Data of Daily and Nece
s/r_o = .0255, $\frac{r}{r_o}$ = 0
NOTE: This data includes slinger tip losses.
Drag Coefficient, C_m
$X10^{-1}$
$X10^{-2}$
$X10^{-3}$
$X10^4$
$X10^5$
$X10^6$
$X10^7$
Reynolds Number

Figure 32

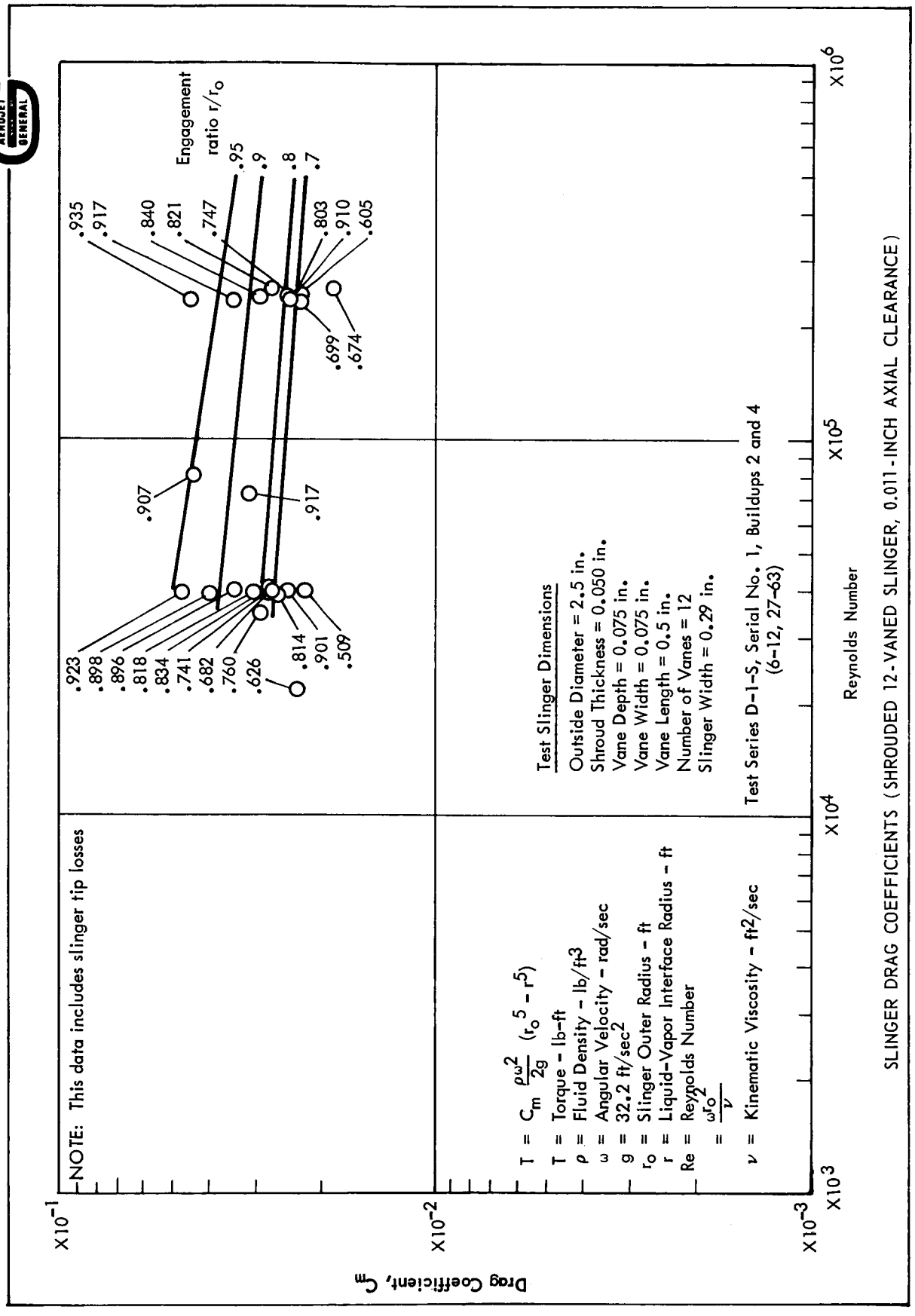
AEROJET GENERAL
SLINGER DRAG COEFFICIENTS (SHROUDED 12-VANED SLINGER, 0.011-INCH AXIAL CLEARANCE)
Drag Coefficient, C_m
Reynolds Number
$\times 10^{-1}$
$\times 10^{-2}$
$\times 10^{-3}$
$\times 10^{3}$
$\times 10^{4}$
$\times 10^{5}$
$\times 10^{6}$
Engagement ratio r/r_o
.95
.9
.8
.7
.935
.917
.840
.821
.747
.803
.910
.605
.699
.674
.907
.917
.923
.898
.896
.818
.834
.741
.682
.760
.626
.814
.901
.509
NOTE: This data includes slinger tip losses
$T = C_m \frac{\rho\omega^2}{2g}(r_o^5 - r^5)$
T = Torque - lb-ft
ρ = Fluid Density - lb/ft^3
ω = Angular Velocity - rad/sec
g = 32.2 ft/sec^2
r_o = Slinger Outer Radius - ft
r = Liquid-Vapor Interface Radius - ft
Re = Reynolds Number $= \frac{\omega r_o^2}{\nu}$
ν = Kinematic Viscosity - ft^2/sec
Test Slinger Dimensions
Outside Diameter = 2.5 in.
Shroud Thickness = 0.050 in.
Vane Depth = 0.075 in.
Vane Width = 0.075 in.
Vane Length = 0.5 in.
Number of Vanes = 12
Slinger Width = 0.29 in.
Test Series D-1-S, Serial No. 1, Buildups 2 and 4 (6-12, 27-63)

Figure 33

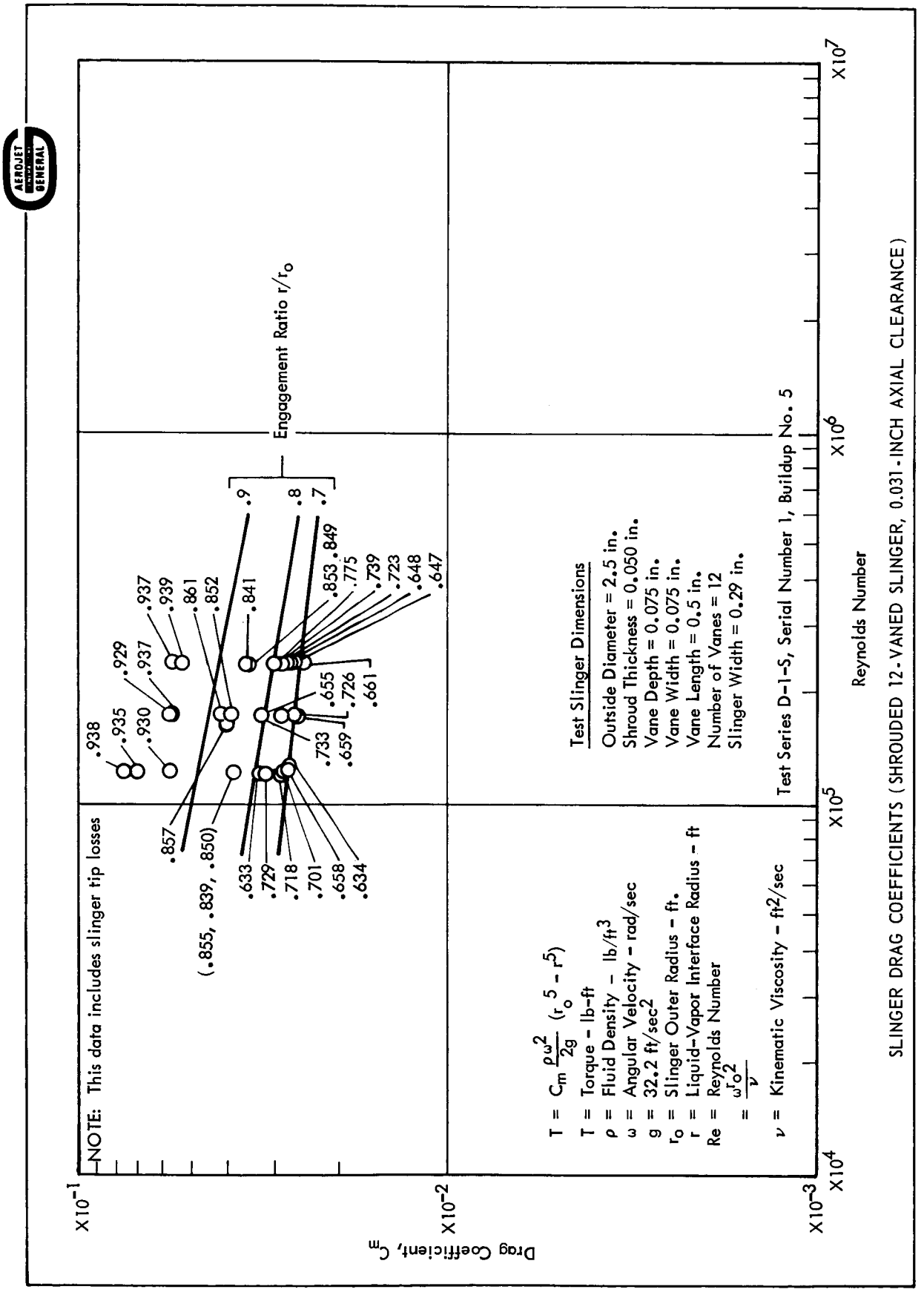
AEROJET GENERAL
SLINGER DRAG COEFFICIENTS (SHROUDED 12-VANED SLINGER, 0.031-INCH AXIAL CLEARANCE)
Drag Coefficient, C_m
Reynolds Number
Engagement Ratio r/r_o
NOTE: This data includes slinger tip losses
$T = C_m \frac{\rho\omega^2}{2g}(r_o^5 - r^5)$
T = Torque - lb-ft
ρ = Fluid Density - lb/ft³
ω = Angular Velocity - rad/sec
g = 32.2 ft/sec²
r_o = Slinger Outer Radius - ft.
r = Liquid-Vapor Interface Radius - ft
Re = Reynolds Number $= \frac{\omega r_o^2}{\nu}$
ν = Kinematic Viscosity - ft²/sec
Test Slinger Dimensions
Outside Diameter = 2.5 in.
Shroud Thickness = 0.050 in.
Vane Depth = 0.075 in.
Vane Width = 0.075 in.
Vane Length = 0.5 in.
Number of Vanes = 12
Slinger Width = 0.29 in.
Test Series D-1-S, Serial Number 1, Buildup No. 5
.938 .935 .930 .929 .937 .937 .939 .861 .852 .841
.857 (.855, .839, .850) .633 .729 .718 .701 .658 .634
.733 .659 .655 .726 .661
.853 .849 .775 .739 .723 .648 .647
.9 .8 .7
$X10^{-1}$ $X10^{-2}$ $X10^{-3}$ $X10^{4}$ $X10^{5}$ $X10^{6}$ $X10^{7}$

Figure 34

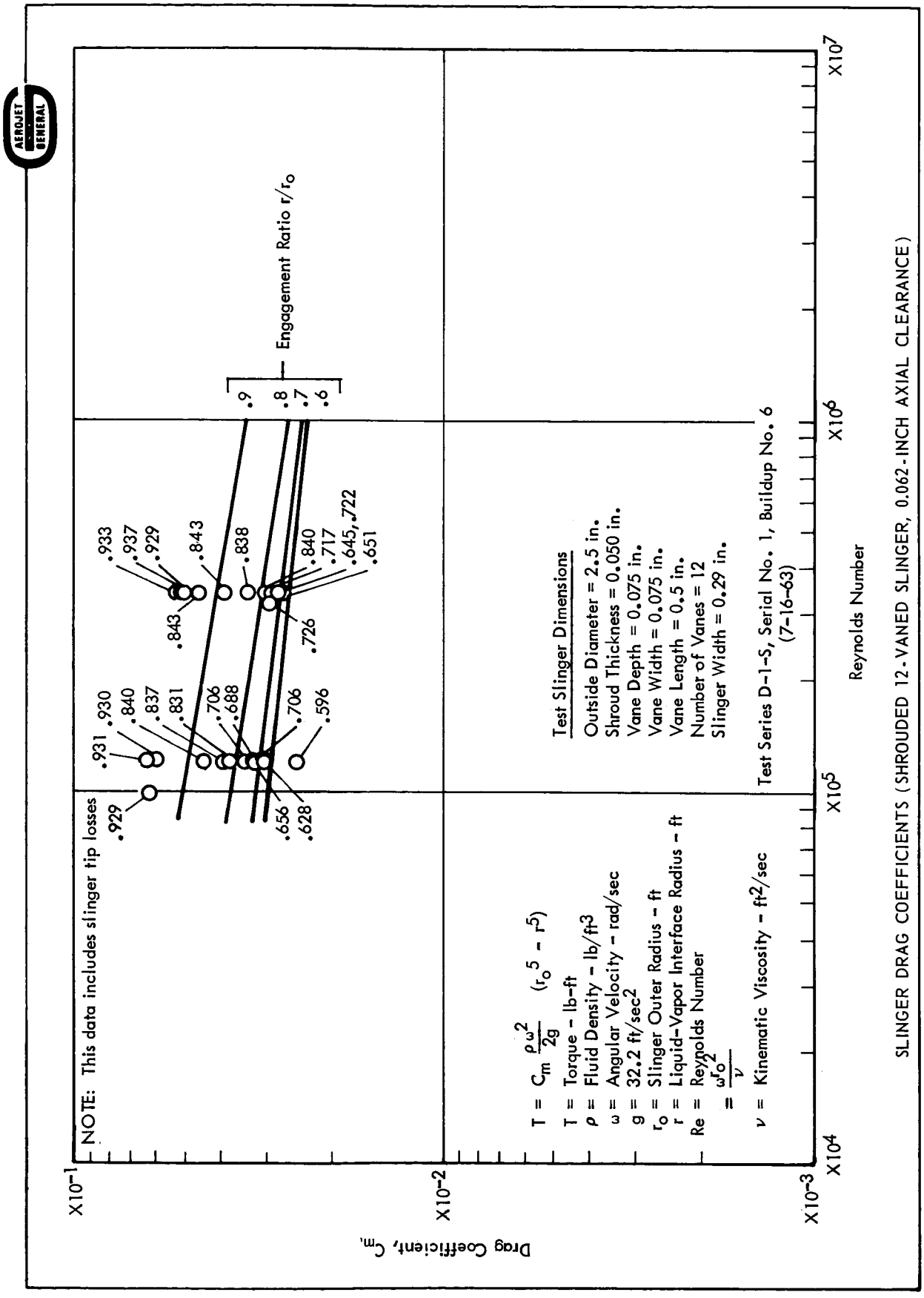
AEROJET GENERAL
SLINGER DRAG COEFFICIENTS (SHROUDED 12-VANED SLINGER, 0.062-INCH AXIAL CLEARANCE)
Drag Coefficient, C_m
Reynolds Number
X10⁻¹
X10⁻²
X10⁻³
X10⁴
X10⁵
X10⁶
X10⁷
Engagement Ratio r/r_o
.9
.8
.7
.6
NOTE: This data includes slinger tip losses
.931 .930 .840 .837 .831 .706 .688 .929
.933 .937 .929 .843 .843 .838 .840 .717 .645, .722 .651 .726 .706 .596 .656 .628
Test Slinger Dimensions
Outside Diameter = 2.5 in.
Shroud Thickness = 0.050 in.
Vane Depth = 0.075 in.
Vane Width = 0.075 in.
Vane Length = 0.5 in.
Number of Vanes = 12
Slinger Width = 0.29 in.
Test Series D-1-S, Serial No. 1, Buildup No. 6 (7-16-63)
$T = C_m \frac{\rho \omega^2}{2g} (r_o^5 - r^5)$
T = Torque - lb-ft
ρ = Fluid Density - lb/ft³
ω = Angular Velocity - rad/sec
g = 32.2 ft/sec²
r_o = Slinger Outer Radius - ft
r = Liquid-Vapor Interface Radius - ft
$Re = \frac{\omega r_o^2}{\nu}$ = Reynolds Number
ν = Kinematic Viscosity - ft²/sec

Figure 35

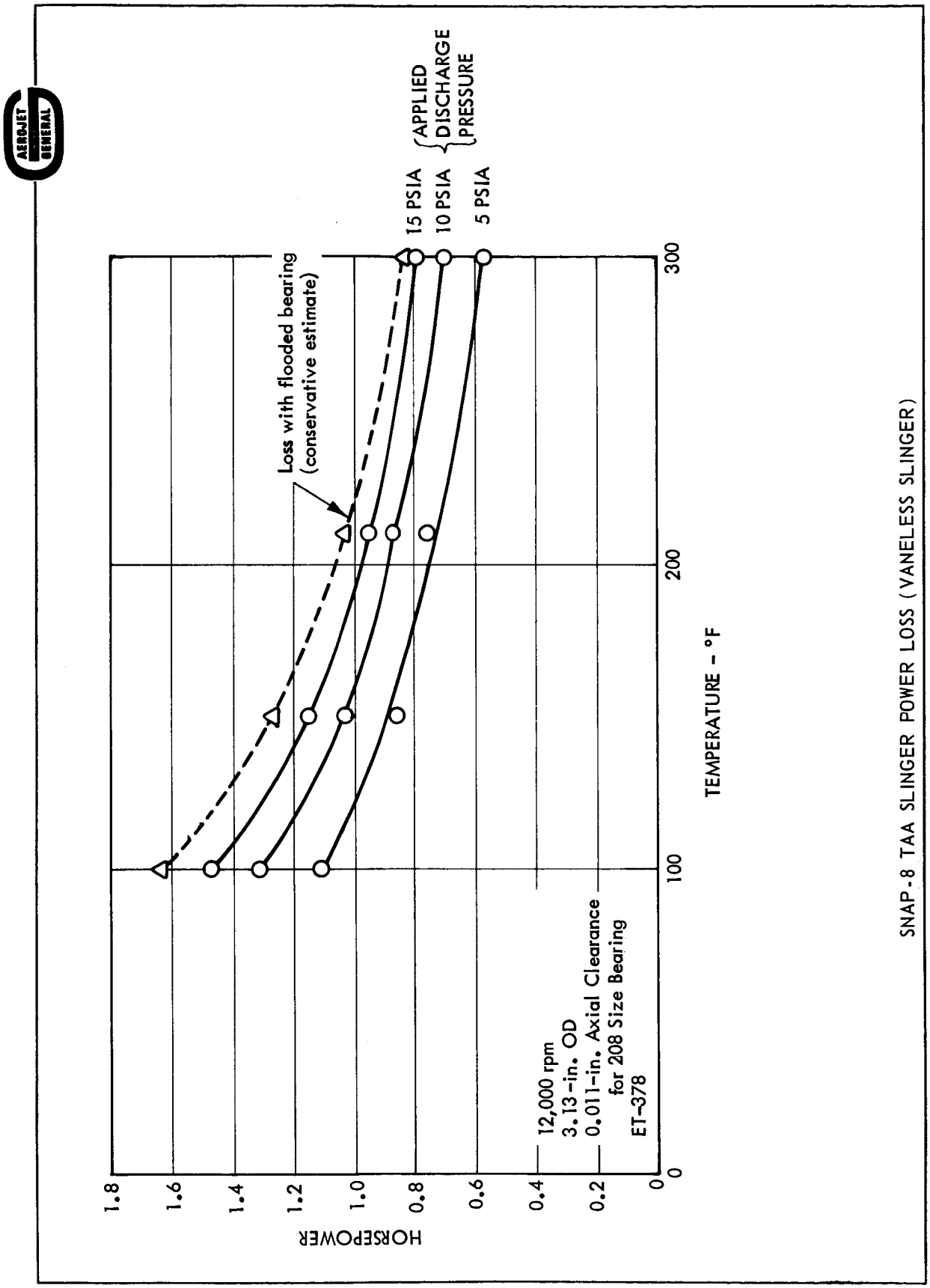
AEROJET GENERAL
SNAP-8 TAA SLINGER POWER LOSS (VANELESS SLINGER)
HORSEPOWER
TEMPERATURE - °F
0
0.2
0.4
0.6
0.8
1.0
1.2
1.4
1.6
1.8
100
200
300
12,000 rpm
3.13-in. OD
0.011-in. Axial Clearance
for 208 Size Bearing
ET-378
Loss with flooded bearing
(conservative estimate)
15 PSIA
10 PSIA
5 PSIA
APPLIED DISCHARGE PRESSURE
10-087-116

Figure 36

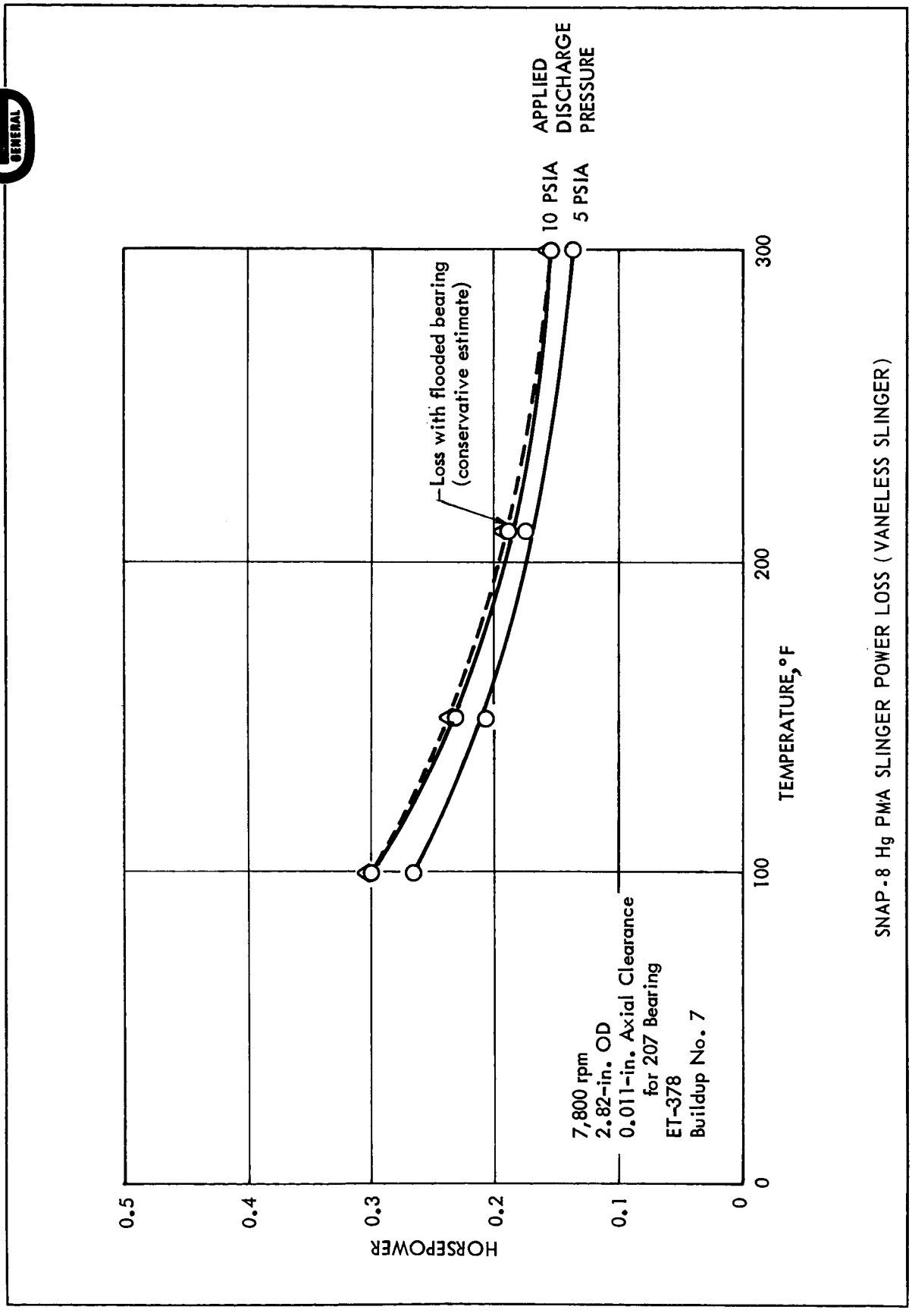
SNAP-8 Hg PMA SLINGER POWER LOSS (VANELESS SLINGER)
APPLIED DISCHARGE PRESSURE
10 PSIA
5 PSIA
Loss with flooded bearing (conservative estimate)
7,800 rpm
2.82-in. OD
0.011-in. Axial Clearance for 207 Bearing
ET-378
Buildup No. 7
HORSEPOWER
0.5
0.4
0.3
0.2
0.1
0
0
100
200
300
TEMPERATURE, °F

Figure 37

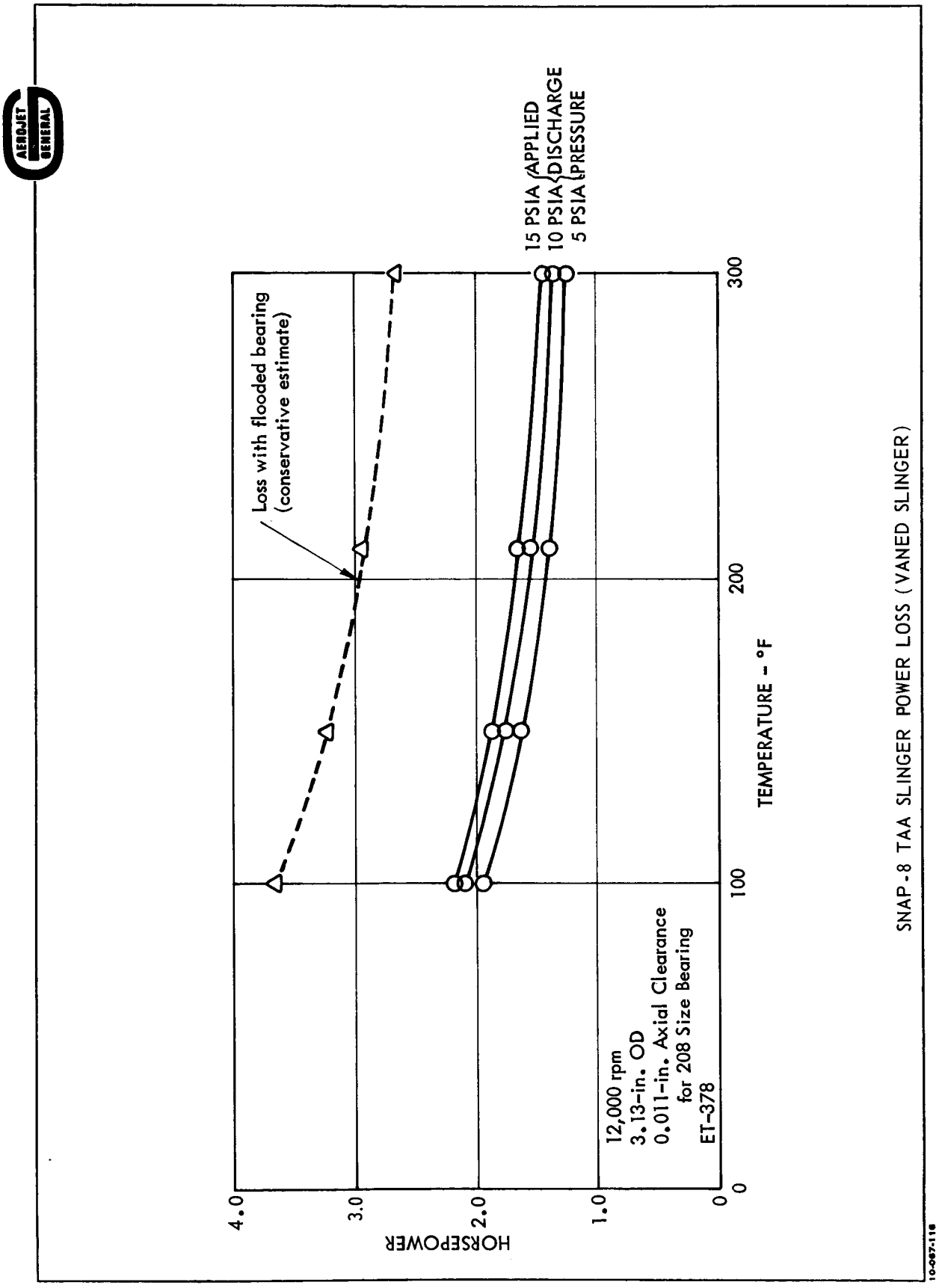
AEROJET GENERAL
SNAP-8 TAA SLINGER POWER LOSS (VANED SLINGER)
HORSEPOWER
4.0
3.0
2.0
1.0
0
100
200
300
TEMPERATURE - °F
Loss with flooded bearing
(conservative estimate)
15 PSIA
10 PSIA
5 PSIA
APPLIED
DISCHARGE
PRESSURE
12,000 rpm
3.13-in. OD
0.011-in. Axial Clearance
for 208 Size Bearing
ET-378
10-087-118

Figure 38

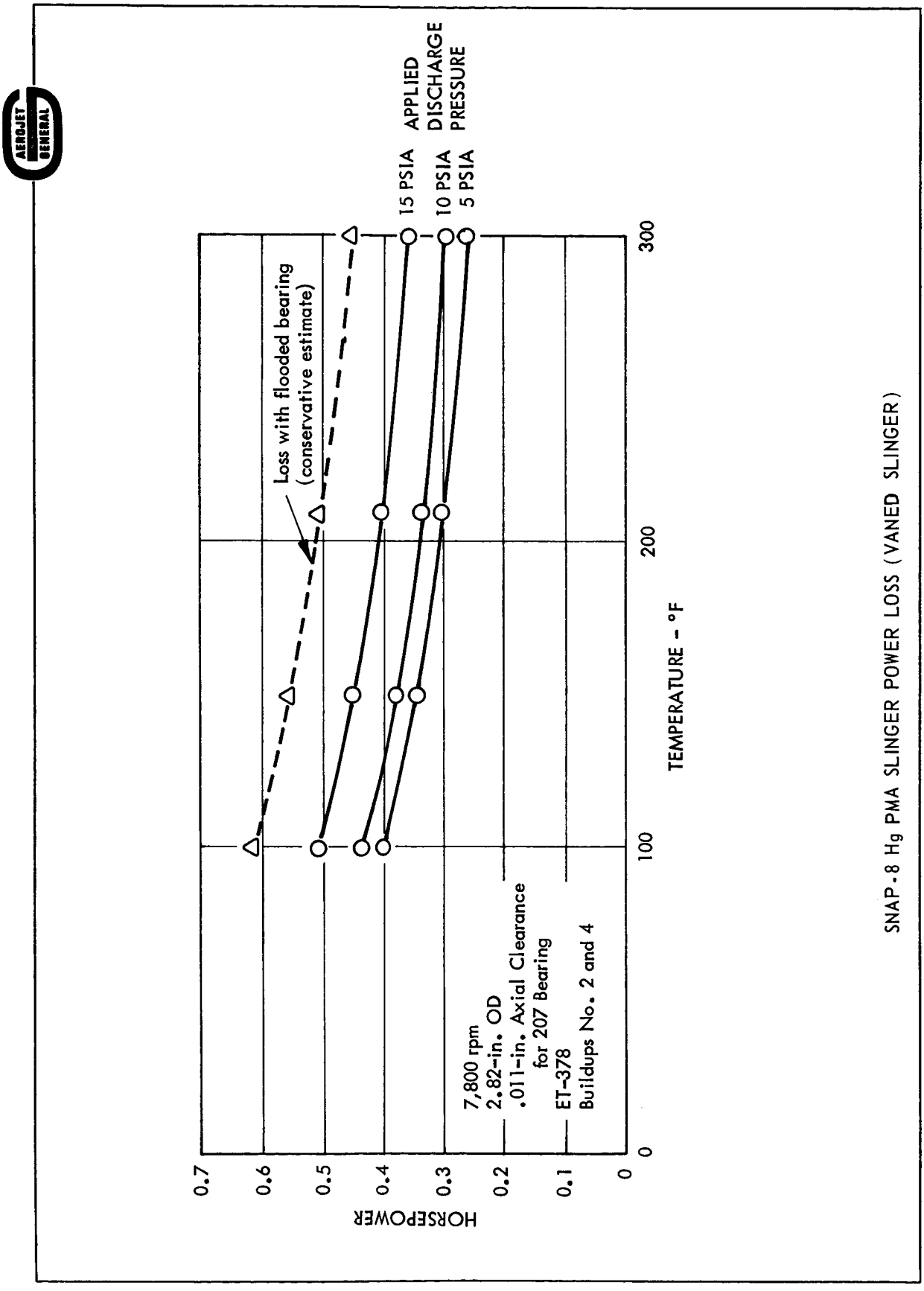
AEROJET GENERAL
SNAP-8 Hg PMA SLINGER POWER LOSS (VANED SLINGER)
HORSEPOWER
TEMPERATURE - °F
0.7
0.6
0.5
0.4
0.3
0.2
0.1
0
100
200
300
15 PSIA
10 PSIA
5 PSIA
APPLIED DISCHARGE PRESSURE
Loss with flooded bearing (conservative estimate)
7,800 rpm
2.82-in. OD
.011-in. Axial Clearance for 207 Bearing
ET-378
Buildups No. 2 and 4
10-067-116

Figure 39

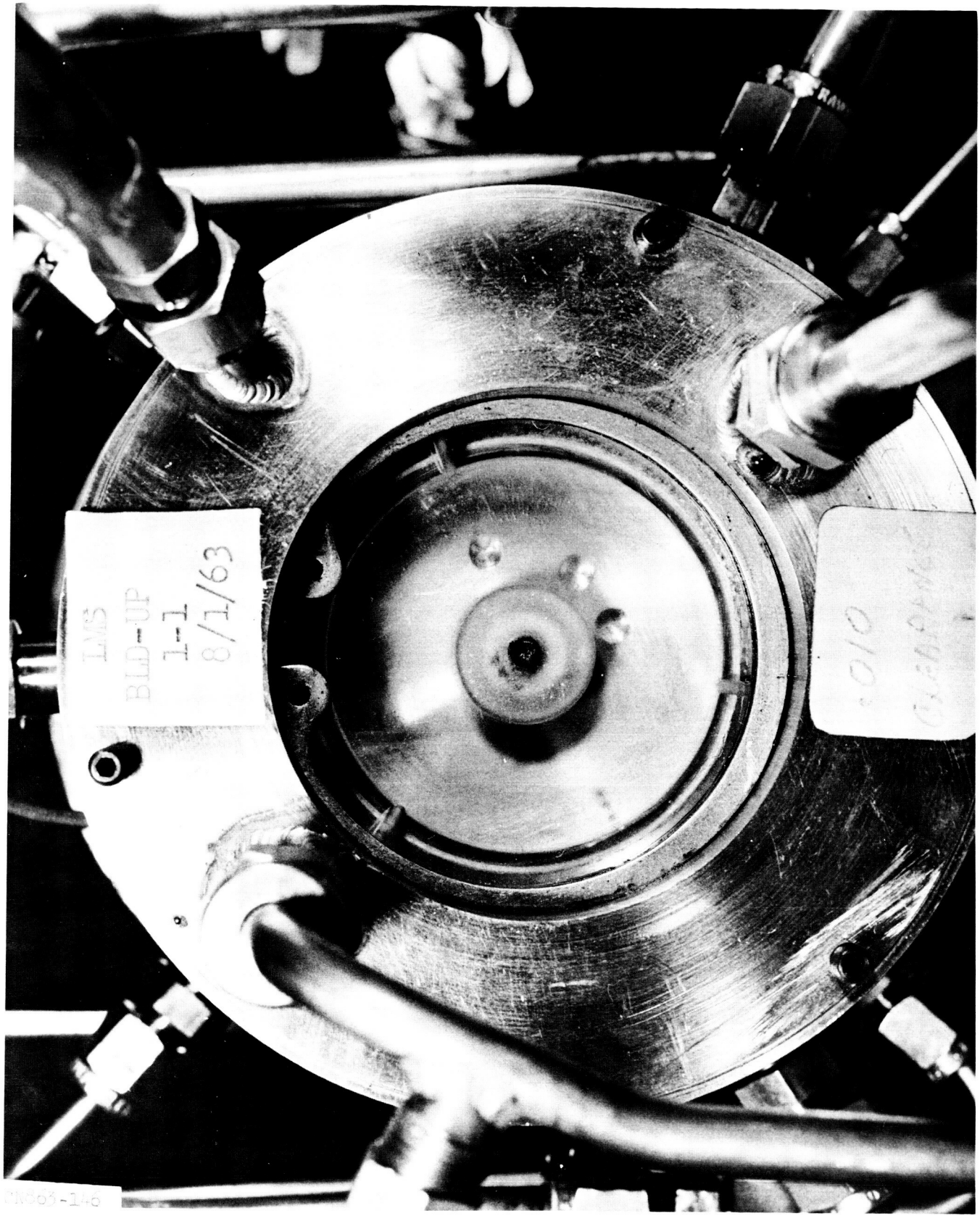

Mercury Slinger Interface
(2-in.-OD Slinger, 12,000 rpm, 0.010-in. Axial Clearance)

Figure 40

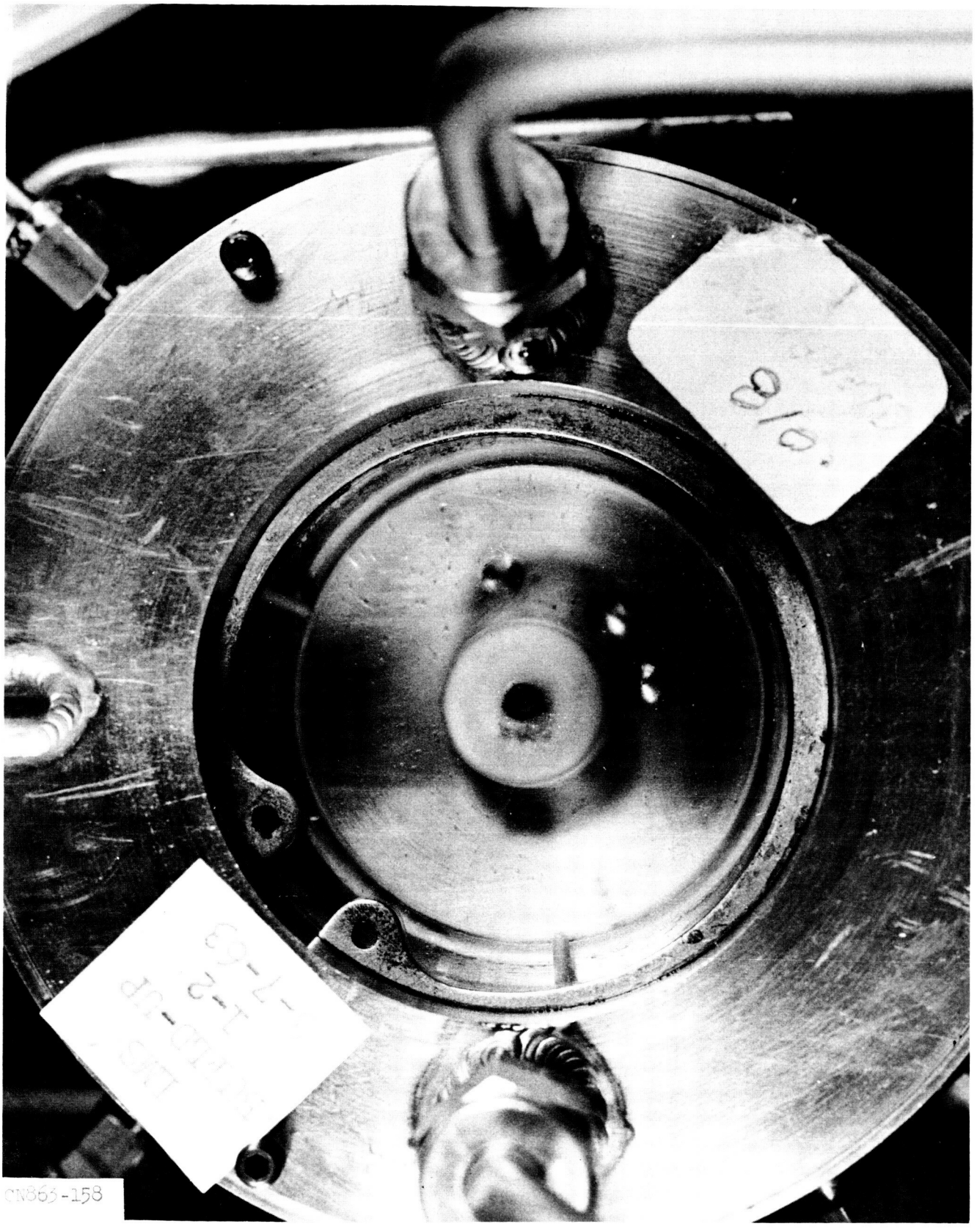

Mercury Slinger Interface
(2-in.-OD Slinger, 12,000 rpm, 0.018-in. Axial Clearance)

Figure 41

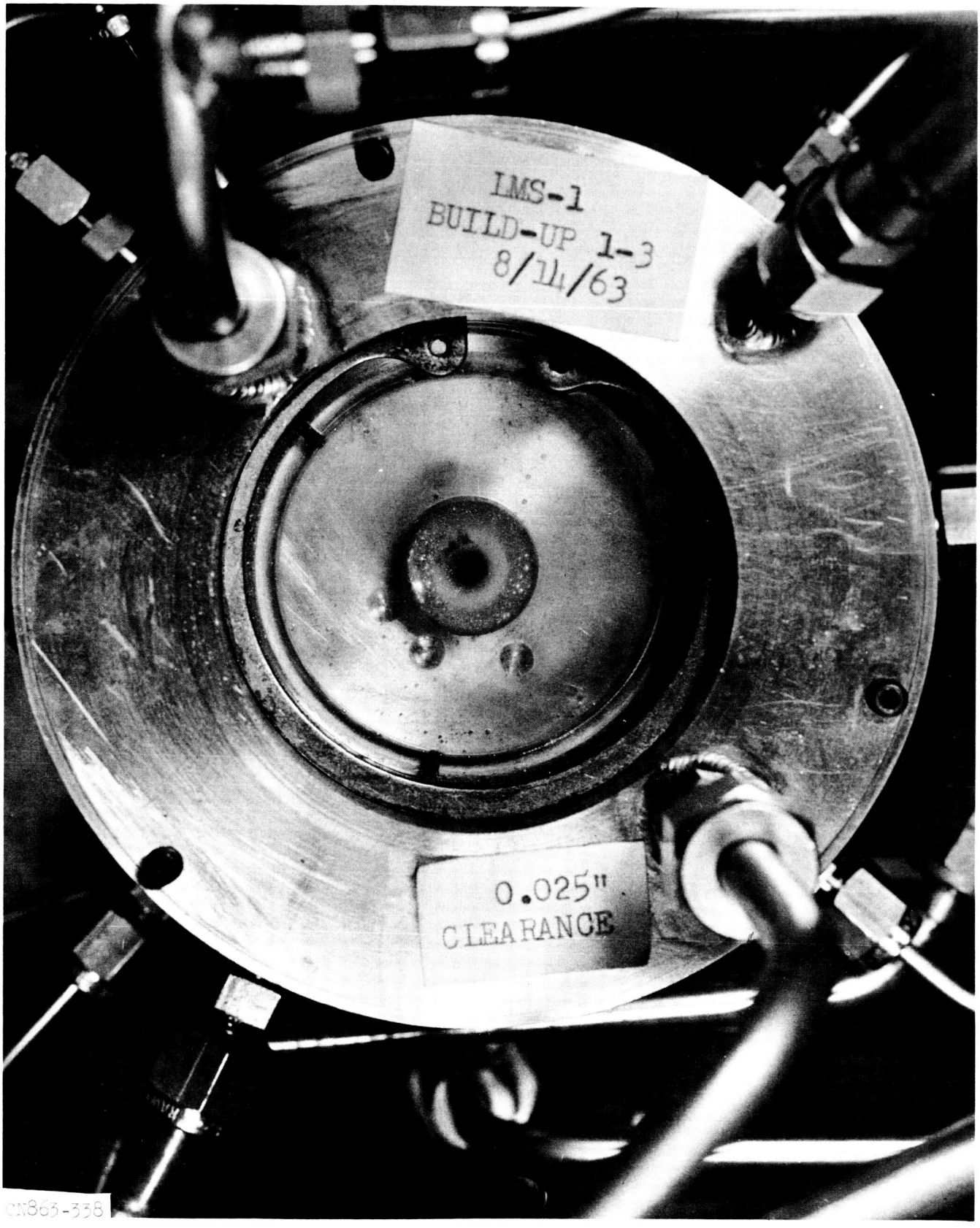

Mercury Slinger Interface
(2-in.-OD Slinger, 12,000 rpm, 0.025-in. Axial Clearance)

Figure 42

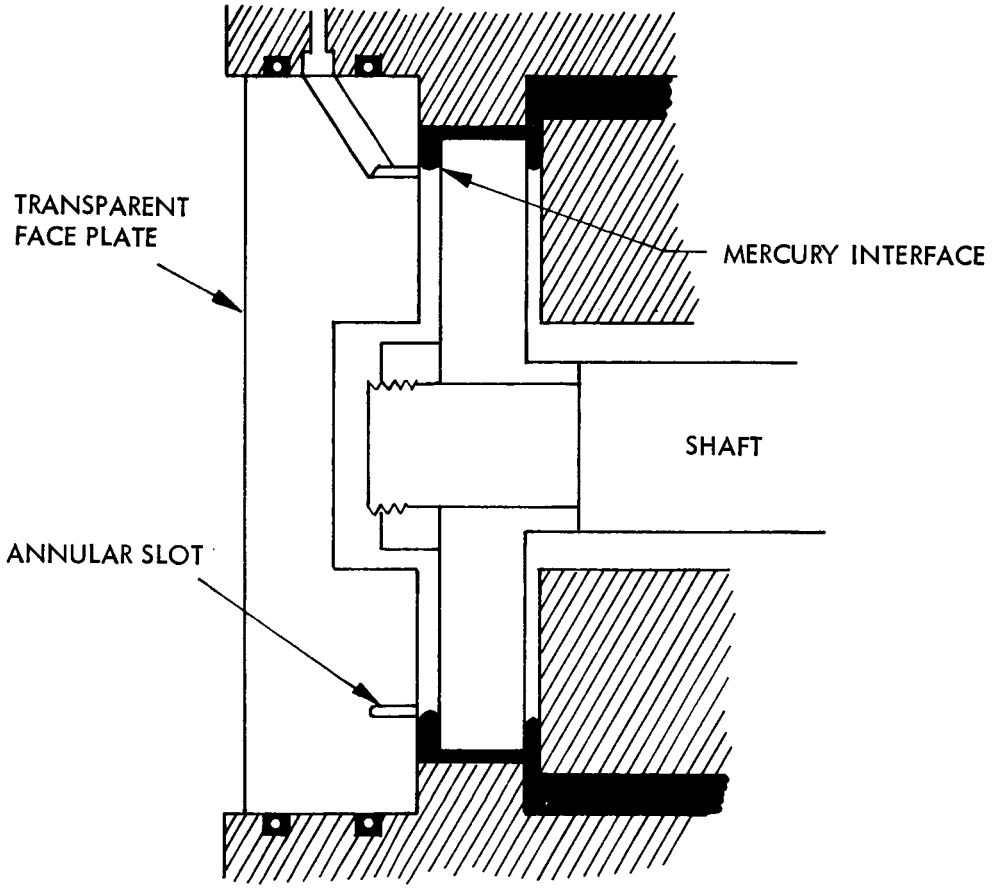

CONFIGURATION OF TRANSPARENT END PLATE, FIGURES 40, 41, AND 42

10-067-11B

Figure 43

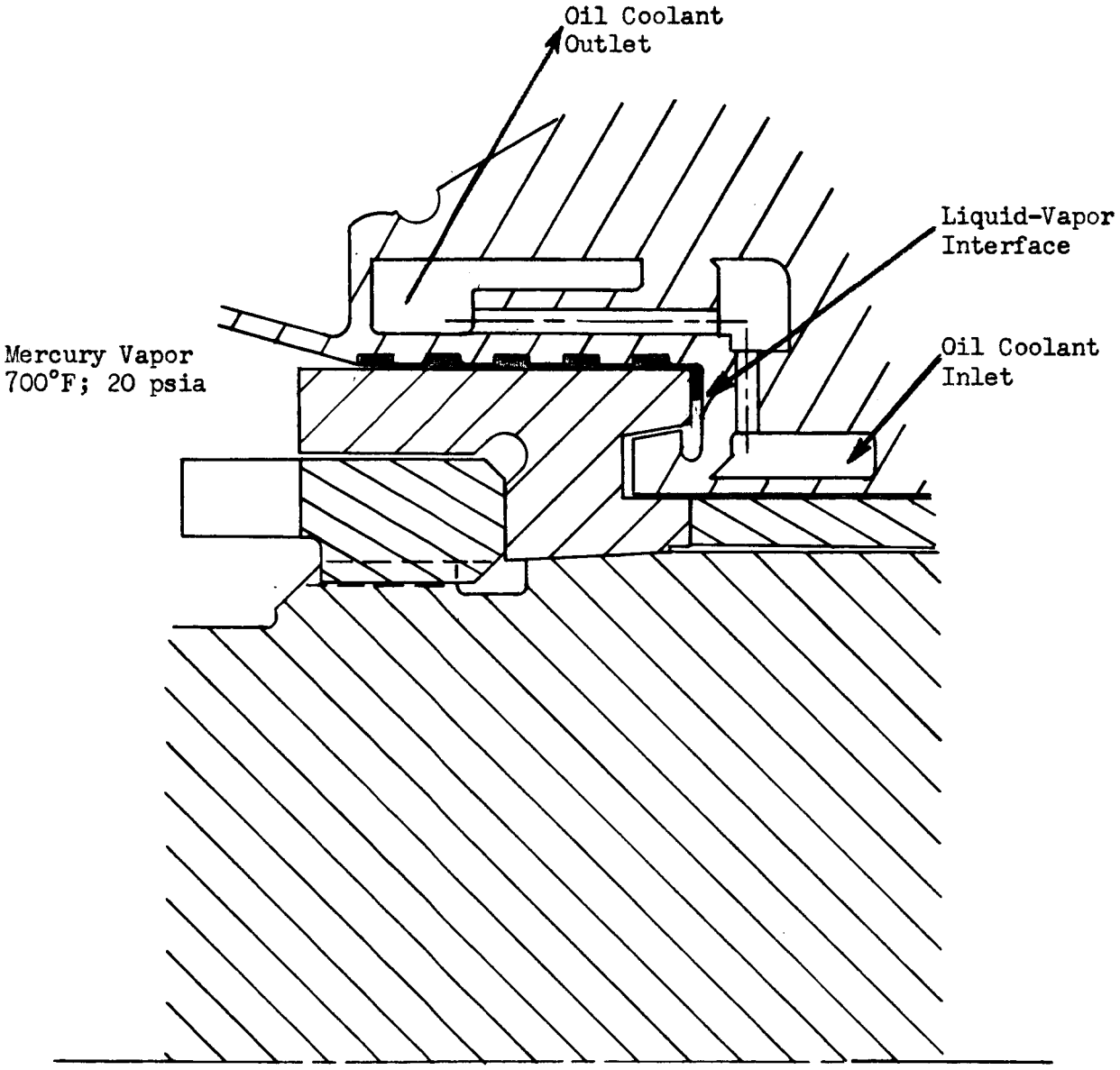

Modified Configuration for the Mercury Slinger

Figure 44

Demonstration of Performance of Modified Mercury Slinger Configuration (No Droplets in Interface Cavity)

Figure 45

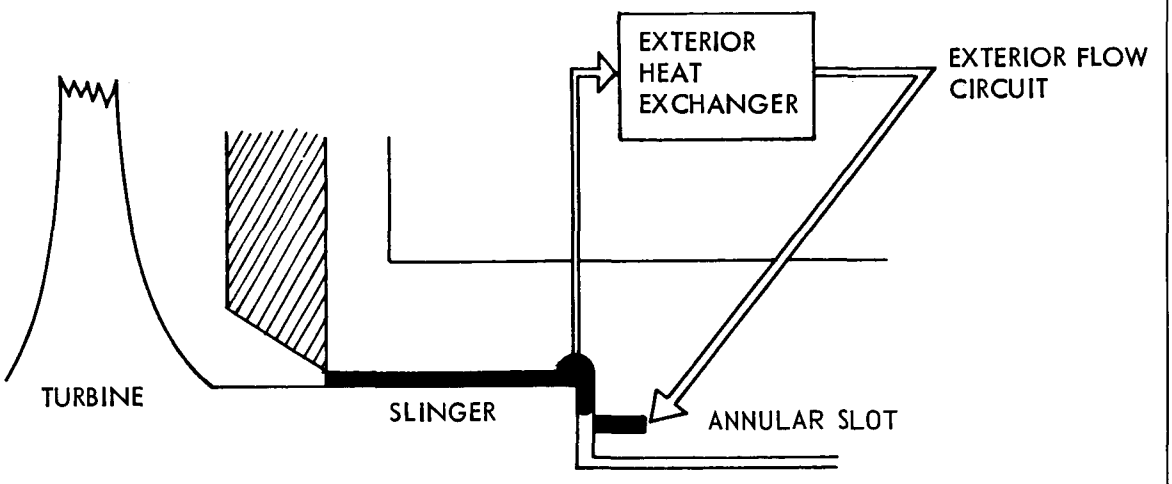

INTERFACE COOLING METHOD, MODEL A SEAL SIMULATOR

10-067-118

Figure 46

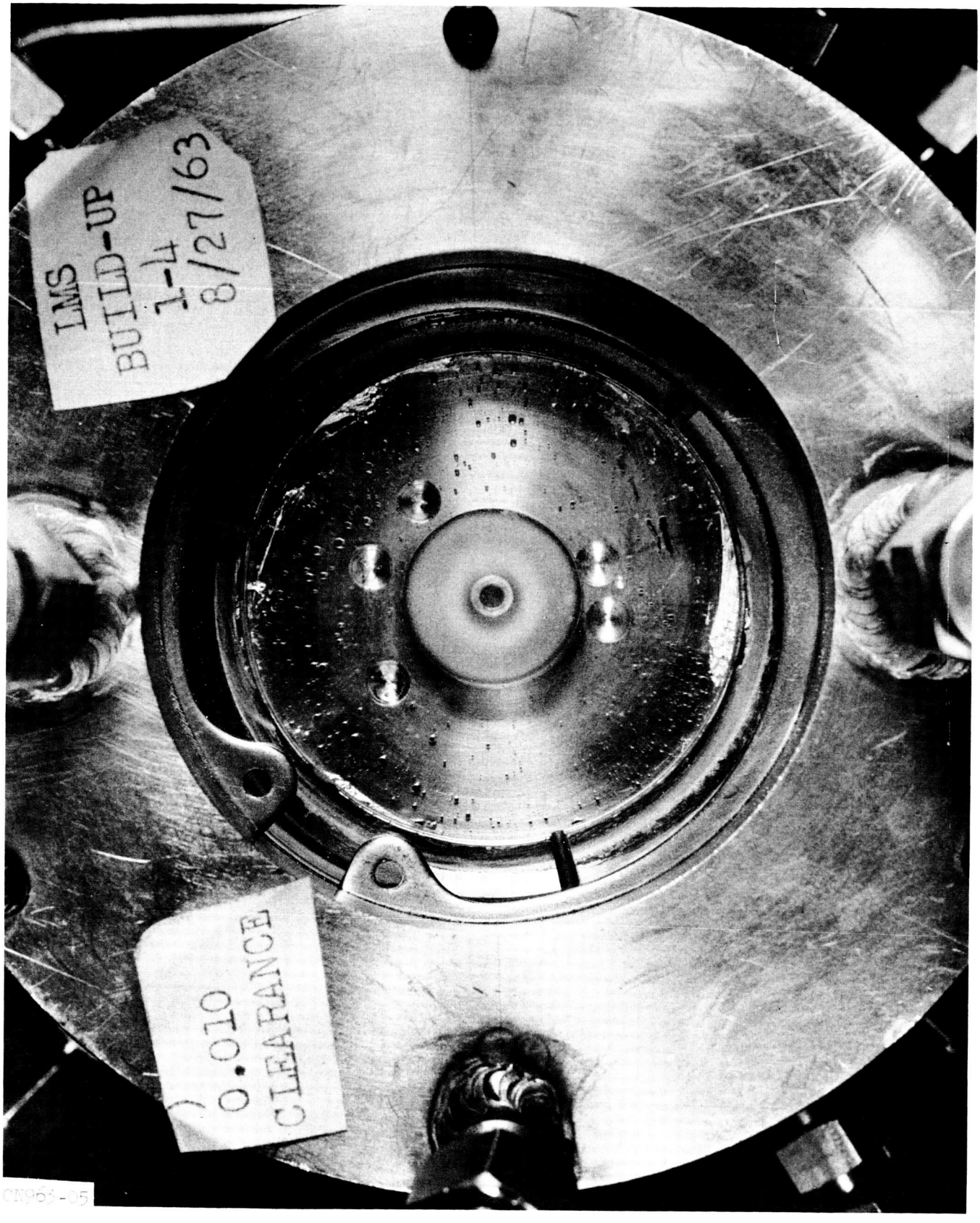

Interface Instability Due to Improper Introduction
of Flow to the Interface

Figure 47

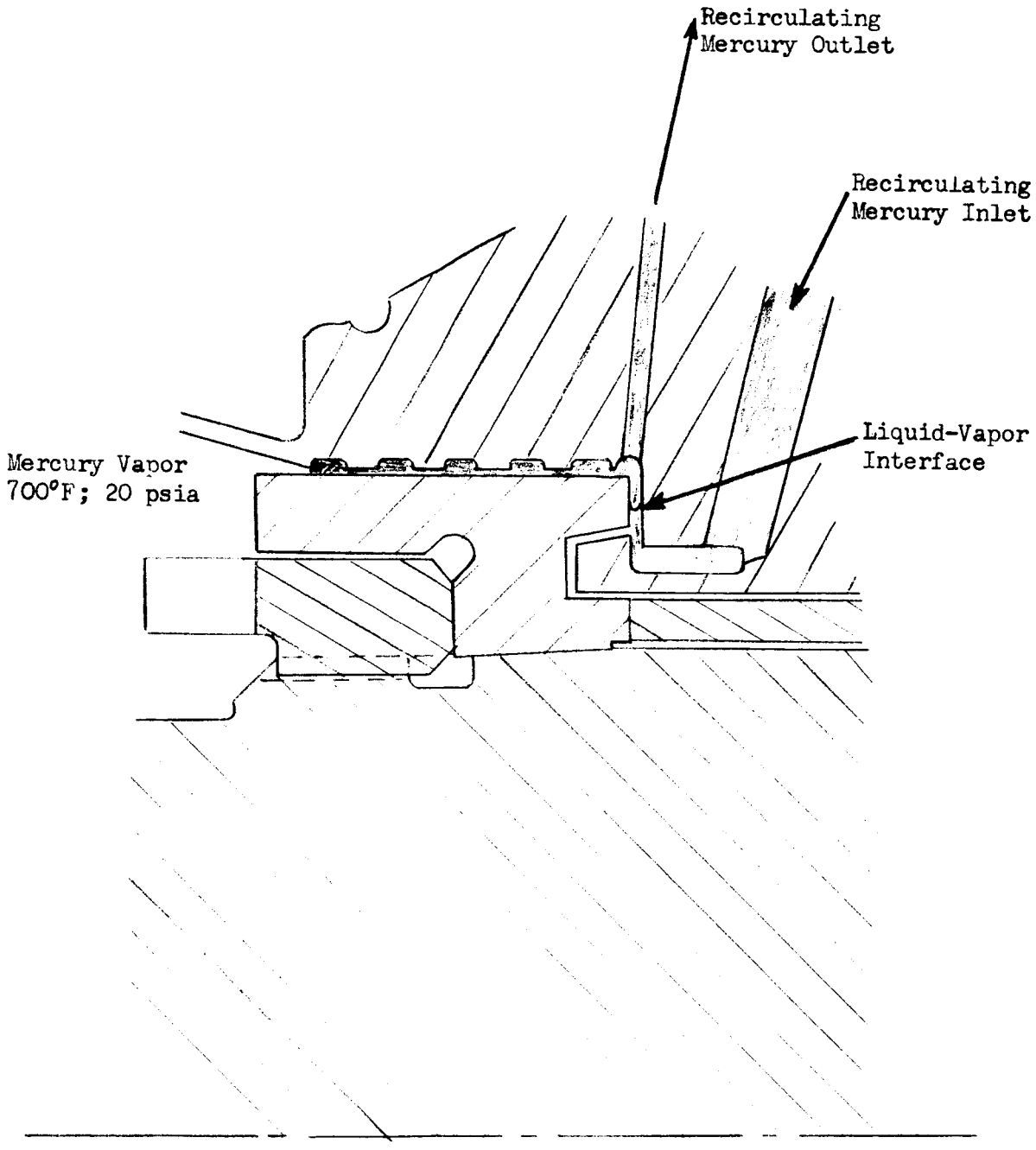

Configuration for Introducing Mercury
Coolant at Slinger Interface

Figure 48

APPENDIX A

INERTIAL METHOD FOR DETERMINING HORSEPOWER LOSS

Given the relationships

$$T = I_o \frac{d\omega}{dt} = \frac{2\pi}{60} I_o \frac{dN}{dt}$$

$$hp = \frac{T\,N}{63000}$$

where

T = torque (inch-lb)

I_o = Mass moment of inertia (inch-lb-sec^2)

N = Revolutions per minute (rpm)

t = time (sec)

ω = angular velocity (radians/sec)

hp = horsepower

It may be seen that if I_o can be accurately evaluated and $\frac{dN}{dt}$ determined, the torque and horse power loss for a rotating assembly may be specified.

For the slinger seal test rigs, the I_o of all rotating parts (including the drive motor) was determined by use of a torsional pendulum; $\frac{dN}{dt}$ was determined from an oscilloscope deceleration trace of a coast down from an equilibrium running condition.

The friction horsepower loss is first determined by use of a deceleration trace obtained with no fluid in the rig and then a total horsepower loss determined with the slinger operating at a desired test condition. The difference between these two values is the net horsepower loss.

The torsional pendulum method for measuring moment of inertia is implemented as follows:

The frequency of oscillation of a torsional pendulum is

$$f = \frac{1}{2\pi}\sqrt{\frac{k}{I_o}} \text{ cycles/second}$$

where

k = torsional spring constant $\frac{(\text{lb-in.})}{(\text{radian})}$

$$k = \frac{\pi d^4 G}{32 \ell}$$

where

G = elastic modulus in shear, psi

d = wire diameter in inches

ℓ = wire length in inches

Rearranging the foregoing expression,

$$I_o = \frac{k}{4 \pi^2 f^2}$$

k is dependent only on the properties of the torsional spring (a long thin wire). It is not necessary to know the exact dimensions and elastic modulus of the wire since k may be evaluated experimentally by measuring the frequency of oscillation of a mass of known I_o attached to the wire. This mass should be a cylinder whose I_o may be readily calculated from the following expression:

$$I_o = \frac{mr^2}{2}$$

where

m = mass (lb-sec^2/in.)

r = radius (in.)

It is not necessary to actually evaluate k since if the same wire is used for both the known (or standard) mass and the unknown mass

$$\frac{I_o}{I_{o\ \text{standard}}} = \frac{\frac{4 \pi^2 f^2 \text{std}}{k}}{\frac{4 \pi^2 f_o^2}{k}} = \left(\frac{f_{o\ \text{std}}}{f_o} \right)^2$$

To summarize: the I_o is determined by (1) rigidly attaching a mass of known I_o to a wire and measuring the frequency of oscillation, (2) replacing the known mass with the mass of unknown I_o and measuring the frequency of oscillation, and (3) calculating I_o with the use of the foregoing expression.

$\frac{dN}{dt}$ is determined by measuring the initial slope of an oscilloscope deceleration trace (rpm vs time).

APPENDIX B

ERROR ANALYSIS

The instrumentation used for data assimilation was a combination of laboratory type and process type. Except where noted, the instrumentation was calibrated prior to the conducting of tests and was considered to be essentially accurate within the limits specified.

For the ET-378 tests, Hiese gages were used for pressure measurement and thermocouples with a Simplytrol readout for temperature measurement. The Hiese gages were considered to be essentially accurate and have a least count of 0.2 psi. This allows the reading to be taken within an accuracy of 0.1 psi. The Simplytrol had a least count of $5^{\circ}F$ and a least readable count of $2\text{-}1/2^{\circ}F$, allowing the reading to be estimated to within an accuracy of $1\text{-}1/4^{\circ}F$. The basic accuracy of the Simplytrol was calibrated to be less than 2% of the indicated reading.

For the mercury tests, a pressure transducer-L&N recorder combination was used for all pressure measurements (including Δp for flow). A thermocouple-Brown recorder combination was used for temperature measurement. The least readable count of the recorder trace is 0.2 millivolt and the maximum error of the pickup readout combination is calibrated to be less than 2%.

Slinger engagements were measured by scaling from photographs using a known diameter to develop a scale factor. The maximum error for this measurement is estimated to be 0.031 in.

The shaft rpm was measured in both instances with a stroboscope. The least count with this instrument was 10 rpm, and the maximum error was less than 1% of the indicated reading.

The expression for the pumping coefficient is as follows:

$$K^2 = \frac{2g\ (P - P_o)}{\rho\, \omega^2\ (r_o^2 - r^2)}$$

where

$g = 32.2\ ft/sec^2$

P and $P_o = lb/ft^2$

$\rho = lb/ft^3$ density of liquid (lb/ft^3)

r_o = slinger radius (ft)

r = interface radius (ft)

ω = angular velocity (rad/sec)

The maximum deviation in the pumping head may be expressed as

$$\frac{\Delta K}{K} = \frac{1}{2}\left[\frac{\Delta P}{P-P_o} + \frac{2\,\Delta\omega}{\omega} + \frac{2\,\Delta r}{r_o^2-r^2}\right]$$

ρ, g, and P_o here were considered to be essentially accurate.

From examination of the foregoing expression, the maximum deviation would occur with a low discharge pressure and high engagement ratio.

The horsepower loss equation is

$$hp = \frac{T\,N}{5250}$$

where

N = rpm

T = torque (ft-lb)

The maximum deviation is

$$\frac{\Delta hp}{hp} = \frac{\Delta T}{T} + \frac{\Delta N}{N}$$

The expression for the torque coefficient for two sides of a disk is

$$Cm = \frac{2Tg}{\rho\omega^2\,(r_o^5-r^5)}$$

where

ω = rad/sec

r and r_o = ft

The maximum deviation may be expressed as

$$\frac{\Delta Cm}{Cm} = \frac{\Delta T}{T} + \frac{2\Delta\omega}{\omega} + \frac{5\Delta r}{r_o^5-r^5} = \frac{\Delta hp}{hp} + \frac{3\Delta\omega}{\omega} + \frac{5\Delta r}{r_o^5-r^5}$$

Here again, the maximum deviation occurs with a high engagement ratio.

The inertial method used to measure the torque T is estimated to have a maximum error of 5%.

Maximum deviations for the various dynamic seal configurations are tabulated below for an engagement ratio (r/r_o) of approximately 0.9.

Seal Configuration	Fluid	Axial Gap in.	ΔP psi	$\frac{r}{r_o}$	$\frac{\Delta K}{K}$	$\frac{\Delta Cm}{Cm}$	$\frac{\Delta Hp}{Hp}$
12-Van Shrouded	ET-378	0.011	15.8	0.90	0.12	0.20	0.05
12-Van Shrouded	↓	0.031	18.8	0.94	0.18	0.25	↓
12-Van Shrouded	↓	0.062	20.8	0.93	0.17	0.26	↓
Smooth Vaneless	↓	0.011	4.0	0.88	0.13	0.21	↓
Smooth Vaneless	↓	0.031	5.6	0.91	0.13	0.21	↓
Smooth Vaneless	ET-378	0.062	4.7	0.89	0.12	0.21	0.05

Report No. 2808, Vol. III

SNAP-8 SEALS-TO-SPACE DEVELOPMENT TEST PROGRAM

Aerojet-General Corporation

ABSTRACT

Tests were conducted to demonstrate that dynamic slingers, using oil and mercury as working fluids, are capable of generating stable liquid-vapor interfaces for use in the SNAP-8 seals-to-space. The test rigs contained transparent housing sections which permitted observation of the liquid-vapor interfaces during operation. Results demonstrated that stable interfaces can be obtained for the operating conditions of the rotating assemblies of the SNAP-8 power conversion system.

Report No. 2808

DISTRIBUTION

	No. of Copies
National Aeronautics and Space Administration Lewis Research Center - SNAP-8 Project Office 21000 Brookpark Road Cleveland, Ohio 44135	
Attn: H. O. Slone, Manager (Mail Stop 500-201)	3 plus repro
Attn: R. E. English	2
Attn: Dr. B. Lubarsky	1
Attn: S. M. Perrone (Quality and Reliability) (Mail Stop 500-203)	1
Attn: W. L. Stewart	1
Attn: G. M. Thur	1
Attn: Librarian	1
Attn: Space Power Systems Procurement Section	1
Headquarters National Aeronautics and Space Administration Washington, D.C. 20546	
Attn: Dr. F. Schulman (Code RNP) Program Director	1
Attn: G. C. Deutsch (Code RRM)	1
Attn: T. B. Kerr (Code RNS)	1
Attn: J. Lazar (Code RNR)	1
Attn: P. R. Miller (Code RNP)	1
Attn: W. H. Woodward (Code RN)	1

DISTRIBUTION (cont.)

	No. of Copies
National Aeronautics and Space Administration Western Operations Office 150 Pico Blvd. Santa Monica, California, 90406	
Attn: J. S. Keeler	1
Attn: Patent Counsel	1
NASA - Azusa Field Office Room 152, Building 160 Aerojet-General Corporation Azusa, California	
Attn: J. G. Kennard	1
Attn: E. F. Morris	1
NASA - Scientific and Technical Information Facility Box 5700 Bethesda 14, Maryland	
Attn: NASA Representative	2
National Aeronautics and Space Administration Marshall Space Flight Center Huntsville, Alabama, 35812	
Attn: Dr. E. Stuhlinger	1
Attn: Claude C. Priest, R-P and VE-ANP	1
National Aeronautics and Space Administration Manned Spacecraft Center Houston 1, Texas	
Attn: Technical Information Division	2
Graham Hagey (ESDE)	1
BuWeps Rep/Azusa - Attn: H. E. Griffin, Bldg. 119	1
Aerospace Corporation P.O. Box 95085 Los Angeles, California, 90045	
Attn: E. R. Berry	1

DISTRIBUTION (cont.)

	No. of Copies
AiResearch Manufacturing Company of Arizona P.O. Box 1947 Phoenix, Arizona	
Attn: H. H. Currey Security Officer	1
Allison Division General Motors Corporation Indianapolis 6, Indiana	
Attn: T. F. Nagey	1
ASRMF-P-1 Aeronautical Systems Division Wright-Patterson AFB, Ohio	
Attn: C. H. Armbruster	1
Atomics International P.O. Box 309 Canoga Park, California	
Attn: Carl E. Johnson	5
The Bendix Corporation Red Bank Division Eatontown, New Jersey	1
Brookhaven National Laboratory Associated Universities, Inc. Upton, Long Island, New York	
Attn: Classified Documents Group	1
Director, USAF Project RAND The RAND Corporation 1700 Main Street Santa Monica, California	
Attn: Library VIA: Air Force Liaison Office	1

DISTRIBUTION (cont.)

	No. of Copies
Electro-Optical Systems 300 N. Halstead Street Pasadena, California	
Attn: Mr. Joseph Neustein	1
Flight Propulsion Laboratory Department General Electric Company Cincinnati 15, Ohio	
Attn: Morris A. Zipkin	1
General Dynamics Astronautics Division San Diego, California	
Attn: Paul Slysh	1
General Electric Company Direct Current Motor and Generator Dept. 3001 East Lake Road Erie 1, Pennsylvania	
Attn: C. M. Mathias	1
General Electric Company Missiles & Space Division P.O. Box 8555 Philadelphia 1, Pennsylvania	
Attn: Edward Ray	1
Institute for Defense Analysis Universal Building 1825 Connecticut Avenue Washington 9, D.C.	
Attn: Dr. N. W. Snyder	1
Jet Propulsion Laboratories California Institute of Technology 4800 Oak Grove Drive Pasadena, California	
Attn: John Paulson	3
Attn: Librarian	1

DISTRIBUTION (cont.)

	No. of Copies
Lockheed Missiles and Space Division Lockheed Aircraft Corporation Sunnyvale, California	
Attn: H. H. Greenfield	1
The Martin Company Nuclear Division Baltimore 3, Maryland	1
McDonnell Aircraft Corporation Advanced Engineering Missiles & Space Systems Division St. Louis 66, Missouri	
Attn: R. A. Pepping	1
Northrop Space Laboratories 3401 W. Broadway Hawthorne, California, 90250	
Attn: E. Naumann Orgn. 600, Zone 65	1
Pratt & Whitney Aircraft East Hartford, Connecticut	
Attn: Wm. H. Podolny	1
Rocketdyne 6633 Canoga Avenue Canoga Park, California	
Attn: R. B. Dillaway	1
Thompson Ramo Wooldridge, Inc. 23555 Euclid Avenue Cleveland, Ohio, 44117	
Attn: E. Vargo	1
Attn: J. Picking	1
U.S. Atomic Energy Commission SNAP-8 Reactors Branch Division of Reactors Development Washington 25, D.C.	
Attn: K. Anderson	1

DISTRIBUTION (cont.)

	No. of Copies
U.S. Atomic Energy Commission Canoga Park, California	
Attn: Mr. Carl Malmstrom	1
U.S. Atomic Energy Commission Division of Technical Information Extension P.O. Box 62 Oak Ridge, Tennessee	1
U.S. Atomic Energy Commission Oak Rdige, Tennessee	
Attn: A. Taboada	1
U.S. Atomic Energy Commission Germantown, Maryland	
Attn: Dr. J. D. Lafleur	1
USA Commander Engineer Research & Development Laboratories Support Equipment Branch Diesel and Turbine Section Fort Belvoir, Virginia	
Attn: J. E. Montgomery	1
Westinghouse Electric Corporation Astronuclear Laboratory Route 51 P.O. Box 10864 Large, Pennsylvania	
Attn: Richard C. Cunningham	1
Westinghouse Electric Corporation Box 989 Lima, Ohio	
Attn: R. W. Briggs	1
R. W. Barret SNAP-8 Resident Office c/o Atomics International Box 309 Canoga Park, California, 91304	
Internal	63